Journal Pre-proofs

A quality by design framework for developing nanocrystal bioenabling formulations

Ana Simões, Ricardo A.E. Castro, Francisco Veiga, Carla Vitorino

PII: S0378-5173(23)00814-1
DOI: https://doi.org/10.1016/j.ijpharm.2023.123393
Reference: IJP 123393

To appear in: *International Journal of Pharmaceutics*

Received Date: 26 June 2023
Revised Date: 23 August 2023
Accepted Date: 6 September 2023

Please cite this article as: A. Simões, R.A.E. Castro, F. Veiga, C. Vitorino, A quality by design framework for developing nanocrystal bioenabling formulations, *International Journal of Pharmaceutics* (2023), doi: https://doi.org/10.1016/j.ijpharm.2023.123393

A quality by design framework for developing nanocrystal bioenabling formulations

Ana Simões [1,2], Ricardo A.E. Castro [1,3], Francisco Veiga [1,2] and Carla Vitorino [1,3] *

[1] Faculty of Pharmacy, University of Coimbra, 3000-548 Coimbra, Portugal; simoesana88@gmail.com (A.S.); rcastro@ff.uc.pt (R.A.E.C.); fveiga@ff.uc.pt (F.V.)

[2] Associated Laboratory for Green Chemistry of the Network of Chemistry and Technology (LAQV/REQUIMTE), Group of Pharmaceutical Technology, Faculty of Pharmacy, University of Coimbra, 3000-548 Coimbra, Portugal

[3] Coimbra Chemistry Centre, Institute of Molecular Sciences - IMS, Department of Chemistry, University of Coimbra 3004-535 Coimbra, Portugal

* Correspondence: csvitorino@ff.uc.pt (C.V.); Tel.: +351-239-488-400

Graphical Abstract

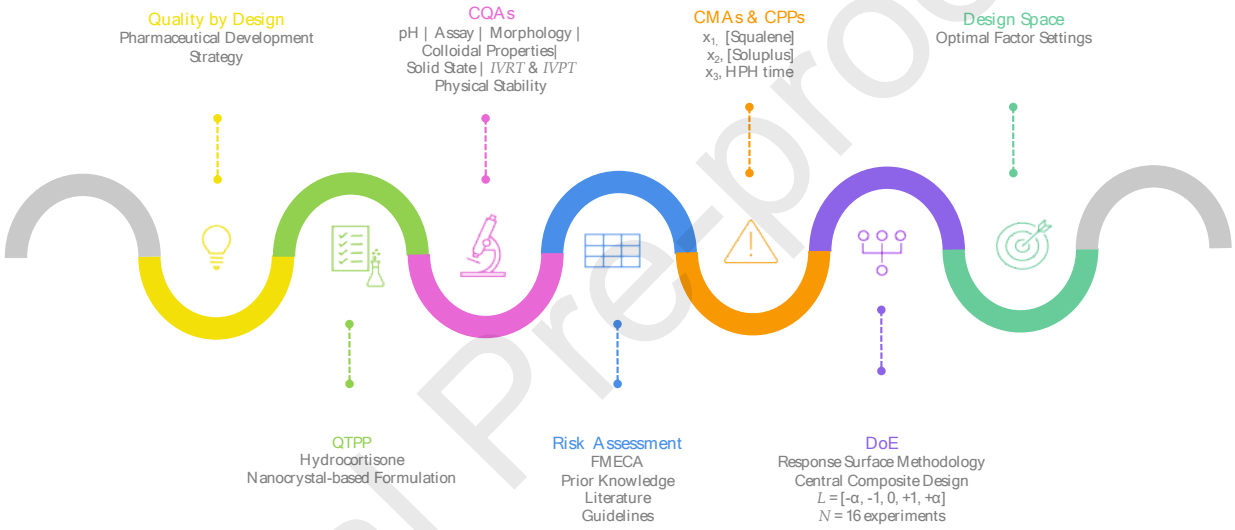

Key: QTPP, Quality Target Product Profile; CQAs, Critical Quality Attributes; *IVRT*, *In Vitro* Release Testing; *IVPT*, *In Vitro* Permeation Testing; FMECA, Failure Mode, Effects and Criticality Analysis; CMAs, Critical Material Attributes; CPPs, Critical Process Parameters; HPH, High-pressure homogenization; DoE, Design of Experiments; *L*, Levels of factors; *L*, number of experiments.

Abstract

The present study aims to outline a rational framework for the design and development of a 1.0% (w/v) hydrocortisone nanocrystal-based formulation, resorting to a simple, efficient, and scalable nanonization methodology, based on the high-pressure homogenization (HPH) technique. Accordingly, the innovative product was comprehensively optimized following a Quality by Design (QbD) approach. The thorough selection of formulation composition was driven by a dual purpose: improving skin permeation and stability. In the early stage of development, a Failure Mode, Effects and Criticality Analysis (FMECA) diagram was employed to identify the most impactful variables for the critical quality attributes (CQAs). In this sense, a rotatable, three-factor and five-level circumscribed central composite design (CCCD) was applied to investigate how squalene concentration (x_1), soluplus concentration (x_2) and HPH-time (x_3) influence physicochemical properties, performance and physical stability of the formulation. A robust Design Space (DS) was defined, establishing the optimal settings for the critical variables, whose combination meets the requirements set in the quality target product profile (QTPP). Morphological analysis revealed the cuboidal shape of hydrocortisone nanocrystals. In what concerns colloidal properties, the most promising formulation disclosed a small particle size (Dx(50) = 311.8 ± 1.5 nm), along with narrow size distribution (span value =

1.91 ± 0.17). Zeta potential results (-2.19 ± 0.15 mV – -12.1 ± 0.4 mV) suggested a steric hindrance stabilization. FTIR spectra showed no chemical interactions between drug and formulation components. XRD diffractograms confirmed loss of crystallinity during the downsizing process. *In vitro* studies revealed an improvement on drug release rate (316 ± 21 – 516 ± 35 μg/cm^2/√t), compared to the coarse suspension and commercial products, and a straight dependence on the stabilizer concentration and HPH time. The permeation flux across the skin (0.16 ± 0.02 – 1.2 ± 0.5 μg/cm^2/h) appeared to be dependent on the drug physicochemical properties, in particular saturation solubility. Further characterization of the experimental formulations pointed out the role of the stabilizing component to prevent against physical instability phenomena. This organic solvent-free, and therefore "green" nanocrystal production technology offers great potential for pharmaceutical R&D and drug delivery by enabling the development of new forms of conventional drugs with optimal physicochemical properties and performance.

Keywords: Central Composite Design; crystallinity; nanocrystals; performance; physical stability; quality by design; solid-state; topical dermatological product

Introduction

Topical drug administration remains the preferred route for the treatment of dermatological conditions. However, the uppermost layer of the epidermis, the *stratum corneum* (SC), still poses the greatest challenge to the penetration of the active substances into the intact or barrier-disrupted skin. In recent years, depending on the physicochemical properties of the studied drug, different nanoparticulate systems have been investigated to overcome skin barrier properties, improving the efficacy and safety of topical drug delivery. Nevertheless, various drawbacks (insufficient drug load, poor long-term stability, high surfactant content, that may lead to skin irritation) have precluded the implementation of nanoparticles in the clinical setting. In this context, nanocrystal-based formulations have emerged as an appealing technology. Drug nanocrystals are solid nanosized particles of drug surrounded by a thin stabilizing layer. With an average particle size between 1 and 1000 nm, nanocrystals are commonly produced as nanosuspensions in a liquid medium (water, aqueous solution or non-aqueous solution) [1-4]. Containing almost 100% drug in their composition, drug nanocrystals do not face the problem of loading capacity often associated with other types of nanoparticles [4]. Also, it endows them with large surface area, faster dissolution rate, and improved stability without requiring high amount of stabilizing agents, consequently minimizing skin irritation phenomena. In addition, skin adhesion and permeation through different pathways are promoted, which may yield an enhanced drug bioavailability to the target site [5-14].

In the dermatological arena, drug permeation through the skin is a premise for successful topical delivery and therapeutic efficacy. The mechanism of action underlying drug nanocrystals relies on increased saturation solubility, leading to an increment in the concentration gradient between the formulation and the skin, resulting in better drug penetration [7, 11]. After topical application, drug molecules can penetrate through several mechanisms: (i) drug nanocrystals are transported to the skin surface, where the drug molecules are dissolved and consequently diffused into the membrane/cell; (ii) the drug nanocrystals (<100 nm) are taken up by the cells via endocytosis, resulting in drug delivery to the cellular compartment or diffusion to the underlying tissue; (iii) after nanocrystal diffusion through the skin layers, endocytosis by the host cells (<100 nm) and phagocytosis by macrophages (>100 nm) can transport nanocrystals to the deeper skin layers; and (iv) via appendageal pathway, especially hair follicles [6, 15].

Relatively easy to produce and cost-effective in large scale production, drug nanocrystals are an interesting approach to improve the dissolution of poorly water-soluble drugs, which is clearly reflected in pharmaceutical industry pipelines. Nanocrystal-based formulations have been widely used in preclinical and clinical studies to increase the oral bioavailability of poorly water-soluble drugs. Moreover, drug nanocrystals have likewise been applied in alternative routes of administration, such as topical route [13, 14, 16, 17]. It is estimated that 90% of new chemical entities belong to BCS class II (70%) and class IV (20%) [18]. As a result of poor solubility, these active substances exhibit a low and erratic bioavailability, remaining a challenging task for formulation scientists [19].

Currently, there are two distinctive approaches for producing drug nanocrystals: bottom-up and top-down technologies [2, 4, 11]. The main top-down methods comprise breaking the drug particle by high-energy mechanical forces and include techniques such as wet media milling or high-pressure homogenization (HPH) [2, 4, 20, 21]. In the bottom-up approach, nucleation, with consequent crystal growth, takes place by employing nanoprecipitation and solvent removal techniques: solvent-antisolvent precipitation, precipitation in supercritical fluids, precipitation by solvent evaporation (spray-drying, freeze-drying or spray-freezing in liquid [2, 4, 16]. More recently, bottom-up and top-down processes have been combined [2, 16]. Despite the high energy consumption and long operating time, top-down technologies are simple, reproducible, easy to scale-up and efficient in reducing particle size to the nanometer scale [2, 10, 16, 22]. However, product contamination can be a hurdle to wet milling application. In contrast, HPH is less prone in generating process impurities [2, 23]. In turn, the complexity of process control, the potential risk of organic solvents, limited reproducibility and scalability have discouraged the implementation of bottom-up approaches by the pharmaceutical industry [4, 22]. Some of the issues related to both top-down and bottom-up techniques comprise cost, time, a wide particle size distribution, and the possibility of recrystallization [24]. Depending on the production method, process parameters, drug and stabilizer properties, and their interactions, a crystalline or amorphous product may result [2, 22, 25]. In the strictest sense, the term "nanocrystal" has been extended to describe drug molecules partially crystalline and even in an amorphous state. More recently, preparations containing drug molecules in a form other than pure crystalline are referred to as "nanocrystals in the amorphous state", "amorphous nanoparticles" or "amorphous drug nanosuspension" [25, 26].

In the nanocrystal design, the selection of the stabilizing agent(s) is of paramount importance to ensure the physical stability of nanosuspensions, and to prevent aggregation and/or the Ostwald ripening effect [3, 19, 25]. Regardless of the modest structure of nanocrystals, the selection of an appropriate stabilizing agent can be challenging [27]. Due to the lack of systematic understanding of the stabilizer, this selection is still made on a trial-and-error basis. Therefore, to ensure the successful design and development of a nanocrystal-based formulation, it is imperative to develop a comprehensive knowledge for the accurate selection of the stabilizer. Moreover, the inclusion of permeation enhancers into the nanocrystal structure, in conjunction with a nanonization process, can be an asset to enhance the topical bioavailability of poorly-water soluble drugs and, consequently, skin permeation [28-31].

Undoubtedly, nanocrystals are a useful strategy for topical drug delivery purposes, where the formulation development stages play an important role in the success of the final product. Indeed, a more comprehensive and rational approach must underlie the design and development of these formulations to consistently deliver the intended quality aspects. In this context, the Quality by Design methodology have been outlined by regulatory authorities as the *status quo* of current pharmaceutical development. QbD relies on a systematic, scientific and risk-driven strategy whose (i) product quality is prospectively defined; (ii) all variability sources are identified, appropriately understood and controlled; (iii) a detailed understanding of the drug product and its manufacturing is mandatory for more flexible regulatory approaches and (iv) a control strategy is delineated to ensure that a product of required quality is produced consistently [32, 33]. The implementation of the QbD methodology begins outlining the quality target product

profile (QTPP), and the selection of critical quality attributes (CQAs). A risk assessment is performed to identify and rank critical material attributes (CMAs) and critical process parameters (CPPs) that potentially impact product CQAs. Thereafter, a design of experiments (DoE) is performed to determine the significance level of individual variables and potential interactions effects in the CQAs. Ultimately, the optimal working ranges for CMAs and CPPs are established within a design space (DS) [34-37].

The main purpose of the present study is to provide a guidance for designing an optimal nanocrystal-based formulation following a prospective and systematic methodology, such as the QbD approach. A detailed understanding of the formulation and manufacturing process was delineated to attain a drug product that meets the QTPP specifications [35]. The effect of formulation and process variability on the quality profile of a nanocrystal-based formulation was evaluated by selecting micronized hydrocortisone as BSC class II drug model.

To find the best compromise for particle size among different combinations of raw materials and manufacturing processes, a preliminary assay was first performed. Subsequently, a feasibility study based on QbD methodology was initiated with QTPP definition, along with CQAs Identification. A Failure Mode, Effects and Criticality Analysis (FMECA) diagram was used to conduct an initial risk assessment for determining the CMAs and CPPs. A circumscribed central composite design (CCCD) was carried out to investigate how critical variables impact the investigated CQAs, interplaying the physicochemical properties of the nanosuspensions with the product performance and stability. To this end, extensive colloidal and solid-state characterization was accomplished, pondering particle size, size distribution, zeta potential, crystallinity, and physical stability. *In vitro* release, and permeation behavior were also appraised. Ultimately, the optimal working conditions were outlined by establishing a DS.

2. Materials

Micronized hydrocortisone was kindly supplied by Laboratórios Basi - Indústria Farmacêutica S.A. (Mortágua, Portugal). Squalene was purchased from Sigma Aldrich (Missouri, USA). Polyethylene glycol 400 was purchased from PanReac AppliChem (Barcelona, Spain). Propylene glycol was acquired from Labchem (Zelienople, USA). Limonene was purchased from Fluka. Kollicream® IPM (isopropyl myristate) and Soluplus® were kindly provided by BASF SE (Ludwigshafen, Germany). MONTANE™ 20 PHA PREMIUM (Span 20), MONTANOX™ 20 PHA PREMIUM (Tween 20), MONTANOX™ 60 PHA PREMIUM (Tween 60) and MONTANOX™ 80 PHA PREMIUM (Tween 80) were gently supplied by SEPPIC SA (Paris, France). Tween 40 was purchased from Sigma Aldrich (Missouri, USA). Water was purified (Millipore®) and filtered through a 0.22 μm nylon filter before use. All other reagents and solvents were from analytical or high-performance liquid chromatography (HPLC) grade.

3. Methods

3.1. Quality by Design Approach

3.1.1. Definition of Quality Target Product Profile

In line with stakeholder expectations (patients, industry and regulators), the QTPP was prospectively established encompassing quality features of a nanocrystal-based formulation capable of improving topical bioavailability and skin uptake of a BSC Class II drug. QTPP summarizes patient-relevant quality, safety and efficacy attributes that ideally should be achieved to ensure the preset quality [35].

3.1.2. Identification of Critical Quality Attributes

To meet the QTPP, potential CQAs were identified as critical quality properties that have the greatest chance of generating product failure and, for that reason, should be studied and controlled for ensuring the required final quality. The acceptance limits and the rationale for designating each CQA were also provided. Derived from the QTPP, these attributes are defined according to guideline requirements, prior knowledge and scientific understanding of the drug product and manufacturing process [35].

3.1.3. Preliminary Study

In order to select the most suitable formulation excipients and nanocrystal production process, and to establish the appropriate levels of the important factors to be further investigated in the experimental design (optimization study), a preliminary study was carried out.

There are different approaches to reduce the average size of the solid drug particles to the nanometer scale. In this context, high-pressure homogenization (HPH) (Emulsiflex®-C3, Avestin, Inc., Ottawa, Canada) and ultrasonication (US) (Branson® Sonifier 250, Branson Ultrasonics Corporation, Connecticut, USA) techniques were explored as potential nanosizing methodologies.

First, the micronized hydrocortisone and the permeation enhancer were dispersed in the stabilizing aqueous solution. This pre-mixing was performed at room temperature with a high shear homogenizer (Ultra-Turrax X10/25, Ystral GmbH, Dottingen, Germany) at 16,000 rpm. The impact of different mixing times (1.0, 2.0, 3.0 and 10.0 min) and dispersing shaft sizes (6G and 18G) on downsizing effectiveness was investigated. The pre-suspension was then transferred to the HPH apparatus and processed over different pressure levels (1000, 1250 and 1650 bar) and periods of time (5.0, 10.0, 17.5, 20.0, 25.0 and 30.0 min). Alternatively, a sonication probe was immersed in the pre-suspension vessel at an amplitude frequency of 100% over different homogenization times (5.0, 10.0, 15.0, 20.0 and 25.0 min). An upper limit of 25.0 min was set up owing to the heat dissipated from the cavitation phenomenon [38]. The temperature was kept constant.

At the same concentration level (2.5% w/v), polyethylene glycol 400 (PEG), propylene glycol (PPG), limonene, isopropyl myristate (IPM) and squalene were screened as skin permeation enhancers, while span 20, tween 20, tween 40, tween 60, tween 80 and soluplus were investigated as stabilizing agents. The impact of different concentrations of tween 80 and soluplus in combination (2.5%:0.0%, 1.875%:0.625%, 1.25%:1.25%, 0.625%:1.875%, 0.0%:2.5%, w/v) on downsizing effectiveness was further tested.

An additional investigation was performed to understand whether particle size and size distribution were affected by different concentrations of squalene (0.5, 1.0, 1.5, 2.0, 2.5, 3.0, 3.7, 4.5 and 5.5% w/v), soluplus (0.3, 1.0, 1.5, 2.0, 2.5, 3.0, 3.7 and 4.5% w/v) and hydrocortisone (0.5, 1.0, 1.5, 2.5, 3.0, 4.5 and 5.5% w/v), HPH time (5.0, 17.5, 25.0 and 30.0 min) and HPH pressure (1000, 1250 and 1670 bar).

3.1.4. Risk Assessment

Risk assessment is a useful approach to systematically gather-up and rank potential factors, inherent to formulation and process manufacturing, that are more likely to affect the final product quality. Therefore, a Failure Mode, Effects and Criticality Analysis (FMECA) diagram was constructed to assign the most critical factors which should be investigated during the development process. FMECA is a comprehensive tool that systematizes information by

presenting modes, causes and effects of failure and the severity, probability of occurrence and detectability of the consequences of that failure [36, 39]. The FMECA allows to rank the risks according to the Risk Priority Number (RPN) as described by the following equation (1):

$$\text{RPN} = \text{Severity (S)} \times \text{Probability (P)} \times \text{Detectability (D)} \quad (1)$$

where a numerical score from 1 to 5 is established, with 1 being a negligible risk, easily detectable, that does not require attention and 5, a severe effect, difficult to detect, that requires the utmost attention.

3.1.5. Design of Experiments

To statistically optimize the nanocrystal-based formulation and manufacturing process, a rotatable, three-factor and five-level circumscribed central composite design (CCCD) was performed, using JMP Pro 17 Software (Cary, NC, USA). CCCD is the most predominant optimizing DoE, providing extensive information on the effects of critical factors with a minimal number of trials. For more than two factors, CCD is cost-effective in experiments and time-consuming. The experimental domain is broader than the (-1) and (+1) levels. As part of the Response Surface Methodology (RSM), the CCD is an appropriate design for exploring quadratic response surfaces. Polynomial quadratic models are constructed to describe the relationship(s) between the investigated factors and the considered responses. Main effects, interaction effects and quadratic effects are well estimated [40-43]. According to risk assessment analysis, squalene concentration (x_1), soluplus concentration (x_2) and HPH time (x_3) were recognized as the most important factors affecting product CQAs. For each independent variable, the CCD selected two extreme levels ($-\alpha$ and $+\alpha$) in addition to low (−1), medium (0) and high (+1) levels. The distance α from the design center to any axial point is $\alpha = 1.68$ ($|\alpha| = (2^f)^{1/4}$, $f = 3$ factors). A total of sixteen experiments were generated, comprising eight factorial points, six axial points and two center points, to increase the accuracy of the method. The selection criteria for electing those factors were based on preliminary study (Section 3.1.4) and risk assessment (Section 3.1.3) results. Different levels of the independent variables are described in Table 1, while DoE experimental runs are presented in Table 2. Experiments were randomly carried out.

[Insert Table 1 and Table 2 around here]

The effects of the independent variables on the different responses/CQAs were examined using the following quadratic polynomial model (2):

$$Y_n = \beta_0 + \beta_1 x_1 + \beta_2 x_2 + \beta_3 x_3 + \beta_{12} x_1 x_2 + \beta_{13} x_1 x_3 + \beta_{23} x_2 x_3 + \beta_{11} x_1^2 + \beta_{22} x_2^2 + \beta_{33} x_3^2 \quad (2)$$

where Y denotes the response associated with each factor level combination; β_0 is the response in the absence of effects; β_1, β_2 and β_3 represent the first order coefficients of the respective independent variables; β_{12}, β_{23} and β_{13} typify the interaction coefficients; β_{11}, β_{22} and β_{33} betokens the quadric coefficients. The greater the absolute regression coefficient value, the greater is the variable impact on the studied response. In turn, the positive and negative sign indicate a synergetic or antagonistic variable effect, respectively.

3.1.6. Design Space

Considering the specifications of each CQA, a Response Surface Methodology (RSM) was conducted to establish a comprehensive Design Space (DS). The DS is an operable region.,

providing several settings of input variables that fulfill CQAs requirements set in the QTPP. This optimal working region provides a more flexible and robust formulation and manufacturing process, without compromising the final product quality [35]. The DS was performed using JMP Pro 17 Software (Cary, NC, USA).

3.2. Preparation of Nanosuspensions

Micronized hydrocortisone (1.0%, w/v) was first blended with different concentrations of squalene (Section 3.1.5). This mixture was then dispersed in 30.0 mL of an aqueous solution of different soluplus concentrations (Section 3.1.5). The dispersion was performed at room temperature with a rotor-stator homogenizer (Ultra-Turrax X10/25, Ystral GmbH, Dottingen, Germany) at 16,000 rpm for 3.0 min.

The pre-suspension was transferred to a high-pressure homogenizer (Emulsiflex®-C3, Avestin, Inc., Ottawa, Canada) at room temperature, and processed at 1,000 bar throughout different periods of time (Section 3.1.5) [44-46].

A coarse suspension of micronized hydrocortisone (1.0%, w/v) was prepared and used as a negative control (NC_{HC}). Commercial hydrocortisone butyrate salt (0.1%, w/w) solution (S_{HCB}) and emulsion (E_{HCB}) were also considered as references. The detailed characterization of unprocessed drug powder, NC_{HC}, S_{HCB} and E_{HCB} is listed in supplementary material Table S1.

3.3. Physicochemical Characterization

3.3.1. pH

The pH values were determined in triplicate at room temperature, resorting to a digital pH meter C3010 (Consort bvba, Turnhout, Belgium), previously calibrated through buffer solutions with pH of 4.00, 7.00 and 10.00. The electrode was immersed directly in the dispersion, and the pH value was recorded.

3.3.2. Assay

Hydrocortisone content was estimated using a specific volume of nanocrystal dispersion adequately diluted in methanol. The dispersion was then centrifugated for 5 min at 11,470 g in a Minispin® (Eppendorf Ibérica S.L., Marid, Spain). The supernatant was collected, diluted in the mobile phase, filtered by a 0.22 μm membrane and determined by HPLC, as described in what follows below.

Briefly, the quantification of hydrocortisone was performed through a reversed-phase HPLC method using a Shimadzu LC-2040C 3D apparatus equipped with a quaternary pump, an autosampler unit, and a D2 Lamp UV-visible photodiode array detector. A LiChrospher100 RP-18 column with 5 μm particle size, 4 mm of internal diameter and 125 mm length, purchased from MZ-Analysentechnik GmbH (Mainz, Germany), was used to perform the chromatographic separation of hydrocortisone at 30°C. The analysis was conducted in an isocratic mode at a constant flow rate of 0.8 mL/min and with a mobile phase consisting of a mixture of water:acetonitrile (75:25, v/v). The detection of hydrocortisone was carried out at 242 nm and an injection volume of 10 μL was considered for all standards and samples. Under these conditions, hydrocortisone was eluted at approximately 8.35 minutes. The acquired data was processed with Shimadzu LabSolutions version 5.82 software.

3.3.3. Morphology

The morphological analysis of the nanocrystals was conducted by scanning electron microscopy (SEM) using a JSM-6010LV scanning electron microscope (Jeol, Tokyo, Japan), at accelerating voltages of 10 kV. Prior to analysis, the samples were placed on a double-side carbon tape mounted onto an aluminium stud, dried and coated with a nanometric layer of gold using a mini sputtering equipment to make them electrically conductive.

3.3.4. Colloidal properties

3.3.4.1. Laser Diffraction

Particle size was determined by laser diffraction (LD), using a Mastersizer 3000 (Malvern Instruments, UK) equipped with a Hydro MV dispersion unit. In this technique, particle size is measured indirectly by the angular variation in the intensity of light scattering as a laser beam passes through a dispersed particle sample. The larger the diffraction angle, the smaller the particle size [47].

After system alignment and background evaluation, the sample was dispersed in 120 mL of ultrapurified water and stirred at a speed of 2000 rpm. No sonication was applied. Measurements were performed with an obscuration of about 10% at room temperature. The particle size distribution was calculated using the Mie theory. Hence, the real RI (1.594) and imaginary RI (0.01) of the sample, and the real RI (1.333) of the dispersant were set up in the optical method [48]. Each determination was carried out in triplicate. The results were expressed as Dx(10), Dx(50), Dx(90), Span, $d_{3,2}$ and $d_{4,3}$. Indicators of fit such as residual and weighted residual provide a clear insight into the quality of the results. The residual is an indication of how well the calculated data were fitted to the measured data [49]. Residual and weighted residual below 2% and in the same order of magnitude consolidate a reliable measurement [50].

Dependent on the volume distribution, Dx(10), Dx(50) and Dx(90) represent the particle diameter corresponding to 10th, 50th and 90th percentiles of the cumulative undersize distribution, respectively [51]. These values allow obtaining a defined statistical parameter, the span value. This parameter is useful for characterizing the particle size distribution and is calculated by the following equation (3):

$$\text{Span} = \frac{Dx(90) - Dx(10)}{Dx(50)} \quad (3)$$

wherein a lower span value indicates a narrow size distribution [52].

The $d_{3,2}$ or Sauter Mean Dimeter is the surface mean diameter and is more sensitive to changes in the fine particle fraction. The $d_{4,3}$ or De Brouckere Mean Diameter is the volume mean diameter and is more sensitive to changes in the large particle fraction [53-55].

3.3.4.2. Zeta Potential

Zeta potential (ZP) was determined by electrophoretic light scattering (ELS), resorting to a Zetasizer Nano ZS (Malvern, Worcestershire, UK) apparatus at a temperature of 25 °C. Prior to measurements, samples were suitably diluted 30-fold with ultrapurified water and analyzed in triplicate. For the ZP calculations, the Helmholtz-Smoluchowsky equation was considered.

3.3.5. Thermal and Solid-state Properties

3.3.5.1. Differential Scanning Calorimetry

Differential scanning calorimetry (DSC) analysis was carried out using a DSC-204 F1 Phoenix differential scanning calorimeter (Netzsch, Germany). Pure compounds (unprocessed hydrocortisone, squalene and soluplus) and lyophilized nanocrystals (approximately 2.5 mg) were placed in aluminum pans with pierced lid. An empty pan with pierced lid was used as reference. The samples were submitted to a heating cycle from 40 °C to 260 °C, under a nitrogen atmosphere flow of 20 mL/min and at a heating rate of 10 °C min^{-1}. Through Proteus Software (Netzsch, Germany), parameters such as onset temperature (T_{onset}), peak temperature (T_{peak}), and enthalpy (ΔH) were determined.

3.3.5.2. Thermogravimetric Analysis

Thermogravimetric Analysis (TGA) were performed at temperatures from 30 to 600 °C using a TG 209 F3 Tarsus (Netzsch, Germany), under a nitrogen atmosphere flow of 20 mL min^{-1} with a heating rate of 10 °C min^{-1}. The initial sample mass was about 15.1 mg, which was weighed in open alumina crucibles. The percentage of mass loss was determined using Proteus Software (Netzsch).

3.3.5.3. Attenuated Total Reflectance Fourier Transform Infrared

Attenuated total reflectance Fourier transform infrared (ATR-FTIR) spectra were recorded at room temperature using a FT-IR/FT-NIR Spectrum 400 spectrometer (Perkin-Elmer, Hopkinton, MA, USA) coupled with an ATR accessory fitted with a Zn-Se crystal plate. The pure compounds (unprocessed hydrocortisone, squalene and soluplus) and lyophilized nanocrystals spectra were recorded using 20 scans for each spectrum, with a resolution of 1 cm^{-1} and a scan speed of 0.5 cm/s. The spectra were collected between 4000 and 650 cm^{-1}. Spectral deconvolution was performed using Origin 2018 Software (Northampton, MA, USA).

3.3.5.4. X-Ray Powder Diffraction

X-ray powder diffractograms (XRPD) of unprocessed hydrocortisone and lyophilized nanocrystals were obtained using a MiniFlex 600 X-ray diffractometer (Rigaku, Tokyo, Japan), with CuKα radiation at 40 kV and 15 mA. The 2θ scan range was 3-40° with a step size of 0.01° and a scan speed of 5 s/°. The relative crystallinity was calculated using the following equation (4):

$$Xc = \frac{Ap}{(Ap + Ab)} \times 100 \quad (4)$$

where *Xc* refers to the relative crystallinity, *Ap* to the crystallinity area of the X-ray diffractogram, and *Ab* to the amorphous area of diffractogram [56].

3.4. Performance Studies

3.4.1. *In Vitro* Release Testing

In vitro release testing (IVRT) was conducted using static vertical Franz diffusion cells (PermeGear, Inc., Pennsylvania, USA) with a diffusion area of 0.636 cm^2 and a receptor compartment of 5 mL. A dialysis cellulose membrane (MWCO ~ 14,000, avg. flat width 33 mm, D9652-100FT, Sigma-Aldrich), as artificial membrane, was placed between donor and receptor

compartments, and a receptor solution composed of water-ethanol (70:30, v/v) was used, safeguarding *sink conditions* [57]. The receptor media was continuously stirred at 600 rpm and maintained at 37 °C by means of a circulating water bath, mimicking skin conditions. 300 µL of experimental formulations were applied in the donor compartment. Throughout the release studies, the donor compartment, as well as the receptor sampling arm, were carefully covered with Parafilm® to avoid unnecessary release medium evaporation and to conduct all the release experiments under occlusive conditions. Samples of the receptor solution (300 µL) were withdrawn at 0.25, 0.5, 1, 2, 3, 4, 6, 8, 10 and 24 h, and immediately replaced with the same volume of preheated receptor solution. IVRT samples were analyzed for the drug content using the RP-HPLC described in Section 3.3.2. Calculated from the slope of the linear portion of the collected data, the amount of drug released per unit area (*In vitro* release rate, IVRR) was considered an important IVRT outcome, as well as the percentage of hydrocortisone released at 6 h (R_{6h}) and 24 h (R_{24h}).

To characterize hydrocortisone release kinetics, the release profiles were fitted with different mathematical models using DDSolver software: Zero order, First order, Higuchi, Korsmeyer–Peppas, Hixson-Crowell, Hopfenberg Weibull and Gompertz. The goodness of fit was assessed pondering statistical outcomes, such as the adjusted coefficient of determination (R^2_{adj}). The Akaike information criterion (AIC), the residual sum of squared errors (SSE), the mean squared error (MSE) and the standard deviation of the residual error (root mean squared error, RMSE) were also considered. The best fitted model presents R^2_{adj} values closest to 1 and lower values of AIC, SSE, MSE and RMSE.

3.4.2. *In Vitro* Permeation Testing

In vitro permeation testing (IVPT) was performed in static vertical Franz diffusion cells in the same conditions of *in vitro* release studies but using newborn pig skin as skin model. The newborn pig was provided by a local slaughterhouse. Full-thickness skin grafts (both the full epidermis, with SC, and dermis) were excised from the trunk area, and subcutaneous fat and excess hair removed. Then, grafts of split-thickness skin (epidermis and a superficial part of the dermis) were cut at a thickness of 0.97 ± 0.22 mm using a manual dermatome (BA706R, AESCULAP, Tuttlingen, Germany) [58]. Each membrane was cut to an appropriate size, wrapped in aluminum foil, and stored at −20 °C for a period not exceeding 3 months. Prior to the experiments, disks of dermatomed skin membrane were thawed and clamped between donor and receptor compartments, with the SC side facing upwards. Skin integrity was monitored by measuring the transepidermal water loss (TEWL). Only those skin samples that were found below 15 g/m^2.h $^{-1}$ were selected for the experiment. A PBS-ethanol (70:30, v/v) solution was found to be suitable as the receptor medium to achieve *sink conditions*. 300 µL of experimental formulations were placed in the donor compartment. Samples of the receptor solution (300 µL) were withdrawn at 0.5, 1, 3, 6, 10, 24, 30, 36 and 48 h, and immediately replenished with the same volume of preheated fresh solution. Hydrocortisone present in IVPT samples was quantified by RP-HPLC depicted in Section 3.3.2. Permeation profiles were acquired by plotting the cumulative amount of permeated hydrocortisone against time.

The cumulative amount of hydrocortisone permeated per unit area of the excised skin (Q_n, µg/cm^2) was calculated as a function of time (t) according to the following equation (6):

$$Q_n = \left[C_n \times V_0 + \sum_{i=1}^{n-1} C_i \times V_i\right] / A \quad (6)$$

where C_n corresponds to the drug concentration of the receptor medium at each sampling time, C_i, to the drug concentration of the ith sample, A to the effective diffusion area, and V_0 and V_i to the volumes of the receptor compartment and the collected sample, respectively. The cumulative

amount of hydrocortisone permeated after 6 h (Q_{6h}), 24 h (Q_{24h}) and 48 h (Q_{48h}) were pondered as IVPT outcomes.

The steady-state flux (Jss) was obtained from the slope of the linear region of the curve, representing the amount of drug permeated per unit area *vs*. time. According to Fick's first law of diffusion, the steady-state flux (J_{ss}, μg/cm^2/h) was determined by the following equation (7):

$$J_{ss} = DC_0P/h = C_0Kp \quad (7)$$

where D is the diffusion coefficient of the drug in the SC, C_0 represents the drug concentration in the donor compartment, P is the partition coefficient between the vehicle and the skin, h is the diffusional path length, and K_p stands for the permeability coefficient. The permeability coefficient (K_p, cm/h) of hydrocortisone from each formulation was calculated by dividing the slope of the straight line portion of the curve (J_{ss}) by drug concentration originally added in the experimental formulations. The lag time of permeation (t_{lag}), a parameter related with the required time to achieve the steady-state flux of a drug through the skin, was determined from de X-intercept of the linear proton of the graph. The enhancement ratio (ER) for flux was calculated as the ratio between the flux of different formulations and the NC_{HC} flux value.

3.5. Stability Testing

3.5.1. Colloidal Stability

Colloidal stability testing was performed over a period of 4 weeks at 4 ± 1°C. Colloidal properties (particle size and zeta potential) were analyzed by performing Sections 3.3.4.1 and 3.3.4.2.

3.5.2. Analytical Centrifugation

Physical accelerated stability testing was conducted through analytical centrifugation, using the LUMiSizer stability analyzer (LUM GmbH, Berlin, Germany). This technique enables to inspect for instability phenomena by measuring the intensity of transmitted near infrared (NIR) light as a function of time and position. A fast stability ranking of undiluted dispersions is achieved in minutes/hours instead of months/years. The shape and progression of transmission profiles provide information on the sample kinetic stability, predicting separation processes over the storage, e.g., aggregation, coalescence, creaming and sedimentation. According to the detected instability phenomena, the separation velocity (μm/s) could be estimated from the linear regression of the clarification zone. A faster separation rate indicates a higher sample instability. Formulation stability can also be quantitatively described through the instability index parameter. This is a dimensionless number ranging from 0 to 1, wherein measurements closer to "0" stand to higher sample stability. The instability index quantifies the clarification in transmission, considering the particle size and separation phenomena, at a given time and under an accelerated gravitational force, divided by the total clarification. The clarification is determined by the increase in transmission or the decrease in particle concentration due to their movement towards the bottom (sedimentation) or to the top (creaming) of the cell. Therefore, for the same total clarification, samples with lower clarification present long-term stability [32, 33, 59-62].

The stability of experimental formulations was evaluated after 1 h 30 min of centrifugation at an acceleration of 4000 rpm and 25 °C. All samples were analyzed in triplicate. The transmission profile analysis was conducted using the SEPView® software (LUM GmbH, Berlin, Germany), from which separation velocity and instability index were calculated.

3.6. Statistical Analysis

Student's *t*-test was performed to assess whether the terms are statistically significant in the regression model, while one-way analysis of variance (ANOVA) was performed to verify the validity of the model's fit. Statistical significance is found when $Prob>|t|<0.05$ and p-value < 0.05. In turn, a regression coefficient (R^2) closer to 1 indicates a suitable fit of the regression model to the experimental data. The adequacy of the model fitting was estimated by Fisher tests. A regression F Ratio (F_1) much greater than 1 with a $Prob>F<0.05$ denotes a good correlation among the experimental and predicted responses and, therefore, the regression model is suitable for describing the variations in responses. In turn, a lack of fit F Ratio (F_2) close to 1 suggests an excellent reproducibility of the purchased data (validity of the model). Pure errors, regardless of the model, e.g., experimental errors, are minimal when a non-significant lack of fit is verified ($Prob>F > 0.05$). Hence, a model will be suitable when a significant regression and a non-significant lack of fit are obtained for the selected confidence level [33].

An ANOVA with Tukey multiple comparison test was also performed using the GraphPad Prism 5 Software (San Diego, CA, USA). Differences among the average values were considered statistically significant when p-value < 0.05.

4. Results and Discussion

4.1. Definition of Quality Target Product Profile and Critical Quality Attributes Identification

The first step in the development and optimization of a drug product based on the QbD approach is to define the QTPP. Therefore, Table 3 comprises quality, efficacy and safety features of hydrocortisone nanocrystals capable of improving dermal bioavailability, solubility and skin permeation of the active substance, towards an improvement of the therapeutic effects under the patient`s perspective. The quality profile was established prospectively using prior knowledge and preliminary experiments [44-46, 63].

The quality attributes more sensitive to formulation and/or process variability were also identified and justified in Table 3. Derived from QTPP, the CQAs encompassed morphological, colloidal and structural properties, performance and stability outcomes. Individual acceptance criteria were also addressed in Table 3.

[Insert Table 3 around here]

4.2. Preliminary Study

A preliminary screening was carried out to select the excipients and process parameters of the nanocrystal-based formulation to be optimized through the response surface methodology (RSM). Furthermore, it is intended to establish lower and upper levels of the critical variables to be explored in the experimental design. Hence, the impact of different manufacturing processes, skin permeation enhancers, stabilizing agents and their concentrations, and drug concentration on Dx(10), Dx(50), Dx(90) and span value was investigated.

In pharmaceutical manufacturing, high shear flows are required to overcome adhesion forces and reduce particle size, which is achieved by high shear homogenizers, high-pressure homogenizers and ultrasonic dispersion [64]. In this context, the first goal of the preliminary analysis was to explore nanocrystal production methods to yield nanosized drug particles with a narrow size distribution.

Inspecting the effect of process parameters on particle size distribution, it was possible to observe how different manufacturing processes influenced downsizing effectiveness (Figure 1).

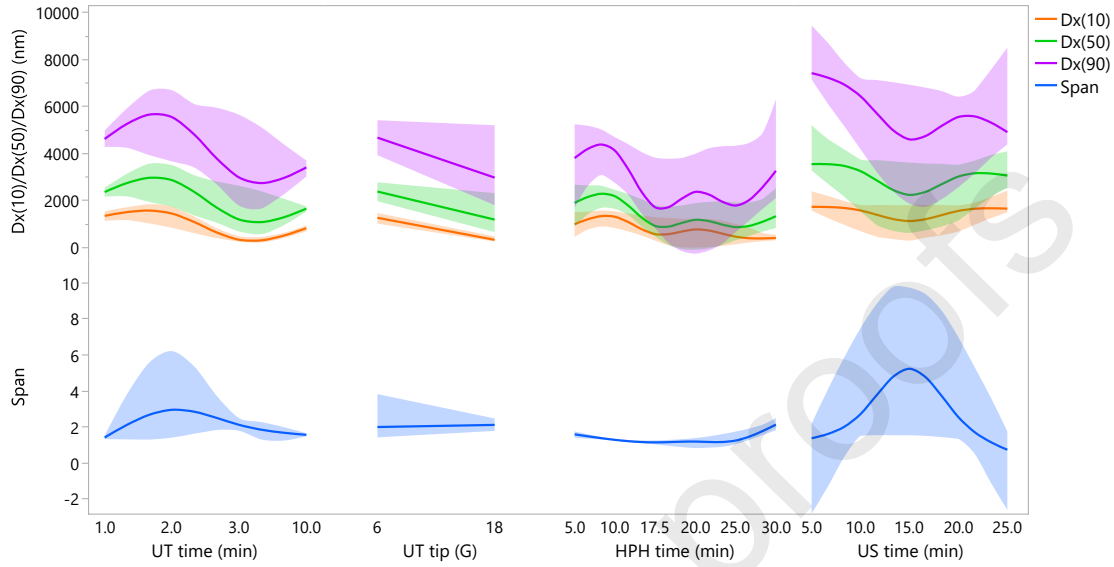

Figure 1 – Dx(10), Dx(50), Dx(90) and Span as function of UT time, UT dispersing shaft size, HPH time and US time.

The first step in the production of nanocrystal suspensions was the pre-mixing of the coarse drug with the dispersion medium, containing the stabilizing system, using a high-speed homogenizer. This procedure is of great importance since when dry powders are first added into a liquid (solid-liquid suspension), clusters can be formed, hampering particle size reduction and clogging the valve homogenizers. The erosion mechanism produced by high shear homogenizers can break up these agglomerates, reducing the starting size material, an important factor for the effective reduction of particle size in the subsequent stage [17, 23, 65].

Considering the pre-mixing settings, at a predetermined homogenization rate (16,000 rpm), variations in particle size were attained at different homogenization times (1.0, 2.0, 3.0 and 10.0 min) (Figure 1). At first glance, an increase in homogenization time produced an efficient particle size reduction to a certain point. Extending the time appears to result in larger particle sizes, possibly due to the formation of agglomerates ascribed to the higher kinetics of the particles generated [66, 67]. The most favorable particle size measurements were achieved at 3.0 min of homogenization time. A significant influence of the dispersing shaft size (8G and 16G) on the particle size distribution was also found. As shown in Figure 1, the lowest values of Dx(10), Dx(50) and Dx(90) were attained with the 18G dispersing shaft, since the breaking mechanism appears to be highly dependent on the input energy. An increase in the shear head size, and therefore in the diameter of the rotor and stator, seems to contribute for improving the bulk mixing since the effectiveness of the deagglomeration process is enhanced by the greater circulation flow and highly localized energy dissipation rate [65, 68]. In what concerns span results, an opposite behavior was observed, suggesting a loss of size uniformity when the 18G dispersing shaft is used.

Regarding nanocrystal production methods, two different approaches were tested entailing high-pressure homogenization (HPH) and ultrasonication (US) techniques. As depicted in Figure 1, the smallest particle size was obtained using the HPH technique. In this methodology, micronized drug particles were subjected to high pressure collisions, cavitation and shear forces, producing an efficient size reduction at the nanometer scale [2, 10, 11, 69]. The results also pointed HPH time as an important factor on particle size reduction and size distribution [16, 46, 70].

Notwithstanding the described effectiveness of the ultrasonic device in particle size reduction, the experimental results demonstrated that the cavitation stress and the oscillation generated by ultrasound waves were not efficient in the deagglomeration mechanism, resulting in a larger particle size [71-73].

Scrutinizing the impact of potential formulation excipients on particle size distribution, it was found how different skin permeation enhancers and stabilizing agents affect the nanosized efficiency (Figure 2). It should be noted that the investigated excipients have an accepted generally recognized as safe (GRAS) designation, being safely applied for topical purposes.

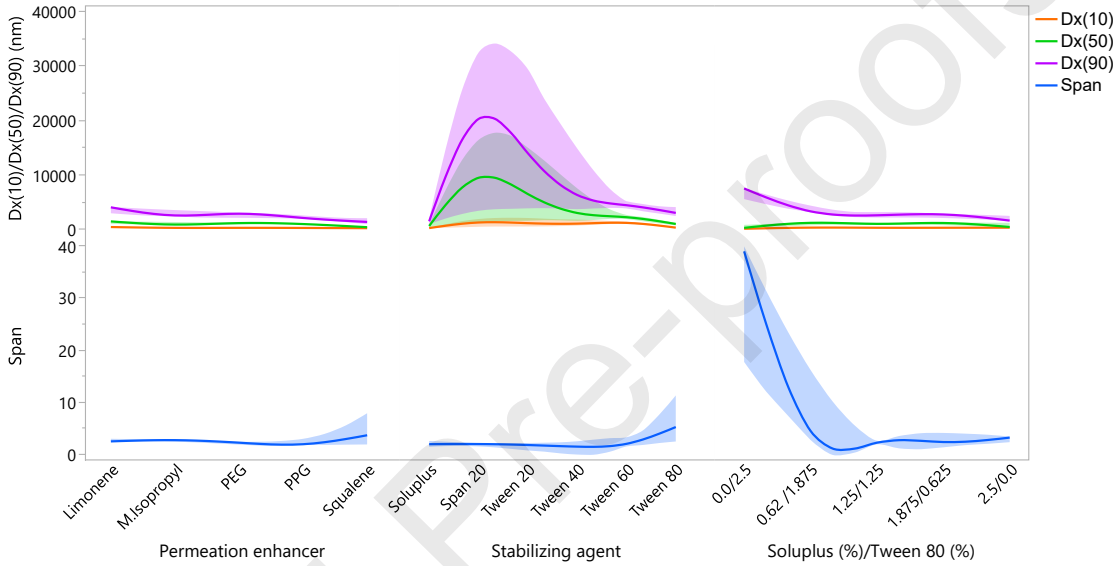

Figure 2 – Dx(10), Dx(50), Dx(90) and Span as a function of different permeation enhancers, stabilizing agents and Soluplus/Tween 80 ratios.

Despite the important advantages of topical and transdermal drug delivery, such administration routes present unique challenges. The greatest hurdle to therapeutic efficacy is the outermost skin layer, the SC. Different approaches have been investigated to overcome this barrier and promote drug transport into and across human skin. In this context, penetration enhancers have been widely used in topical and transdermal formulations due to their effect on the barrier function of the skin and/or on increasing drug solubility in SC [29-31, 74].

Currently, several molecules have been described to promote percutaneous absorption. Thereby, an initial screening of skin permeation enhancers was imperative. Based on well-established use for topical and transdermal application, isopropyl myristate (IPM) [28, 75], polyethylene glycol 400 (PEG 400) [76, 77], propylene glycol (PG) [78, 79], limonene [80, 81] and squalene [82, 83] were screened. As shown in Figure 2, the smallest particle size and narrowest distribution were observed when squalene was incorporated into the formulation. Squalene is a natural acyclic triterpene (polyunsaturated hydrocarbon), widespread in nature and in living organisms, being a precursor in the cholesterol biosynthesis pathway. Squalene is the main component of skin surface polyunsaturated lipids. These molecule presents some advantages as an emollient and antioxidant, as well as contributing to skin hydration. Due to its biocompatibility, non-toxicity, therapeutic effects (e.g., antitumoral) and potential as drug delivery vehicle, squalene has been extensively studied for pharmaceutical applications [84-86]. In the dermatological field, this molecule has been used as penetration enhancer to improve skin permeation of poorly water-soluble drugs by partitioning into the SC and disrupting the structure of the organized lipid bilayer [30, 84, 85, 87].

In addition to permeation enhancer selection, the selection of a suitable stabilizing agent is challenging and a critical step, as influences the size, performance, and stability of the nanosuspension particles [3, 88]. Selecting an appropriate ionic or steric stabilizer at the optimum concentration is essential to prevent aggregation of thermodynamically unstable suspended particles. Indeed, there is no systematic procedure or theoretical guideline for proper stabilizer selection and optimization. Therefore, a preliminary investigation of the stabilizer was conducted considering the well-established use of different stabilizing agents in topical formulations, biocompatibility, nature (i.e., surfactant *vs.* polymer) and hydrophilic-lipophilic balance (HLB). Six stabilizers were screened: span 20 (HLB = 8.6), showing a more lipophilic character, and tween 20 (HLB = 16.7), tween 40 (HLB = 15.6), tween 60 (HLB = 14.9), tween 80 (HLB = 15) and soluplus (HLB = 16), presenting more hydrophilic properties [89].

It has been reported that lipophilic molecules (HBL<10) exhibit a better interaction with hydrophobic particles, producing smaller particle sizes [22, 89-91]. However, as represented in Figure 2, the smallest size was attained with tween 80 and soluplus, hydrophilic stabilizers (HLB>10) [10, 92-94]. Figure 2 also illustrates the changes in particle size obtained with different concentrations of tween 80 and soluplus. It was perceived that polymeric molecules produced suspensions with smaller particle size and more uniform distribution [95]. Tween 80 is a low-molecular weight surfactant (MW=1,310 g/mol) that forms a thin adsorption layer around the surface of the drug particle, offering less effective steric stabilization than high-molecular weight polymers, such as soluplus (MW= 90,000 – 140,000 g/mol) [27, 96]. Soluplus is a non-ionic polyvinyl caprolactam-polyvinyl acetate-polyethylene glycol graft copolymer (57% PLC/30% PVAc/13% PEG 6000), originally developed to stabilize solid dispersions. However, it has been investigated as potential pharmaceutical excipient to stabilize nanosuspensions of poorly water-soluble drugs via steric hindrance.

The production of nanosized drug particles generates high surface energy, which makes them thermodynamically unstable and prone to aggregation and Ostwald ripening. Accordingly, soluplus reduces the surface energy of the drug particles by decreasing the interfacial tension, preventing against instability/separation phenomena and assuring the formation of particles with reduced sizes. Because of its amphiphilic nature, soluplus also increases the solubility and wettability of poorly water-soluble drugs, contributing to more efficient manufacturing, bioavailability and nanosuspension performance [3, 97-100].

Once the nanocrystal production process and the foremost formulation excipients were selected, the important material attributes and process parameters were explored in more detail. Figure 3 depicts the impact of different concentrations of squalene, soluplus and hydrocortisone, HPH time and HPH pressure on drug particle size and size distribution, pointing out critical material attributes (CMAs) and critical process parameter (CPPs) for further optimization.

Taking into account Dx(10) Dx(50), DX(90) and span results, the experimental levels for the squalene concentration were set at 0.75% (low level) and 3.00% (high level) and for soluplus concentration from 1.5% (low level) to 4.5% (high level). In the present study, the impact of soluplus concentration was tested over a wide concentration range, allowing to assess the impact of the stabilizing agent at concentrations below and above its critical micelle concentration (CMC = 7.6 mg/L) [101].

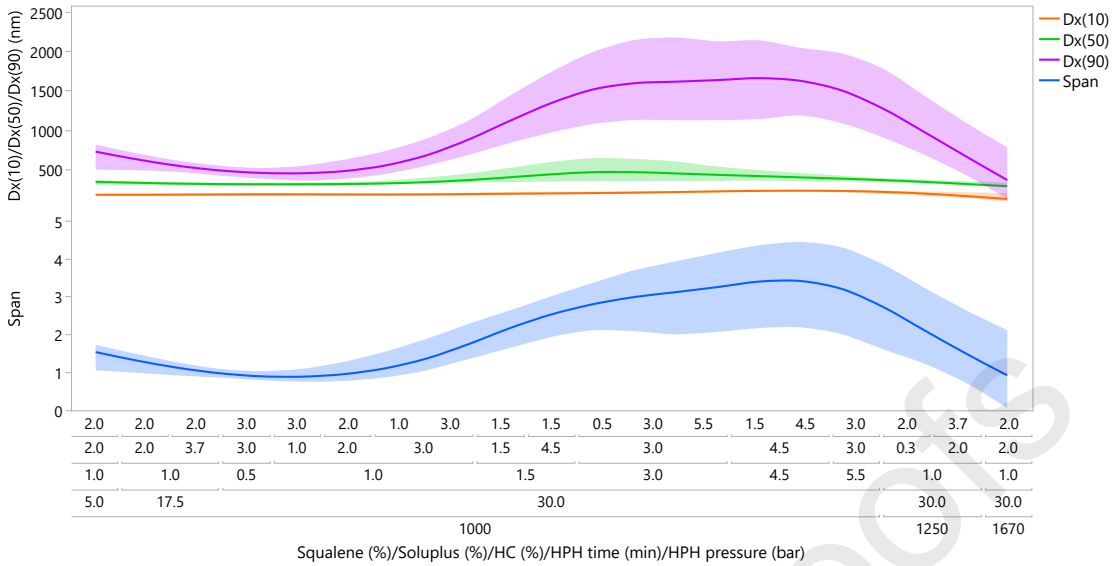

Figure 3 – Dx(10), Dx(50), Dx(90) and Span as a function of Squalene concentration, Soluplus concentration, HPH time, HPH pressure and Hydrocortisone (HC) concentration.

Although HPH pressure is considered to be an important process parameter, Figure 3 shows a slight effect on drug particle size reduction when HPH pressure increased from 1000 to 1650 bar [17, 102]. Considering energy consumption and scalability aspects, 1000 bar was selected as the optimal homogenization pressure for subsequent investigations. In turn, significant differences in particle size were observed when HPH time raised from 5.0 to 30.0 min. As the most impactful process parameter (CPP), the HPH time was studied at experimental levels of 7.5 min (low level) and 22.5 min (high level).

Figure 3 also illustrates how hydrocortisone concentration significantly influenced particle size and size distribution. An increase in hydrocortisone concentration from 0.5 to 5.5%, resulted in suspensions with larger particle sizes and worse homogeneity. At lower drug concentrations, the polymer appears to stabilize the drug particles more efficiently, preventing aggregation [98]. Safeguarding formulation therapeutic efficacy, 1.0% (w/v) of hydrocortisone was considered as the suitable dosage strength to produce nanosuspensions with reduced particle sizes and uniform distribution.

4.3. Initial Risk Assessment

As a valuable science-driven tool, risk assessment assists in identifying, ranking and mitigating variability sources, making an important contribution to a detailed understanding of how formulation and/or process parameters affect product quality expectations. Hence, based on prior knowledge, an initial risk analysis was performed to estimate the risk of each factor variation [36]. As shown in Table 4, a FMECA diagram was constructed to distinguish the most important factors. In such a representation, failure modes, causes and effects were identified. The impact of severity of each failure, along with the probability of occurrence and detectability were also classified [103]. Any failure mode with an RPN score of 18 or greater was classified as critical and eligible for further investigation. Thus, the RPN values pointed permeation enhancer concentration, stabilizing agent concentration and HPH time as the major risk factors, corroborating the preliminary results.

[Insert Table 4 around here]

4.4. Scrutinizing DoE

In addition to conventional strategies to improve topical drug delivery, innovative drug delivery systems have been explored to enhance the therapeutic efficacy of poorly water-soluble active substances, such as corticosteroid molecules. In this context, nanocrystals have emerged as a groundbreaking nanotechnology for dermal application due to their undeniable benefits in terms of drug solubility and bioavailability, skin penetration and toxicity [11, 104].

According to the formulation and manufacturing process, nanocrystals can exhibit significant variability in size, size distribution and solid state, which affects product performance and stability. Thereby, a multivariate optimization strategy was carried out to understand the impact of independent variables on CQAs and to assist in establishing the optimal working conditions to consistently deliver a drug product that meets QTPP specifications. Hence, the most important factors found from the risk analysis were detailed investigated using the rotatable circumscribed central composite design (CCCD). CCCD is an experimental design method extensively used in process optimization studies, establishing a second-order response surface model. The axial points, defined by the α value, differentiate CCD from other designs [40, 105-107]. Depending on where the axial points are located, three types of CCD can be considered: circumscribed CCD, inscribed CCD, and face-centered CCD. In selecting the most suitable CCD, it is important to compare the operability region with the interest region. The different variations of the CCD allow investigating the same region of interest but differ in the levels settings to be tested. The circumscribed CCD and inscribed CCD are rotatable designs, a demanded property for response surface designs. Rotatability refers to the uniformity of the prediction error. In such design, all points are at the same radial distance from the center point and have the same magnitude of prediction error. In the circumscribed CCD, the axial points are located outside the initial region of interest, at a distance α from the center point, given by $\alpha = (2^f)^{1/4}$, where f is the number of factors. The operability region is larger than the initial region of interest. In turn, in the inscribed CCD, the axial points are located at levels -1 and +1, while factorial points are brought into the region of interest, at a distance of $1/\alpha$ from the center point. In both designs, each factor must be tested at five levels coded as $-\alpha$, -1, 0, +1 and α. In the face-centered CCD, the axial points are located on the faces of the region of interest, at a distance $|\alpha| = 1$ from the center point, and factorial points also range at -1 and +1 levels. The operability region must encompass the region of interest. This design requires three levels of each factor coded as -1, 0 and +1 [108-114].

Despite the reduced number of experiments, the relationship between factors and the responses was determined by the least square methodology, where a multiple regression technique fitted a quadratic model to the experimental data [40, 115].

In order to inspect the effect of x_1, x_2 and x_3 terms, and their interactions, on the CQAs, the experimental formulations were characterized for key quality attributes, comprising assay, physicochemical properties (pH, colloidal and solid-state properties), product performance (release and permeation) and physical stability (instability index, separation rate and colloidal properties) as represented in Tables 5-9. An overall analysis of the regression models discloses that the best fits were retrieved from the pH response, followed by drug solid state (X_c), the release outcomes (R_{6h} and R_{24h}) and, ultimately, the stability indicators (instability index at t = 0 days and zeta potential at t = 30 days). Figure 4 represents the observed vs. predicted values for those CQAs that exhibit a better goodness of fit.

Scrutinizing the experimental data, different second-order polynomial models were generated. ANOVA appraisal was also performed for model fit and summarized in supplementary Table S2, revealing the suitability of the selected mathematical model to predict the considered responses. The values of the coefficient and the corresponding significance levels are displayed in the supplementary material Table S3.

An overview pointed out F_{10} as the most promising experimental formulation. Compliant with QTPP specification for topical application, this formulation exhibited the smallest particle

size and narrow size distribution, appropriate surface charge, slight drug amorphization, optimal drug release and permeation performance, and long-term stability.

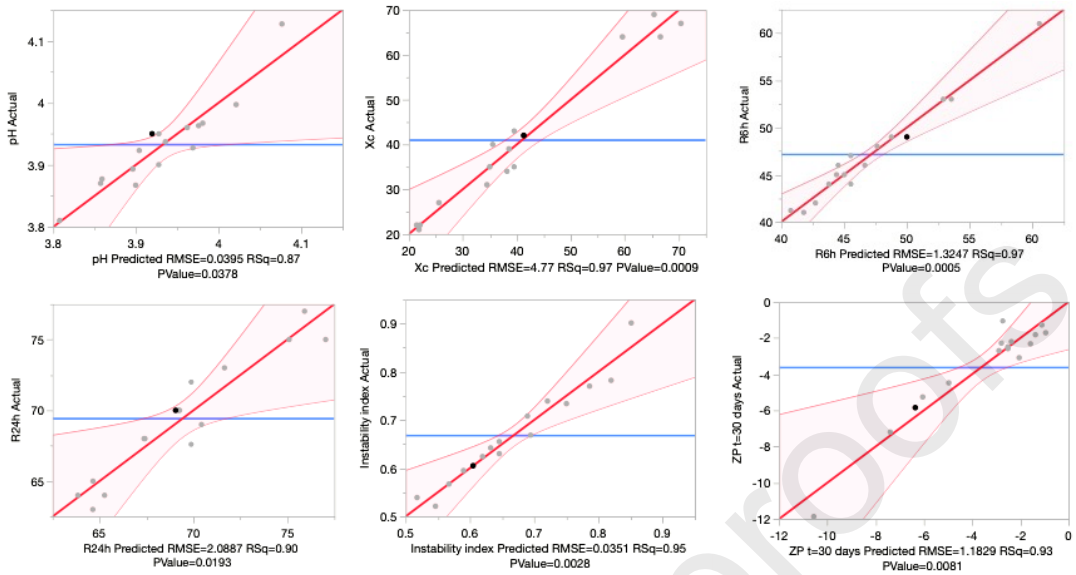

Figure 4 - Actual by predicted plots for the responses (CQAs) presenting a better goodness of fit. The diagonal line corresponds to the Y = X line. For a perfect fit, all the points would be on this diagonal.

[Insert Table 5 around here]

4.5. Assay

Inspecting the effect of formulation and process variables on the assay of experimental formulations, no significant differences ($p > 0.05$) were observed for the considered response, ranging from 59 ± 3 % (F_9) to 77.3 ± 1.7 % (F_{11}) (Table 5). Note that this range reflects the yield of HPH process. As shown in Table S3, the investigated factors had no important impact on the hydrocortisone assay (*Prob*>|*t*| > 0.05).

4.6. Physicochemical Characterization

4.6.1. pH

Assessing the influence of formulation and process variability on the physicochemical properties of the experimental formulations, significant differences ($p < 0.05$) were observed for the pH response. The value of the dependent variable ranged between 3.810 ± 0.014 (F_{14}) and 4.13 ± 0.02 (F_{11}) (Table 5). As displayed in Table S3, squalene concentration (x_1) and soluplus concentration (x_2) were the most critical factors for the pH response (*Prob*>|*t*| < 0.05). The increase in concentration had a negative impact on the considered CQA, resulting in a decrease in pH values. Although the results are slightly lower than the physiological pH of the skin surface (4.5-5.5), acidified formulations appear to offer both preventive and therapeutic benefits, being recommended for the maintenance of key skin functions (e.g., permeability barrier homeostasis, SC integrity and cohesion, and antimicrobial defense) and for the treatment of skin with impaired barrier function [116-118].

4.6.2. Morphological Structure

Regarding the impact of formulation and process variability on the morphological properties of nanocrystals, differences were perceived in the shape and size of hydrocortisone particles. Figure 5 depicts different SEM images of unprocessed hydrocortisone powder, coarse suspension (NC_{HC}) and experimental formulations. SEM micrographs revealed that the unprocessed powder forms clusters of irregular shape without size uniformity. The NC_{HC} formulation exhibited fractured, irregularly shaped particles of various sizes. In contrast, the particles generated by HPH were smaller in size, cuboidal in shape, more regular and uniform. Figure 5 also demonstrates how HPH is an effective downsizing technique, converting the original drug microparticles into the submicron range [119-122].

Depending on the production method, nanosized drug crystals can be produced in amorphous or crystalline state [2]. Even though the high energy input during HPH processing contributes to a more amorphous state of the drug [46], the crystalline nature of hydrocortisone in the experimental formulations is clearly observed through the elongated cobblestone-like structures with smooth surfaces.

Although soluplus contributes for producing more amorphous drug particles [97], the shape of the particles indicate that morphology is independent on the permeation enhancer and stabilizing agent concentrations.

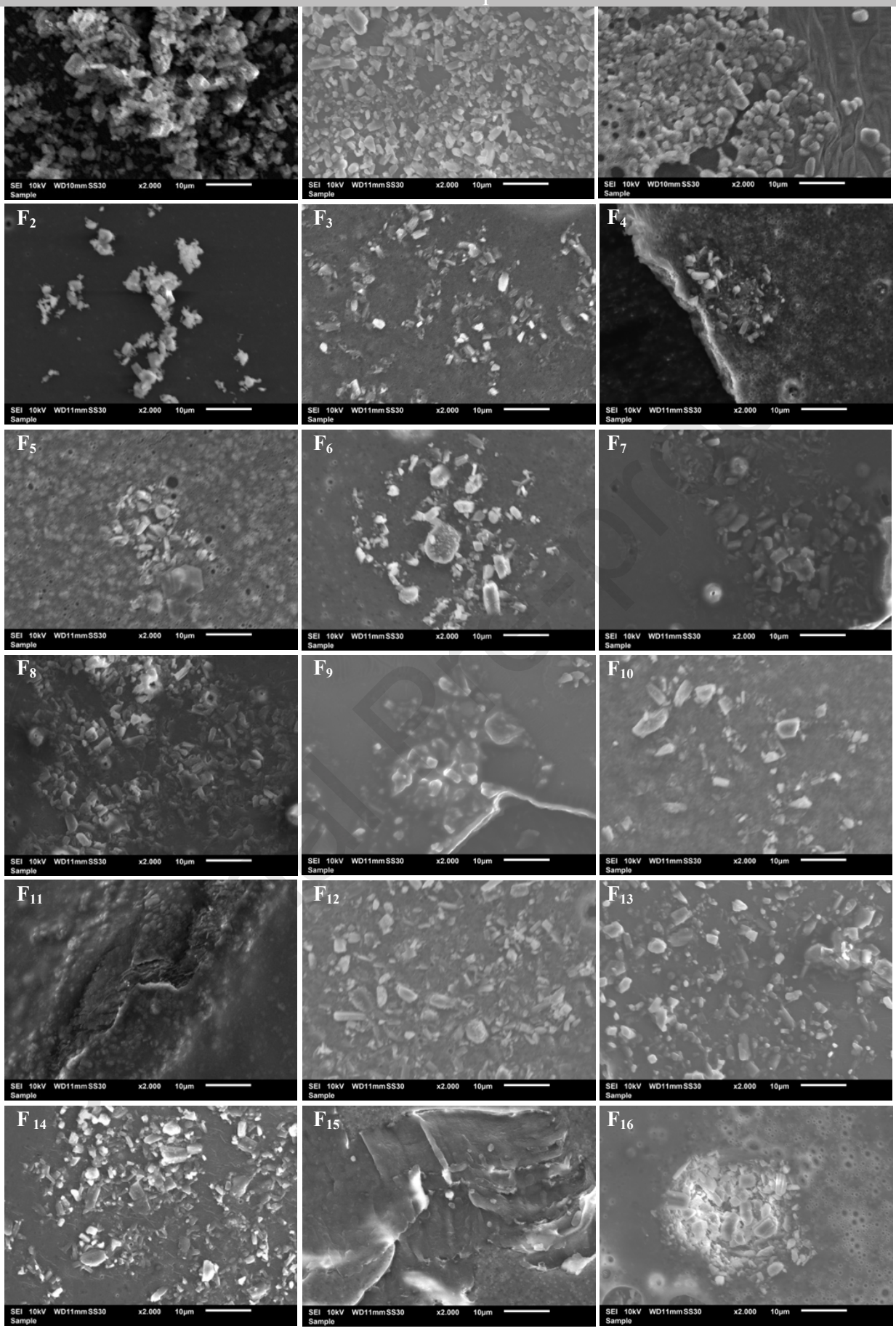
F2
F3
F4
F5
F6
F7
F8
F9
F10
F11
F12
F13
F14
F15
F16
SEI 10kV WD11mm SS30 x2.000 10μm
Sample

\

Figure 5 – SEM micrographs of unprocessed hydrocortisone powder (HC), negative control (N_{HC}) and experimental formulations (F_1-F_{16}).

4.6.3. Colloidal Poperties

Considering the effect of formulation and process variability on nanocrystal particle size and size distribution, significant differences ($p < 0.05$) were observed on Dx(10), Dx(50), Dx(90), span, $d_{3;2}$ and $d_{4;3}$ results, ranging from nanometer to micrometer. As displayed in Table 5, the Dx(50) response ranged between 174 ± 5 nm (F_{15}) and 3,282 ± 255 nm (F_3) and the span value between 1.48 ± 0.05 (F_{11}) and 21.4 ± 1.0 (F_{13}). Dx(10) varied from 28.9 ± 0.5 nm (F_2) and 1,289 ± 31 nm (F_{11}) and Dx(90) from 732 ± 49 nm (F_{10}) and 11,094 ± 175 nm (F_{13}).

As represented in Table S3, HPH time (x_3) was the most impactful factor for the Dx(50) response ($Prob>|t| < 0.05$) with increasing levels of x_3 producing smaller particle sizes. In the HPH technique, the coarse suspension is forced through a valve under high pressure. A longer homogenization process is more efficient in the breaking of agglomerates, resulting in reduced particle sizes and narrow size distribution.

The magnitude and negative value of the coefficient revealed the positive impact of squalene concentration (x_1) on the downsizing process. In light of current knowledge, the use of squalene as a excipient in nanocrystal formulations has not yet been described. Due to its high percutaneous enhancement abilities and skin compatibility, this molecule has been widely used to formulate nanostructured lipid carriers (NLCs) and oil-in-water (o/w) emulsions for topical application, with nanosized range and uniform size distribution. However, the mechanism by which squalene produces smaller particle/droplet sizes has not been elucidated [82, 83, 123].

In what concerns soluplus concentration (x_2), the reduction in particle size did not appear to be directly proportional to the stabilizer concentration. Increasing the polymer concentration had a negative impact on particle size, resulting in high values of Dx(50). There is an optimum level of polymer concentration which results in a decrease in the contact angle between the drug molecules and the aqueous phase, leading to the formation of smaller particles and, consequently, an increase in the surface area. Below the CMC, monomers bind to the nanocrystal surface with high affinity, but at concentrations above the CMC, micelles will be formed. The micelles begin to compete for surface adsorption so that the total adsorption at the interface begins to decrease as the micelles become more numerous. Therefore, a stabilizer concentration higher than the CMC could actually result in less surfactant adsorption, which would further destabilize the nanosuspensions and thereby contributed to increased particle size [102, 124].

The investigated variables had no significant influence on span response. This CQA relies on Dx(10), Dx(50) and Dx(90) results. A narrow size distribution was obtained for experimental formulations with a size range both the nanometer (F_{10}) and micrometer (F_{11}) ranges.

As shown in Table 5, $d_{3;2}$ and $d_{4;3}$ fluctuating from 86.3 ± 0.9 nm (F_{15}) to 2,182 ± 39 nm (F_{11}) and from 903 ± 74 nm (F_{10}) to 6,608 ±124 nm (F_3), respectively. The Sauter Mean Dimeter and the Brouckere Mean Diameter are important indicators of the particle size distribution. If the aim is to monitor the size of the coarse particles, then $d_{4,3}$ is considered. In turn, if it is more important to monitor the proportion of fine particles, then the use the $d_{3,2}$ is more appropriate [55]. Usually, $d_{3,2}$ describes the average ratio between volume and surface area. At a constant volume, the greater the surface area, the lower the value of $d_{3,2}$. In comparison, $d_{4,3}$ is more susceptible to large particles. The difference between $d_{3,2}$ and $d_{4,3}$ decreases with increasing particle size uniformity. $d_{3,2}$ and $d_{4,3}$ will be identical only for a completely monodisperse distribution [125]. The experimental formulations that showed high span results and, therefore, a more polydisperse distribution, also exhibited significant differences between $d_{3,2}$ and $d_{4,3}$ values.

Inspecting the goodness of fit, important fluctuations were observed in the fit quality indicators with the residual term ranging from 0.7 ± 0.3 % (F_{10}) to 3.62 ± 0.32 % (F_1) and the weighted residual varying from 0.27 ± 0.07 % (F_{11}) to 1.31 ± 0.05 % (F_{10}) (Table 5). A general trend was observed for formulations with polydisperse distributions towards the highest residual and

weighted residual values, exceeding, in some cases, the recommended 2%. The best fits/data quality were observed for the formulations with lower span values. The residual is the difference between the predicted value, based on the regression equation, and the observed value [126]. In this context, high residual values do not mean an incorrect analysis (e.g., incorrect selection of the refractive index or absorption index for the sample and dispersant, wrong selection of the calculation model or too high obscuration) or data quality problems, but rather that there is some unexplained variations by the fitted model [127], probably due to their dependence on particle size distribution. The lowest values for both fit indicators were found for F_{11}. A good fit was found for the experimental formulations that present the largest particle size and narrow size distribution.

Monitoring the effect of formulation and process variability on nanocrystal surface properties, no significant differences ($p > 0.05$) were observed for ZP response, fluctuating between -12.3 ± 0.4 mV (F_1) and -2.19 ± 0.2 mV (F_8) (Table 5). The ZP measurement in the original dispersion medium is an indirect measure of the thickness of the diffuse layer and is used to predict long-term stability [128]. In general, an absolute ZP value above 30 mV provides good stability. A ZP around 20 mV provides only short-term stability. ZP values in the range -5 mV to +5 mV undergo pronounced aggregation. This is valid for low-molecular weight surfactants and pure electric stabilization, but not for high-molecular weight stabilizers, which act mainly by steric stabilization. In this case, a ZP value of only 20 mV or even less can provide an appropriate stabilization [17, 128, 129]. Experimental formulations exhibited lower ZP values, between -12 and 0 mV, indicating that nanocrystals were neutral in nature and sterically stabilized [17, 130-132]. Electrostatic stabilization was discarded [129, 130].These results suggest that experimental formulations will not be physically long-term stable if they present a thin layer of sterically stabilizing soluplus on the particle surface [128]. As displayed in Table S3, soluplus concentration (x_2) was the most critical variable to the ZP response ($Prob>|t| < 0.05$). As the polymer concentration increased, the surface charge became less negative. This decrease may be attributed to a reduction in the free energy of the system due to the interaction between the hydrophobic functionalities of soluplus and the drug particles. ZP values close to zero suggest a complete coverage of hydrocortisone nanocrystals by soluplus molecules, a ZP dependence on the type and concentration of the stabilizing agent and predict a moderate long-term stability of experimental formulations [120, 128].

4.7. Thermal and Solid-state Properties

4.7.1. Differential Scanning Calorimetry, and Thermogravimetric Analysis

To determine physical reaction patterns in response to increasing temperature, pure compounds were analyzed by DSC. As displayed in Figure 6, unprocessed hydrocortisone was characterized by a single, sharp melting endothermic event at 225.4 °C, consistent with the melting point of pure drug [121]. The thermogram of soluplus revealed a broad endothermic peak around 64 °C, consistent with the glass transition temperature (*Tg)*, i.e., molecules in glassy state gain mobility [97, 132, 133]. The TGA curve of squalene (Figure 7) revealed compound stability until 110 °C, above this temperature, a complete degradation was observed [134]. Thermograms of the NC_{HC} and the formulations were not analyzed since the thermal degradation of squalene hinders the detection of hydrocortisone melting temperature.

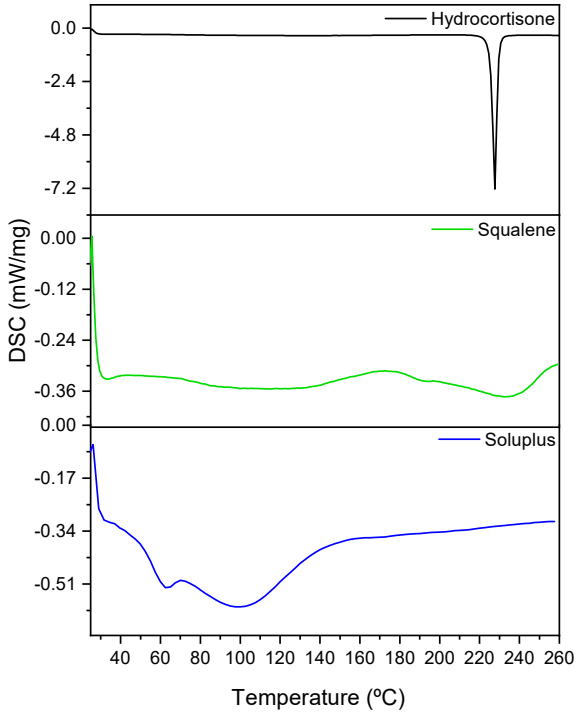

Figure 6 –DSC thermograms of the pure compounds: unprocessed hydrocortisone, squalene and soluplus.

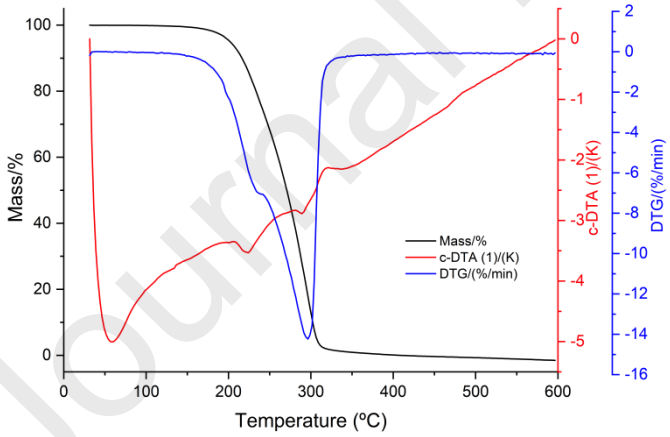

Figure 7 –TGA curves of squalene component.

4.7.2. Attenuated Total Reflectance Fourier Transform Infrared

Inspecting the occurrence of interactions between hydrocortisone and formulation excipients at a molecular level, pure compounds (Figure 8A), coarse suspension (NC_{HC}) and experimental formulations (Figure8B and 8C) were analyzed by ATR-FTIR. The FTIR spectrum provides identification of the different functional groups and can detect the presence of newly formed hydrogen bonds [121, 135].

The FTIR spectrum of unprocessed hydrocortisone (Figure 8A) showed three intense and well-defined absorption bands at 3415 cm^{-1} (O-H stretching), 2913 cm^{-1} (C-H stretching), 1706 and 1641 cm^{-1} (C=O stretching) [121].

The squalene spectrum (Figure 8A) presented three intense C–H stretching bands at 2966 cm^{-1} (antisymmetric CH_3 stretching), 2917 cm^{-1} (antisymmetric CH_2 stretching and 2853 cm^{-1} (symmetric CH_2 stretching). Vibrational bands at 1443 cm^{-1} (CH_2 scissor stretch), 1376 cm^{-1} ($C(CH_3)$ symmetric stretching) and 835 cm^{-1} (C-H waging of trialkyl alkene function) were also noticeable. The low intensity band at 1668 cm^{-1} (C=C stretching) was also of analytical importance [136-138].

The soluplus spectrum (Figure 8A) exhibited a broad peak at 3471 cm^{-1} (O-H stretching). A vibrational band at 2923 cm^{-1} (C-H stretching) appeared prominent. Characteristic bands at 1731 cm^{-1} and 1625 cm^{-1} (C=O stretching), and at 1477 cm^{-1} (C-O-C stretching) were also observed [135].

For the experimental formulations samples (Figure 8B and 8C), no significant spectral shift was observed. All samples exhibited similar behavior, with characteristic bands in the stretching vibration of O-H, C-H, C=O, C-O-C and C=C groups. However, there is a general trend towards a decrease in the peak intensity corresponding to the O-H and C=O stretches. This effect can be attributed to the possible interaction, at the molecular level, between the hydroxyl and the carbonyl functional groups of hydrocortisone and carbonyl, hydroxyl and ether functional groups of soluplus, capable of establishing hydrogen bonds. Furthermore, there was no addition of new peaks or the absence of any existing peak in the experimental formulations spectra, suggesting that there were no intermolecular interactions between the raw materials selected for the production of nanocrystals [135].

Figure 8 - ATR-FTIR spectra of (A) pure compounds and the different experimental formulations: (B) F_1-F_8 and (C) F_9-F_{16}.

Examining the impact of formulation and process variability on the hydrocortisone crystallinity, significant differences ($p < 0.05$) were attained for the relative area percentage (%) response, varying from 4.29 % (F_9) to 22.19 % (F_1) (Table 6).

Fourier self-deconvolution is a mathematical resolution enhancement method by which the spectrum is split by the instrumental function to reverse signal distortion in the Fourier domain. The method provides a way of computationally resolving multicomponent band, that cannot be instrumentally resolved. Hence, it separates and sharpens the overlapping hidden peaks [139, 140]. In the infrared spectra, the deconvolution of the band corresponding to the O-H stretching was performed, allowing to identify different formulation components. The relative concentration of each component was calculated from the area under the deconvoluted peaks hidden in the original spectrum. The small shoulder identified around 3265 cm^{-1} seemed to be significantly influenced by hydrocortisone concentration. Therefore, the relative amount of such a component was determined by the relative area % of the corresponding deconvoluted peak. In this context, the 3265 cm^{-1} band provided a near concentration of hydrocortisone in the formulation, influenced by soluplus and squalene concentration represented in the additional deconvoluted peaks.

As presented in Table S3, soluplus concentration (x_2) assumed a relevant importance for the response in an antagonistic way ($Prob>|t| < 0.05$). At high levels of surfactant concentration, the drug-stabilizer interaction (hydrogen bonding) significantly influenced the characteristics of the hydrocortisone deconvoluted band by reducing its intensity and therefore, the relative area % values.

[Insert Table 6 around here]

4.7.3. X-Ray Powder Diffraction

In what pertains the effect of formulation and process variability on the hydrocortisone crystallinity, meaningful differences ($p < 0.05$) were observed for the relative crystallinity (Xc) response, ranging from 21 % (F_{14}) to 69 % (F_1) (Table 6).

As shown in Figure 9A, the diffractogram of the unprocessed hydrocortisone exhibited intense and sharp peaks at 14.5°, 16.1° and 17.4°, confirming the crystalline nature of the drug [121]. Characteristic peaks of hydrocortisone were observed for the experimental formulations (Figure 9B and 9C), although with a slight decrease in intensity, suggesting that formulation components and manufacturing process may influence drug crystallinity towards a more amorphous solid state [24]. Closer inspection of the X-ray patterns indicated the existence of the polymorphic form I of hydrocortisone, the most thermodynamically stable form [141, 142].

As displayed in Table S3, squalene concentration (x_1) and soluplus concentration (x_2) were the most important factors for the considered response ($Prob>|t| < 0.05$). Crystallinity appeared to be negatively influenced by x_1 and x_2 with increasing squalene and soluplus concentrations contributing to hydrocortisone amorphization, with diffractograms showing lower Xc values [97, 120]. Compared to the crystalline state, the amorphous form displays random position of drug molecules and presents differences in physical properties, including solubility [96]. Although the decrease in drug crystallinity has been described for the HPH technique, data analysis suggests that the HPH time did not significantly interfere with the crystalline state of hydrocortisone.

(A)

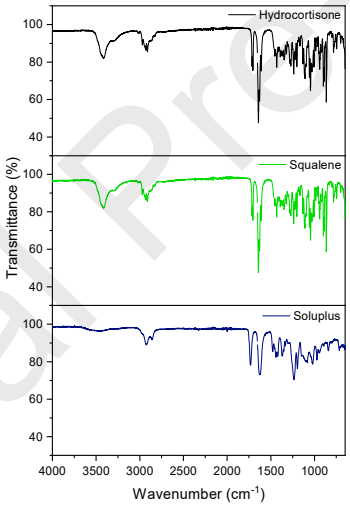

(B)

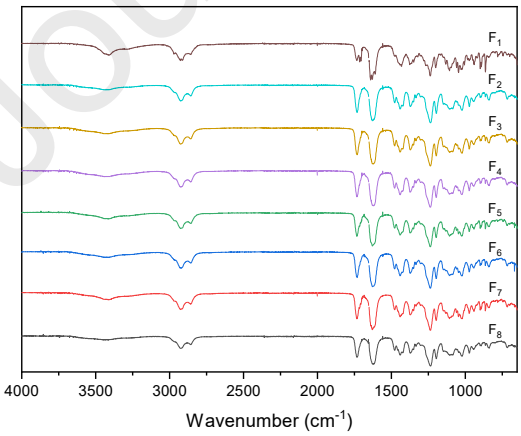

(C)

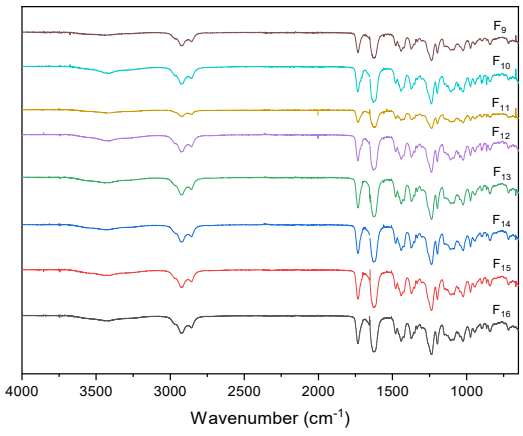

Figure 9 – X-ray powder diffractogram of (A) unprocessed hydrocortisone and the different experimental formulations: (B) F_1-F_8 and (C) F_9 - F_{16}.

4.8. Product Performance

4.8.1. *In Vitro* Release Testing

Assessing the impact of formulation and process variability on the release behavior of experimental formulations, important differences ($p < 0.05$) were observed for the pondered responses. The *in vitro* release rate (IVRR) of hydrocortisone fluctuated between 316 ± 21 μg/cm²/√t (F_8) and 516 ± 37 μg/cm²/√t (F_1), and the cumulative percentage (%) of hydrocortisone released at 6 h (R_{6h}) and 24 h (R_{24h}) ranged from 41 ± 5 % (F_{13}) to 61 ± 3 % (F_1) and from 63 ± 8 % (F_8) to 77 ± 5 % (F_9), respectively (Table 7).

[Insert Table 7 around here]

As represented in Figure 10A-10D, in the release profiles of experimental formulations, a burst release is observed with about 20% of hydrocortisone released in 2 h. A slower release rate is evidenced in the first 6 h, followed by a greater extent of drug released in 24 h. The biphasic pattern shows that the experimental formulations allow a sustained release of hydrocortisone. For dermal application, sustained drug release is extremely useful to improve drug penetration, as drug is available over a prolonged period of time [82].

A comparative release study was carried out to assess the improvement of hydrocortisone release from nanocrystal-based formulations compared to NC_{HC} and commercialized formulations (Figure 10E and supplementary material Table S1). The experimental formulations exhibited a drug released around 60-80% at the end of the experiment (24 h). In turn, the coarse suspension (NC_{HC}) released about 25% of the drug at the same time. Surprisingly, the experimental formulations presented better release performance than the marketed formulations. This finding corroborates the added value of the nanosizing approach to improve the physicochemical properties of poorly-water soluble drugs, in particular their solubility and dissolution.

The cumulative percentage of hydrocortisone released confirms the readability of nanocrystals as efficient drug vehicles for topical application, as it ensures an appropriate drug bioavailability for skin uptake. The nanometer scale produces a substantial increase in surface area, resulting in higher saturation solubility and faster dissolution rate [2, 23]. Increased saturation solubility helps to maintain the concentration gradient between the suspension of drug nanocrystals and the target cells. This effect aids to keep the prolonged and continuous drug release from the nanocrystals, acting as a reservoir that provides a fast replacement of diffused molecules through a fast-continuing dissolution from the large nanocrystal surface [6, 15].

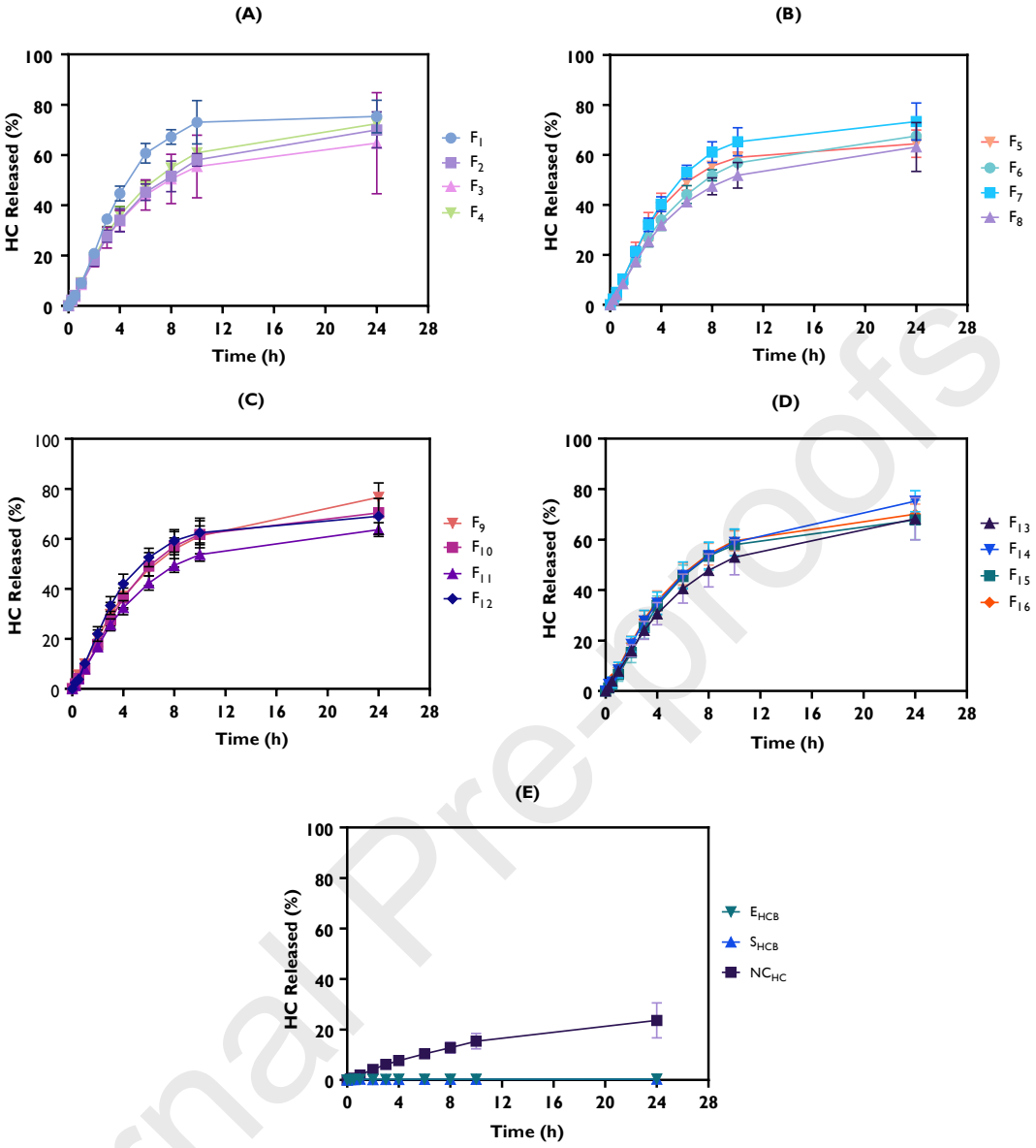

Figure 10 – *In vitro* release profiles of hydrocortisone (HC) from the different experimental formulations: (A) F_1-F_4, (B) F_5-F_8, (C) F_9-F_{12}, (D) F_{13}-F_{16} and (E) Negative control (NC_{HC}) and Commercialized formulations (S_{HC} and E_{HCB}).

As displayed in Table S3, squalene concentration (x_1) induced an important positive effect on the R_{24h} response ($Prob>|t| < 0.05$). During the manufacturing of experimental formulations, squalene appeared to contribute for hydrocortisone powder wettability, producing nanocrystals at the nanometer scale more efficiently, with greater solubility and bioavailability. Soluplus concentration (x_2) was found to have a significant antagonistic effect on IVRR and R_{6h} responses. An increasing concentration of soluplus seemed to hamper the release of hydrocortisone from nanocrystals during the first 6 h. Soluplus is an amphiphilic polymer that may contribute to a slower dissolution rate due to its own slow dissolution rate. At high levels of x_2, hydrocortisone exhibited slower release rate probably due to the increased medium viscosity [5, 135]. Furthermore, soluplus presents a bifunctional character: a matrix polymer for solid dispersions and an active solubilizer through the formation of polymeric micelles in aqueous medium. In the present study, soluplus seems to form polymeric micelles, where a controlled release probably takes place. Drug

release from micelles is an out-diffusion process through the core-shell structure. A higher soluplus concentration leads to greater polymer-drug interaction in the micellar structures, resulting in slower release kinetics. A lower soluplus concentration induces a weaker polymer-drug interaction, generating a greater driving force for drug release [97, 135, 143, 144].

Despite not presenting a significant impact on the R_{24h} response, the positive sign of the β_2 coefficient (Table S3) highlights the effect of soluplus concentration on the continuous release of hydrocortisone from the experimental formulations. Literature reports that soluplus increases oral bioavailability and absorption, because of its contribution to a smaller particle size and greater drug wettability [122, 131, 132, 145].

Regarding the release behavior of the experimental formulations, x_{23} was the most decisive interaction term, exerting a positive effect on the R_{6h} and R_{24h} responses (Table S3 and Figure 11) due to the fundamental role of stabilizing agent concentration and input energy in the production of drug nanocrystals with small and stable particle size. As previously reported, high levels of x_2 and x_3 seem to contribute for reducing drug crystallinity and particle size, respectively, playing a key role in governing the physicochemical properties of hydrocortisone, with amorphous forms and smaller sizes presenting greater solubility and, consequently, higher dissolution rate and bioavailability [132].

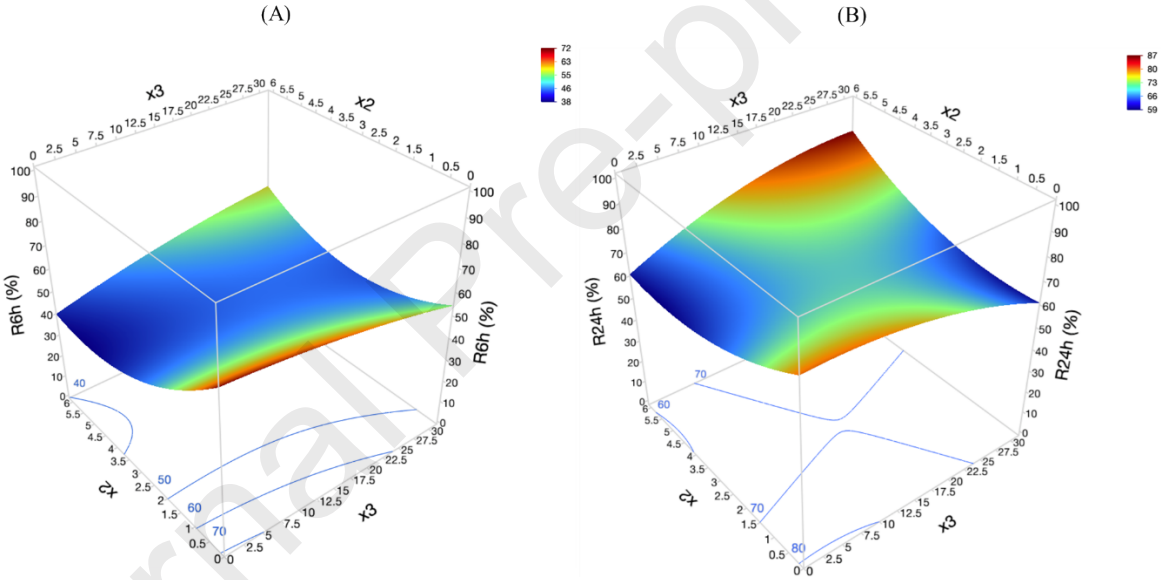

Figure 11 – Response surface plots showing the effect of soluplus concentration and HPH time on: (A) R_{6h} response and (B) R_{24h} response.

Mathematical modeling is useful to establish a prediction of *in vivo* drug release for better understanding of release kinetics and drug release pattern. Indeed, the use of *in vitro* drug release models to predict *in vivo* performance can be considered part of the rational development of new products with time and cost savings [146]. Therefore, to provide a comprehensive analysis of the mechanism underlying drug release kinetics from the experimental formulations, different mathematical models were fitted to the release profiles. The estimated parameters for each model, along with the goodness of fits, are represented in supplementary material Table S4. According to statistical criteria, the Weibull function was considered the best model for describing the release mechanism of hydrocortisone from experimental formulations (Table S4). In the Weibull model [$F = F_{max}.(1\text{-}e^{t^{\beta}/\alpha})$], F is the fraction (%) of drug released in time t, F_{max} represents the maximum fraction of the drug released at infinite time, α is the time scale parameter and β is the shape parameter of the dissolution/release curve, either exponential (β=1), sigmoidal (β>1) or

parabolic (β<1). In addition, the β parameter also describes the release mechanism of a drug molecule through a polymeric matrix [146-148]. Depending on β values, different circumstances can be considered: (i) $\beta \leq 0.75$ - Fickian diffusion mechanism (Case I transport), (ii) $0.75 < \beta < 1$ - Anomalous transport (Fickian diffusion and Case II transport), frequently observed in release studies, (iii) $\beta = 1$ - First-order kinetics (Case II transport) and (iv) $\beta > 1$ - a complex mechanism governs the release process. Higher values of β indicate that the release rate initially increases nonlinearly up to the inflection point and then decreases asymptotically [149]. The experimental results acquired for the β parameter were in the range of 1.023 (F_9) and 1.403 (F_1) (Table S4), indicating a sigmoidal release curve, with an upward curvature (abrupt increase in the initial drug release/burst effect) followed by a turning point (Figure 10A-10D), and a drug transport governed by a complex release mechanism. The Weibull function is a mathematical model that fits a greater number of points (release zone and final stabilization zone) [150]. In fact, when the drug release mechanism follows a pure Fickian diffusion, the Weibull model successfully describes the entire release profile [149]. However, as an empirical model, with no kinetic fundament, this model may not adequately characterize the release kinetics. Indeed, Weibull function is of limited use for establishing *in vitro*/*in vivo* correlation. For a better understanding of the release mechanism, an integrated analysis, with different kinetic models or experiments, is required [151, 152].

In order to provide additional information on the mechanism of hydrocortisone release, the Korsmeyer–Peppas fitting ($F = k_{KP}.t^n$) was also analyzed, where F is the fraction of active compound released until time t, k_{KP} is the Korsmeyer-Peppas constant which incorporates structural and geometric characteristic of the release form (sphere, film, cylinder) and n is the release exponent (diffusional), a parameter that defines the release mechanism [146]. As per the n values, four scenarios can be possible: n close to 0.5 - Fickian diffusion mechanism (Case I transport), (ii) $0.5 < n < 1.0$ - or Anomalous transport (combined mechanism of Fickian diffusion and Case II transport), (iii) $n = 1{,}0$ - Zero-order model (Case II transport), and finally (iv) $n > 1.0$ - Super case II transport. In Case I transport, solvent diffusion is much greater than the polymeric relaxation process. In the three classes of non-Fickian diffusion (Case II, Anomalous Case and Super Case II transport), the main difference is the solvent diffusion velocity. In Anomalous transport, the velocity of solvent diffusion and polymeric relaxation present similar magnitudes (diffusion- and relaxation-controlled release mechanism). In Case II, the solvent diffusion velocity is lower than the polymeric relaxation process (relaxation-controlled release mechanism). However, in Super Case II, the higher solvent diffusion velocity produces an acceleration of solvent penetration and, thus, a drug release controlled by stress-induced relaxations (erosion/relaxation-controlled release mechanism) [150, 152, 153]. This semi-empirical model is a useful tool to in-depth knowledge of the phenomena involved in drug release from a matrix system [152].

The n values of the experimental formulations ranged from 0.667 (F_5) to 0.963 (F_1) (Table S4). The main release mechanism that described the experimental results was the anomalous transport. These results may be related to the XRD results, with the high degree of crystallinity (lower surfactant concentration) contributing to hinder drug diffusion [151]. Nanocrystals are not considered polymeric matrix systems but rather micellar-like structures, whose drug release mechanism can be governed by relaxation of the soluplus polymeric network, which surrounds drug molecules, and by drug diffusion.

The exponent β of the Weibull model is linearly related to the release exponent (n) of the power law (Korsmeyer-Peppas) [149]. Regarding the nanocrystals release mechanism, β values describe a complex transport mechanism, while n results denote a prevalence of Anomalous transport. The non-agreement between the models can be attributed to the fact that the Korsmeyer-Peppas model only describes the first 60% of the release profile where a first Fickian diffusion took place, followed by a Case II transport [154].

As previously mentioned, the Weibull and Korsmeyer-Peppas functions are mathematical models suitable for comparing the release profiles of matrix systems. Although nanocrystals are

not polymeric in nature, these functions were fitted to the experimental release profiles for a better elucidation of the nanocrystals release mechanism.

Note that NC_{HC} formulation followed a first order kinetics [$F_{max}.(1-e^{k_1.t})$] (Table S4), corroborating how the downsizing process significantly influences drug release behavior.

4.8.2. *In Vitro* Permeation Testing

Regarding the impact of formulation and process variability on the permeation profile of experimental formulations, no significant differences ($p > 0.05$) were observed for the pondered responses. The flux (J_{ss}), determined from the slope of the resulting linear plot, alternated between 0.16 ± 0.02 μg/cm²/h (F_8) to 1.2 ± 0.5 μg/cm²/h (F_{11}). K_p varied from 4.84x10^{-05} cm/h (F_8) to 31.4x10^{-05} cm/h (F_{11}). The cumulative amount of hydrocortisone permeated across split skin ranged from 0.44 ± 0.06 μg/cm² (F_8) to 6 ± 7 μg/cm² (F_2) at 6 h (Q_{6h}), from 2.0 ± 0.2 μg/cm² (F_8) to 22 ± 7 μg/cm² (F_{11}) at 24 h (Q_{24h}) and from 6.9 ± 1.0 μg/cm² (F_8) to 61 ± 17 μg/cm² (F_{11}) at 48 h (Q_{48h}) (Table 8).

[Insert Table 8 around here]

As shown in Figure 12A-12D, the permeation profiles evidenced an increase in permeated hydrocortisone over time, with slight differences among the experimental formulations. In what concerns J_{ss}, K_p, Q_{24h} and Q_{48h} responses, F_{11} was statistically different from the remaining formulations.

A comparative permeation study was also performed to assess the enhancement in hydrocortisone permeation from nanocrystal-based formulations compared to NC_{HC} and marketed formulations (Figure 12E and supplementary material Table S1). The experimental formulations and showed better performance than the coarse suspension (NC_{HC}) and commercialized formulations.

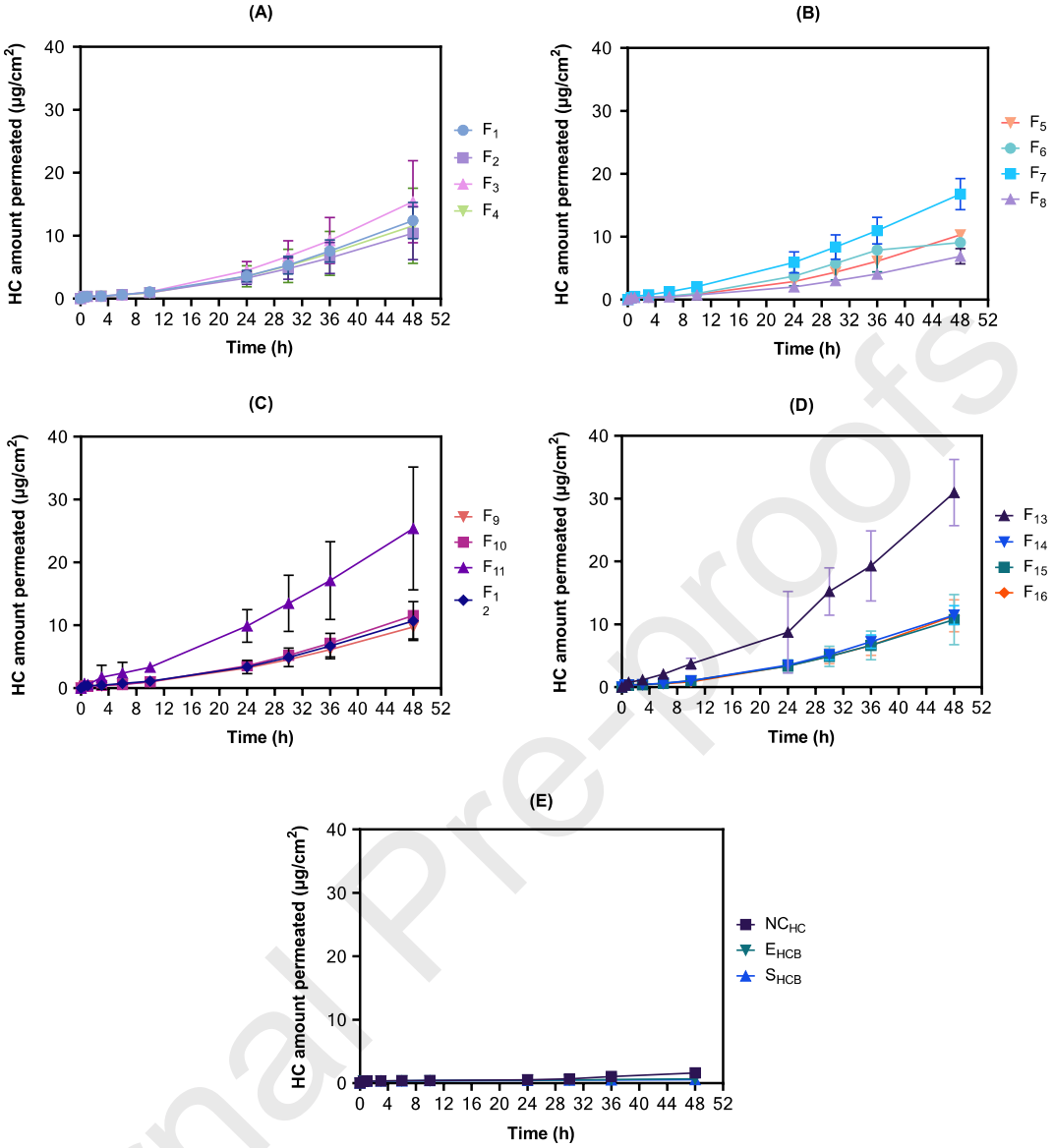

Figure 12 – *In vitro* permeation profiles of hydrocortisone (HC) nanosuspensions and according to independent variables: (A) F_1-F_4, (B) F_5-F_8, (C) F_9-F_{12}, (D) F_{13}-F_{16} and (E) Negative control (NC_{HC}) and Commercialized formulations (S_{HC} and E_{HCB}).

As displayed in Table S3, the regression models did not point out any factor that significantly impacted the permeation results. Indeed, hydrocortisone nanocrystals presented an erratic permeation behavior with unpredictable effects of independent variables on pondered responses.

According to Fick`s first law of diffusion, the steady-state flux, J_{ss}, directly depends on the drug concentration in the vehicle (C_0) and on the drug permeability coefficient (K_p). K_p is given by the product of the diffusion coefficient of the drug in the *SC* (D) by the partition coefficient of the drug between the vehicle and the skin (P), divided by the diffusion path (h) [155, 156].

In the experimental formulations, C_0 was kept constant. Therefore, superior values of K_p and J_{ss} may be attributed to the formulation effect on hydrocortisone D and P values. The main goal of the design and development of a nanocrystal-based formulation was to improve the bioavailability of hydrocortisone, as well as its permeation through the skin. Therefore, a critical

selection of formulation composition was carried out. In addition to the permeation enhancer, a stabilizing agent was carefully selected. This excipient appears to serve a dual purpose of improving formulation stability and performance by increasing hydrocortisone permeation flux. As a permeation enhancer, squalene acts by partitioning into the SC and disrupting the highly ordered structure of the SC lipid bilayer, causing its fluidization and then, greater permeant diffusion coefficient (*D*). Once inserted into the intercellular SC lipid bilayers, squalene may also change their solubility and thereby increase partition coefficient of the drug in the SC (*P*). Consequently, there is an increase in the steady-state flux (J_{ss}) of the drug through the skin [30, 74]. Although not reported in the literature, due to the lipophilic nature of squalene, increasing concentrations of this excipient in the formulation may contribute to occlusive effects, promoting skin hydration and thus drug permeation [10]. In fact, high levels of x_1 negatively affected the permeation outcomes. This finding is not in agreement with the expected results since squalene was selected to enhance skin permeation. In the absence of squalene (F_{11}), a significant improvement in drug transport across the skin was attained, highlighting the effect of soluplus as a permeation enhancer. As a drug delivery vehicle, soluplus has been reported to enhance ocular and oral absorption of different BCS class II drugs, but no evidence was found to enhance skin permeation [97, 131, 145, 157]. The general contribution of x_3 in reducing particle size to the nanometer range may produce important changes in drug physicochemical properties, particularly in the saturation solubility, leading to an increase in the concentration gradient and, consequently, to increased drug penetration into the skin [11]. The enhanced surface area also helps to intensify the interaction among drug nanocrystals and surface/cells membrane and thus, the adhesive properties [2]. By prolonging the residence time of nanocrystals on the skin surface, a rise on drug permeation is achieved. The increasing effect of x_2 on hydrocortisone permeation may result from the soluplus contribution to the amorphous state of hydrocortisone nanocrystals [2, 23]. In fact, drug amorphization may improve hydrocortisone permeation due to the superior solubility observed for the amorphous form [135].

In addition, it has also been reported that drug nanocrystals may accumulate in hair follicles, generating a reservoir that gradually increases drug penetration into contiguous skin layers in a concentration-dependent manner [6, 15].

4.9. Stability Testing

4.9.1. Analytical Centrifugation

Inspecting the effect of formulation and process variability on the physical stability of experimental formulations, significant differences ($p < 0.05$) were observed for the instability index, ranging from 0.521 ± 0.197 (F_{16}) to 0.901 ± 0.225 (F_{11}), and for the separation velocity, varying from -12.8 ± 0.3 μm/s (F_7) to 41.5 ± 0.7 μm/s (F_{11}) (Table 9). These observations reveal a relative long-term physical stability of the experimental formulations.

The shape and progression of the transmission profiles provide information on the kinetics of the separation process, particle characterization, as well as estimates particle-particle interactions [158]. Hence, the transmission profiles progress represented in Figure 13 enables to infer that the creaming phenomenon (represented by the negative values of separation velocity) was the predominant separation process. A deviation to this finding was observed for the F_{11} formulation, where the sedimentation phenomenon (denoted by the positive value of separation velocity) was prevalent.

An overall analysis of transmission profiles, particle size and stability indicators allow to conclude that the experimental formulations with smaller particle sizes tend to present a lower instability index (close to 0.5) and separation velocity and, therefore, a greater stability level. Moreover, formulations presenting more uniform particle size distribution showed symmetrical

spacing between acquired profiles and better stability, while formulations exhibiting multimodal particle size distribution (e.g., F_{11}) showed decreasing spacing between profiles and greater instability [158].

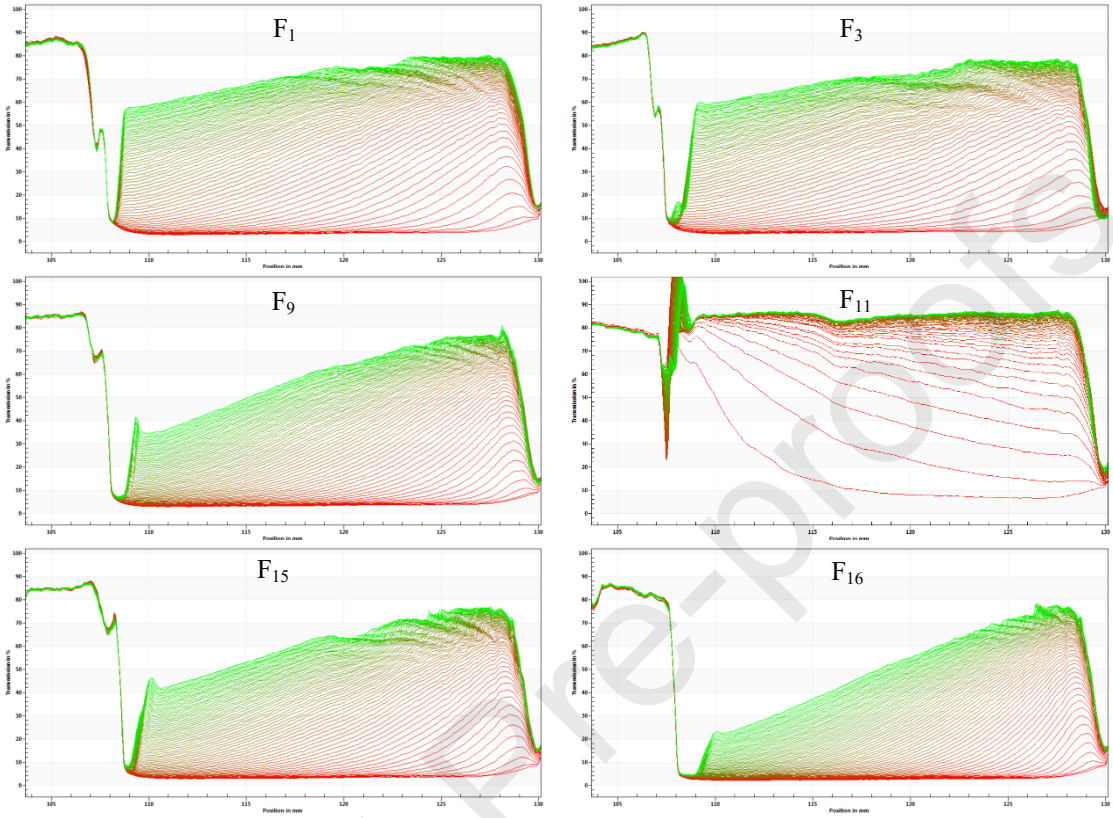

Figure 13 – Transmission profiles of different experimental formulations: F_1 (lower stabilizer agent concentration), F_3 (lower HPH time), F_9 (higher stabilizer agent concentration), F_{11} (absence of squalene and more unstable), F_{15} (higher HPH time) and F_{16} (higher squalene concentration and more stable formulation).

Physical instability phenomena are straight related to particle migration (sedimentation and/or creaming) or, because of interactions among particles, variations in particle size distribution potentiate their movement [62]. In general, these interactions occur naturally due to Brownian motion, where the collision between dispersed particles can generate aggregation. These collisions may be accelerated by physical forces, such as centrifugal acceleration and result in separation phenomena, predicted by analytical centrifugation. However, phenomena related to physicochemical and biological processes, which includes Ostwald ripening, may not be accelerated through centrifugal forces [159].

As represented in Table S3, squalene concentration (x_1) demonstrated a significant impact on instability index response in an antagonistic manner ($Prob>|t| < 0.05$). Increasing concentrations of the squalene component contributed to lower values of the pondered response. In addition to the main function of promoting skin permeability, permeation enhancers can also exhibit emulsifying effects, contributing to a more efficient particle size reduction and formulation stability [30]. Although not described in the literature for nanocrystals, squalene has been widely selected as an oil component to produce stable emulsions with small droplet sizes [160, 161]. In the present study, the importance of squalene as a formulation component was observed throughout the characterization of the F_{11} formulation, where the absence of squalene seemed to produce a significant physical instability with the highest values of instability index and

separation velocity. The stability effect relies on the affinity of the stabilizing agent for the drug surface, the resulting packaging density, and the thickness of the stabilizing layer. In fact, when the squalene is present in the formulation, its lipophilic nature may reinforce the hydrophobicity of the hydrocortisone particles and thus, increase the thickness of the stabilizing agent layer, contributing to a better nanosuspension stabilization, less susceptible to physical separation phenomena [17].

As displayed in Table S3, soluplus concentration (x_2) also impacted the instability index and separation velocity responses in an indirect trend. Increasing concentrations of the stabilizing agent resulted in lower values of the considered responses, since the soluplus polymer interacts with the hydrocortisone and covers the newly formed surfaces, providing adequate steric hindrance to prevent particle aggregation and improve physical stability of experimental formulations.

[Insert Table 9 around here]

4.9.2. Colloidal Stability

Colloidal stability is a fundamental feature to predict the long-term storage of a nanosuspension, once drug particles in the nanosized range are thermodynamically unstable [102, 162]. Indeed, ensuing formulation stability throughout its life cycle is mandatory since instability phenomena impact product safety and efficiency. The particle size reduction process comprises fracturing of drug crystals, adsorption and desorption of polymer molecules on drug surfaces, drug dissolution and precipitation, formation of polymeric micelles, particle aggregation and segregation, and crystal growth [69, 163]. In this context, the control of nanocrystal growth and zeta potential deviations were investigated as fundamental quality features to predict long-term stability of experimental formulations.

Considering formulation and process variability on the colloidal stability of experimental formulations, important differences ($p < 0.05$) in the particle size, size distribution and surface charge of nanocrystal were detected at 30 days of storage.

Taking into account particle size in the original dispersion medium (t = 0 days), for the experimental formulations that initially exhibited small particle size and narrow distribution, a slight increase in Dx(10) values were perceived throughout storage, ranging from 61 ± 8 nm (F_9) and 239 ± 8 nm (F_3) (Table 9). For the original formulations with larger particle dimensions and lower uniformity, a significant increase for the Dx(90) response was observed, changing from 27,956 ± 6,104 nm (F_1) to 562 ± 14 nm (F_{15}) (Table 9). An opposite trend was detected for the Dx(50) results, varying from 190 ± 6 nm (F_2) to 1,154 ± 132 nm (F_3) (Table 9).

The decrease in Dx(50) values may result from sedimentation/precipitation of larger nanocrystals, with smaller and more stable nanocrystals remaining in suspension [17]. As exhibited in Table S3, HPH time (x_3) was the most significant variable for the investigated response ($Prob>|t| < 0.05$). A positive correlation was observed for x_3 and the small particle size with increasing homogenization time contributing to produce more stable formulations, apparently because of the de-aggregation velocity of soluplus micelles, whose monomers are available for diffusion on newly formed surfaces [17]. Furthermore, a longer homogenization process promotes the fracture of micronized drug particles into nanometer sizes, resulting in more uniform nanosuspensions.

As previously outlined, experimental formulations exhibited improved saturation solubility. When stored in a fridge, a decrease in drug solubility may occur, leading to its recrystallization in the form of large crystals [17]. These colloidal changes can also be attributed to agglomeration and/or crystal growth by the Ostwald ripening effect [90, 119]. Nanosuspensions provides an improvement in the surface area of drug particles, associated with a high interfacial free energy of the system. Thermodynamically unstable, nanosuspensions tend to minimize their

total energy by aggregation or by crystal growth, through the Ostwald ripening effect [20, 69, 119, 120]. The aggregation process results from Van der Waals or hydrophobic forces during the manufacturing process or storage. Aggregation phenomenon can be prevented in the presence of a suitable stabilizing agent through electrostatic and/or steric repulsion between nanocrystals [19, 131]. Ostwald ripening phenomena is the process of particle growth at the expense of smaller particles, due to the higher saturation solubility of finely dispersed particles. Driven by the concentration gradient, molecules near to the small particles settle to the surface, resulting in larger particles. Hence, due to recrystallization on the surface of larger particles, the formation of microparticles occurs [2, 119]. Differences in saturation solubility, as a result of different particle sizes, can be avoided when a narrow size distribution is achieved [4, 19, 164].

Hydrocortisone solid state can also be an instability source, as the enhanced solubility of the amorphous form presents great potential for the Ostwald ripening process [10]. Additionally, the amorphous state is a higher-energy solid form, thermodynamically unstable and prone to aggregation, which tends to convert to a more stable crystalline stage over storage [4, 98, 164].

According to the size distribution percentiles, span values fluctuated from 1.68 ± 0.14 (F_{14}) and 62 ± 10 nm (F_1) (Table 9). As shown in Table S3, the regression model did not elect any factor that significantly impacted the considered response.

Considering the surface charge of colloidal particles, the experimental formulations exhibited an increase in the ZP response throughout the storage period, ranging from -11.9 ± 0.2 mV (F_1) to -1.06 ± 0.09 mV (F_9) (Table 9). ZP values remained within the range of ±20 mV, which suggests that the diffuse layer remained intact over time, ensuring the steric stabilization of the nanocrystals.

As displayed in Table S3, soluplus concentration (x_2) was the most important factor for the considered response ($Prob>|t| < 0.05$). The ZP appeared to be positively influenced by the concentration of the stabilizing agent As the soluplus concentration increased, the surface charge also increased for less negative values. Small values of ZP (closer to zero) may be indicative of complete coverage of the hydrocortisone particles by the stabilizer , providing adequate steric stabilization to prevent particle aggregation and crystal growth and hence, long-term physical stability of experimental formulations [120].

4.10. Design Space

Design Space (DS) is a multidimensional combination and interaction of input variables that have been demonstrated to provide quality assurance that establishes the optimal settings of CMAs and CPPs, fulfilling CQAs requirements set forth in the QTPP. Working within the DS is not considered a change. Movement out of the DS is considered to be a change and would normally initiate a regulatory post approval change process [35].

In the present work, RSM was used to achieve the optimal factor conditions. The responses acquired from the DoE experiments were statistically analyzed to provide the model relationship between responses and independent variables [165]. Based on this model, a DS was established for all investigated CQAs (Figure 14 and 15). The target value of each CQA is detailed in Table 3. Figure 14 shows an *InSpec Portion* value close to zero. It means that, not defining the operational boundaries, the variables will hardly predict any response within the target values of the CQAs. In this context, the optimal operating limits were defined comprising the following ranges: x_1, 2.85 – 3.0 %, x_2, 1.98 – 2.66%. and x_3, 19.2– 22.5 min. A narrow DS (Figure 15) alerts to the sensitivity of the responses towards the factors and for this reason a strict control of input variables must be implemented [166]. Scatter plots (Figure 15 and 16) provide a visual representation of the operating limits and their impact on response results. Predicted responses that are within the specification limits are colored green, and predicted responses that fall outside the specification limits are colored red. Selected points contain factor levels that are within the operational limits. Monte-Carlo simulations were carried out to simulate product quality profiles, and define operating ranges, without performing experiments. This powerful tool enables simulating random disturbances within the investigated operating range for all factors and thus, estimating the likelihood of meeting CQAs specifications [167].

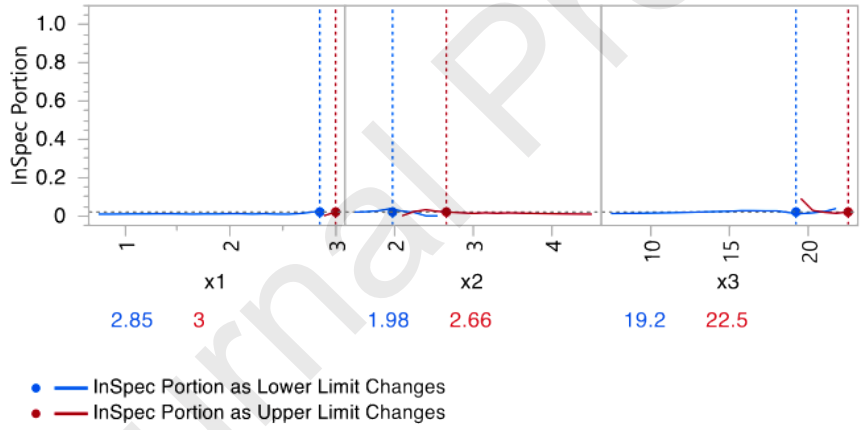

Figure 14 – Design Space settings established for the independent variables.

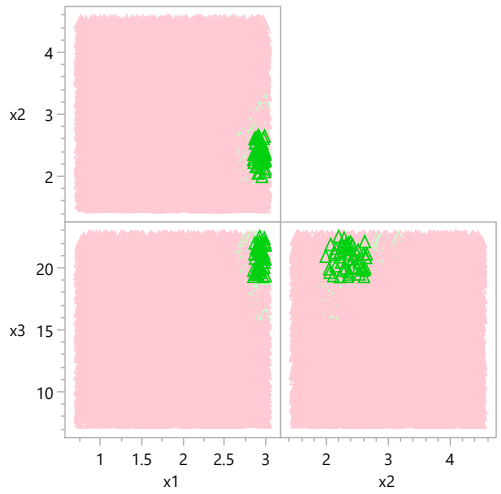

Figure 15- Scatterplot Matrix X highlighting the Design Space.

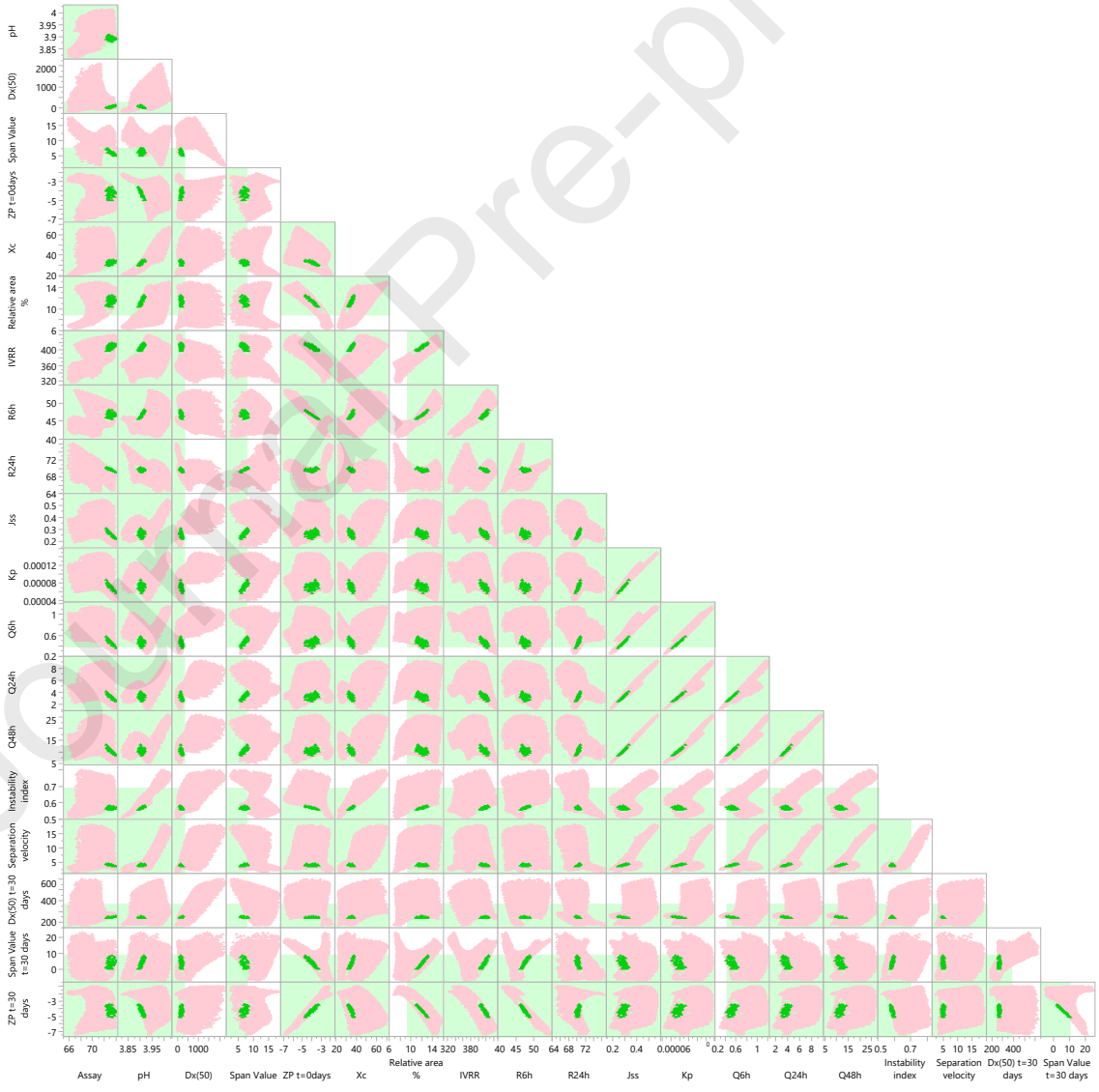

Figure 16 –Scatterplot Matrix Y highlighting the Design Space.

5. Conclusions

Nanocrystals offer great potential for drug delivery that is far from being exhausted. Designing nanocrystal-based formulations is not straightforward due to a lack of systematic understanding of the formulation and manufacturing process. The mechanism underlying nanocrystal performance remains unclear. In this regard, a QbD methodology was successfully implemented to enable comprehensive and systematic product development that meets QTPP requirements. The most critical factors were accurately identified through an FMECA approach. A CCD was carried out to understand the impact of CMAs and CPP and their interactions on the product quality profile. From the combinatorial factor analysis, squalene concentration and soluplus concentrations were considered impacting factors for pH, drug crystallinity, drug release and stability. HPH time was identified as a critical parameter affecting particle size. Soluplus produced a steric stabilization with great impact on ZP results. The study indicates that the hydrocortisone release rate notably depends on the particle size and lower crystallinity of the drug, resulting in better saturation solubility and faster dissolution rate. The sustained release profile of hydrocortisone from experimental formulations shows long-term activity with improved permeation. The investigated variables had no effect on drug permeation. The rise in hydrocortisone skin uptake seemed to be dependent on higher drug bioavailability, prolonged residence time of nanocrystals on the skin surface, and their accumulation in hair follicles. The nanosuspension systems were found to be relatively stable for the studied period. The present study shows a significant progress compared to the marketed formulations. The improved solubility and permeability exhibited by hydrocortisone nanosuspension are responsible for the better *in-vivo* performance. Considering quality criteria outlined in the QTPP, a DS was established comprising the optimal working limits for the most significant variables, within which the prospective product quality is ensured. Innovative approaches such as the QbD methodology has been revolutionizing the pharmaceutical development field, allowing a more robust, less time-consuming and costly, and flexible development process, able to accommodate minor variations without regulatory burden.

Declaration of competing interest

The authors declare that they have no known competing financial interests or personal relationships that could have appeared to influence the work reported in this paper.

Data availability

Data will be made available on request.

Acknowledgments

Ana Simões acknowledges the PhD research grant PD/BDE/135074/2017 assigned by FCT (Fundação para a Ciência e a Tecnologia) and Dendropharma, Investigação e Serviços de Intervenção Farmacêutica, Sociedade Unipessoal Lda, from Drugs R&D Doctoral Program.

The authors acknowledge LAQV/REQUIMTE supported by National Funds (FCT/Ministério da Educação e Ciência, MEC) through project UID/QUI/50006/2013, co-financed by European Union (FEDER under the Partnership Agreement PT2020) and Coimbra Chemistry Center (CQC), supported by FCT through, through the projects UID/QUI/00313/2020.

The authors acknowledge Laboratórios Basi – Indústria Farmacêutica S.A., for the kind donation of micronized hydrocortisone. The authors also thank UCQFarma for making available the Mastersizer 3000 (Malvern Instruments, UK), DSC-204 F1 Phoenix differential scanning calorimeter (Netzsch, Germany), TG 209 F3 Tarsus (Netzsch, Germany), FT-IR/FT-NIR Spectrum

400 spectrometer (Perkin-Elmer, Hopkinton, MA, USA), MiniFlex 600 X-ray diffractometer (Rigaku, Tokyo, Japan) and LUMiSizer stability analyzer (LUM GmbH, Berlin, Germany).

Appendix A. Supplementary material

Supplementary material data to this article can be found online at XXXXX.

List of abbreviations

ANOVA	Analysis of variance
ATR-FTIR	Attenuated Total Reflectance Fourier Transform Infrared
BSC	Biopharmaceutics Classification System
CCCD	Circumscribed central composite design
CCD	Central composite design
CMA	Critical material attribute
CMC	Critical micelle concentration
CPP	Critical process parameter
CQA	Critical quality attribute
D	Detectability
DoE	Design of experiment
DS	Design space
DSC	Differential scanning calorimetry
E_{HCB}	Commercial emulsion of hydrocortisone butyrate salt
ELS	Electrophoretic light scattering
ER	Enhancement ratio
FMECA	Failure Mode, Effects and Critically Analysis
GRAS	Accepted generally referred as safe
HLB	Hydrophilic-lipophilic balance
HPH	High pressure homogenization
HPLC	High performance liquid chromatography
IPM	Isopropyl myristate
IVPT	In vitro permeation testing
IVRR	In vitro release rate
IVRT	In vitro release testing
LD	Laser diffraction
MSE	Mean squared error
MW	Molecular weight
NC_{HC}	Negative control
NIR	Near infrared
P	Probability
PEG	Polyethylene glycol
PG	Propylene glycol
PLC	Polyvinyl caprolactam
PVA	Polyvinyl acetate
QbD	Quality by Design
RMSE	Root mean squared error
RP-HPLC	Reversed-phase high performance liquid chromatography
RPN	Risk Priority Number
RSM	Response Surface Methodology
S	Severity
S_{HCB}	Commercial solution of hydrocortisone butyrate salt
SC	Stratum corneum
SEM	Scanning electron microscopy
SSE	Sum of squared errors
TEWL	Transepidermal water loss
TGA	Thermogravimetric analysis
tlag	Lag time of permeation
UV	Ultraviolet
XRPD	X-Ray Powder Diffractometry
ZP	Zeta potential

References

1. J. Li, Z. Wang, H. Zhang, J. Gao and A. Zheng, *Drug delivery*, 2021, **28**, 19-36.
2. F. Fontana, P. Figueiredo, P. Zhang, J. T. Hirvonen, D. Liu and H. A. Santos, *Advanced Drug Delivery Reviews*, 2018, **131**, 3-21.
3. A. Tuomela, J. Hirvonen and L. Peltonen, *Pharmaceutics*, 2016, **8**, 16.
4. M. Ermelinda S. Eusébio, Ricardo A. E. Castro and J. Canotilho, in *Nanoparticles for Brain Drug Delivery*, eds. Carla Vitorino, Andreia Jorge and A. Pais, Jenny Stanford Publishing, New York, 1st edn., 2021, ch. 7, pp. 209-253.
5. A. Homayouni, F. Sadeghi, J. Varshosaz, H. Afrasiabi Garekani and A. Nokhodchi, *Colloids and Surfaces B: Biointerfaces*, 2014, **122**, 591-600.
6. V. Patel, O. P. Sharma and T. Mehta, *Expert opinion on Drug Delivery*, 2018, **15**, 351-368.
7. R. Shegokar and R. H. Müller, *International Journal of Pharmaceutics*, 2010, **399**, 129-139.
8. L. Al Shaal, R. H. Mueller and C. M. Keck, *Pharmazie*, 2010, **65**, 86-92.
9. Q. Yu, X. Wu, Q. Zhu, W. Wu, Z. Chen, Y. Li and Y. Lu, *Asian Journal of Pharmaceutical Sciences*, 2018, **13**, 518-526.
10. I. S. Mohammad, H. Hu, L. Yin and W. He, *International Journal of Pharmaceutics*, 2019, **562**, 187-202.
11. R. H. Müller, S. Gohla and C. M. Keck, *European Journal of Pharmaceutics and Biopharmaceutics*, 2011, **78**, 1-9.
12. S. B. Lohan, S. Saeidpour, M. Colombo, S. Staufenbiel, M. Unbehauen, A. Wolde-Kidan, R. R. Netz, R. Bodmeier, R. Haag, C. Teutloff, R. Bittl and M. C. Meinke, P*harmaceutics*, 2020, **12**, 400.
13. K. Mitri, R. Shegokar, S. Gohla, C. Anselmi and R. H. Müller, *International Journal of Pharmaceutics*, 2011, **420**, 141-146.
14. H. Piao, N. Kamiya, F. Cui and M. Goto, *International Journal of Pharmaceutics*, 2011, **420**, 156-160.
15. R. H. Müller, R. Shegokar, S. Gohla and C. M. Keck, in *Intracellular Delivery: Fundamentals and Applications, Fundamental Biomedical Technologies*, ed. A. Prokop, Springer Nature BV, Dordrecht, 2011, vol. 5, pp. 411-432.
16. B. Sinha, R. H. Müller and J. P. Möschwitzer, *International Journal of Pharmaceutics*, 2013, **453**, 126-141.
17. P. R. Mishra, L. A. Shaal, R. H. Müller and C. M. Keck, *International Journal of Pharmaceutics*, 2009, **371**, 182-189.
18. L. Peltonen and J. Hirvonen, *International Journal of Pharmaceutics*, 2018, **537**, 73-83.
19. V. B. Junyaprasert and B. Morakul, *Asian Journal of Pharmaceutical Sciences*, 2015, **10**, 13-23.
20. B. Van Eerdenbrugh, G. Van den Mooter and P. Augustijns, *International Journal of Pharmaceutics*, 2008, **364**, 64-75.
21. C. M. Keck and R. H. Müller, *European Journal of Pharmaceutics and Biopharmaceutics*, 2006, **62**, 3-16.
22. B. Sun and Y. Yeo, *Current Opinion in Solid State and Materials Science*, 2012, **16**, 295-301.
23. J. P. Möschwitzer, *International Journal of Pharmaceutics*, 2013, **453**, 142-156.

24. F. O. David and T. V. Goran, *Micromachines*, 2016, **7**, 236-236.
25. A. H. J. R. H. M. Jens-Uwe, *International Journal of Nanomedicine*, 2008, 295.
26. M. Dhaval, J. Makwana, E. Sakariya and K. Dudhat, *Current Drug Delivery*, 2020, **17**, 470-482.
27. P. Liu, X. Rong, J. Laru, B. van Veen, J. Kiesvaara, J. Hirvonen, T. Laaksonen and L. Peltonen, *International Journal of Pharmaceutics*, 2011, **411**, 215-222.
28. P. Santos, A. C. Watkinson, J. Hadgraft and M. E. Lane, *International Journal of Pharmaceutics*, 2012, **439**, 260-268.
29. M. E. Lane, *International Journal of Pharmaceutics*, 2013, **447**, 12-21.
30. P. Karande and S. Mitragotri, *Biochimica et Biophysica Acta* (*BBA) - Biomembranes*, 2009, **1788**, 2362-2373.
31. J. Hadgraft and M. E. Lane, *International Journal of Pharmaceutics*, 2016, **514**, 52-57.
32. C. Vitorino, S. Silva, F. Gouveia, J. Bicker, A. Falcão and A. Fortuna, *European Journal of Pharmaceutics and Biopharmaceutics*, 2020, **153**, 106-120.
33. A. Simões, F. Veiga and C. Vitorino, *Pharmaceutics*, 2020, **12**.
34. M. Fowler, *American Pharmaceutical Review*, 2015.
35. International Council for Harmonisation of Technical Requirements for Pharmaceuticals for Human Use (ICH), ICH Harmonised Tripartite Q8(R2) Guideline: Pharmaceutical Development, 2009. https://database.ich.org/sites/default/files/Q8%28R2%29%20Guideline.pdf (acessed November 11, 2022).
36. International Council for Harmonisation of Technical Requirements for Pharmaceuticals for Human Use (ICH), ICH Harmonised Tripartite Q9(R1) Guideline: Quality Risk Management, 2021. https://database.ich.org/sites/default/files/ICH_Q9-R1_Document_Step2_Guideline_2021_1118.pdf (accessed November 22, 2022).
37. International Council for Harmonisation of Technical Requirements for Pharmaceuticals for Human Use ICH, ICH Harmonised Tripartite Q10 Guideline: Pharmaceutical Quality System, (2008). https://database.ich.org/sites/default/files/Q10%20Guideline.pdf (accessed November 22, 2022).
38. S. M. Dizaj, F. Lotfipour, M. Barzegar-Jalali, M. H. Zarrintan and K. Adibkia, *Materials Science and Engineering: C*, 2014, **44**, 278-284.
39. J. Henriques, J. Sousa, F. Veiga, C. Cardoso and C. Vitorino, *International Journal of Pharmaceutics*, 2019, **554**, 21-35.
40. D. O. Aksoy and E. Sagol, *Fuel*, 2016, **183**, 609-616.
41. B. Dejaegher and Y. Vander Heyden, *Acta Chromatographica*, 2009, **21**, 161–201.
42. B. Dejaegher, A. Durand and Y. V. Heyden, in *Chemometric Methods in Capillary Electrophoresis* . J ohn Wiley & Sons, Inc., New York, U.S.A., 2010, pp. 11-74.
43. B. Dejaegher and Y. V. Heyden, *Journal of Pharmaceutical and Biomedical Analysis*, 2011, **56**, 141-158.
44. M. A. Kassem, A. A. Abdel Rahman, M. M. Ghorab, M. B. Ahmed and R. M. Khalil, *International Journal of Pharmaceutics*, 2007, **340**, 126-133.
45. J. P. Möschwitzer and R. H. Müller, *Drug Development and Industrial Pharmacy*, 2013, **39**, 762-769.
46. J. Möschwitzer and R. H. Müller, *European Journal of Pharmaceutics and Biopharmaceutics*, 2006, **62**, 282-287.

47. M. Mendes, H. T. Soares, L. G. Arnaut, J. J. Sousa, A. A. C. C. Pais and C. Vitorino, *International Jjournal of Pharmaceutics*, 2016, **515**, 69-83.
48. H. Xiao, F. Yang, Q. Lin, Q. Zhang, L. Zhang, S. Sun, W. Han and G.-Q. Liu, *International Journal of Biological Macromolecules*, 2020, **160**, 437-445.
49. Malvern Instruments, Mastersizer 3000 User Manual, https://www.montana.edu/eal-lres/documents/Mastersizer-3000-user-manual-English-MAN0474-2-1.pdf, (accessed 8 of Sept 2022).
50. E. De Cleyn, R. Holm and G. Van den Mooter, *Journal of Pharmaceutical Sciences*, 2019, **108**, 1905-1914.
51. International Organization for Standardization (ISO), ISO 13320:2020 - Particle size analysis - Laser diffraction methods, Switzerland, 2020.
52. L. Bai, S. Huan, J. Gu and D. J. McClements, *Food Hydrocolloids*, 2016, **61**, 703-711.
53. P. P. Anihouvi, S. Danthine, Y. Kegelaers, A. Dombree and C. Blecker, *Food Research International*, 2013, **53**, 156-163.
54. X. Feng, H. Dai, L. Ma, Y. Fu, Y. Yu, H. Zhou, T. Guo, H. Zhu, H. Wang and Y. Zhang, *Colloids and Surfaces B: Biointerfaces*, 2020, **196**.
55. M. Instruments, *Journal*, 2015.
56. V. C. Ito, E. Schnitzler, I. M. Demiate, M. E. S. Eusebio, L. G. Lacerda and R. A. E. Castro, *Starch - Stärke*, 2018, **70**.
57. United States Pharmacopeia (USP), 〈3〉 Topical and Transdermal Drug Products - Product Performance Tests, 2012, 37-41. http://www.triphasepharmasolutions.com/Private/USP%203%20TOPICALS.pdf (accessed September 10, 2022)
58. H. Takeuchi, M. Ishida, A. Furuya, H. Todo, H. Urano and K. Sugibayashi, *Biological and Pharmaceutical Bulletin*, 2012, **35**, 192-202.
59. C. Vitorino, F. A. Carvalho, A. J. Almeida, J. J. Sousa and A. A. C. C. Pais, *Colloids and Surfaces B: Biointerfaces*, 2011, **84**, 117-130.
60. T. Sobisch and D. Lerche, *Colloids and Surfaces A: Physicochemical and Engineering Aspects*, 2008, **331**, 114-118.
61. M. Yerramilli and S. Ghosh, *Journal of Food Science and Technology*, 2017, **54**, 82-92.
62. C. Caddeo, M. Manconi, A. M. Fadda, F. Lai, S. Lampis, O. Diez-Sales and C. Sinico, *Colloids and Surfaces B: Biointerfaces*, 2013, **111**, 327-332.
63. A. Simões, F. Veiga, A. Figueiras and C. Vitorino, *International Journal of Pharmaceutics*, 2018, **548**, 385-399.
64. V. Vikash, K. D. P. Nigam and V. Kumar, *Chemical Engineering Science*, 2021, **232**,.
65. L. Xie, C. D. Rielly and G. Özcan-Taşkin, *Journal of Dispersion Science and Technology*, 2008, **29**, 573-579.
66. A. N. Oktay, S. Ilbasmis-Tamer and N. Celebi, *Pharmaceutical Development and Technology*, 2019, **24**, 1278-1286.
67. B. H. Duong, H. N. Truong, Q. A. P. Nguyen, T. N. N. Phu and L. T. H. Nhan, *Processes*, 2020, **8**.
68. J. Zhang, S. Xu and W. Li, *Chemical Engineering and Processing*, 2012, **57/58**, 25-41.
69. J. Möschwitzer and R. H. Müller, *Journal of Nanoscience and Nanotechnology*, 2006, **6**, 3145-3153.
70. H. Rachmawati, L. Al Shaal, R. H. Müller and C. M. Keck, *Journal of Pharmaceutical Sciences*, 2013, **102**, 204-214.

71. J. Bałdyga, Ł. Makowski, W. Orciuch, C. Sauter and H. P. Schuchmann, *Chemical Engineering Research & Design: Transactions of the Institution of Chemical Engineers Part A*, 2008, **86**, 1369-1381.
72. R. R. Retamal Marín, F. Babick, G.-G. Lindner, M. Wiemann and M. Stintz, *Nanomaterials*, 2018, **8**.
73. S. Pradhan, J. Hedberg, E. Blomberg, S. Wold and I. Odnevall Wallinder, *Journal of Nanoparticle Research*, 2016, **18**, 285.
74. D. Mohammed, K. Hirata, J. Hadgraft and M. E. Lane, *European Journal of Pharmaceutical Sciences*, 2014, **51**, 118-122.
75. A. S. Zidan, N. Kamal, A. Alayoubi, M. Seggel, S. Ibrahim, Z. Rahman, C. N. Cruz and M. Ashraf, *Journal of Pharmaceutical Sciences*, 2017, **106**, 1805-1813.
76. H. K. Vaddi, L. Z. Wang, P. C. Ho and S. Y. Chan, *International Journal of Pharmaceutics*, 2001, **212**, 247-255.
77. M. Chessa, C. Caddeo, D. Valenti, M. Manconi, C. Sinico and A. M. Fadda, *Pharmaceutics*, 2011, **3**, 497-509.
78. L. Trottet, C. Merly, M. Mirza, J. Hadgraft and A. F. Davis, *International Journal of Pharmaceutics*, 2004, **274**, 213-219.
79. A. Mehdizadeh, M. H. Ghahremani, M. R. Rouini and T. Toliyat, *Acta Pharmaceutica (Zagreb, Croatia)*, 2006, **56**, 219-229.
80. P. F. C. Lim, X. Y. Liu, L. Kang, P. C. L. Ho, Y. W. Chan and S. Y. Chan, *International Journal of Pharmaceutics*, 2006, **311**, 157-164.
81. M. H. F. Sakeena, S. M. Elrashid, F. A. Muthanna, Z. A. Ghassan, M. M. Kanakal, L. Laila, A. S. Munavvar and M. N. Azmin, *Journal of Oleo Science*, 2010, **59**, 395-400.
82. J.-Y. Fang, C.-L. Fang, C.-H. Liu and Y.-H. Su, *European Journal of Pharmaceutics and biopharmaceutics*, 2008, **70**, 633-640.
83. Y.-K. Lin, S. A. Al-Suwayeh, Y.-L. Leu, F.-M. Shen and J.-Y. Fang, *Pharmaceutical Research*, 2013, **30**, 435-446.
84. L. H. Reddy and P. Couvreur, *Advanced Drug Delivery Reviews*, 2009, **61**, 1412-1426.
85. L. T. Fox, M. Gerber, J. du Plessis and H. H. Josias, *Molecules*, 2011, **16**, 10507-10540.
86. F. Jia-You, H. Zih-Rou and L. Yin-Ku, *Molecules*, 2009, **14**, 540-554.
87. H. Marwah, T. Garg, A. K. Goyal and G. Rath, *Drug Delivery*, 2016, **23**, 564-578.
88. B. Van Eerdenbrugh, J. Vermant, J. A. Martens, L. Froyen, J. Van Humbeeck, P. Augustijns and G. Van den Mooter, *Journal of Pharmaceutical Sciences*, 2009, **98**, 2091-2103.
89. F. Dehghani, N. Farhadian, S. Golmohammadzadeh, A. Biriaee, M. Ebrahimi and M. Karimi, *European Journal of Pharmaceutical Sciences*, 2017, **96**, 479-489.
90. S. Verma, R. Gokhale and D. J. Burgess, *International Journal of Pharmaceutics*, 2009, **380**, 216-222.
91. M. George and I. Ghosh, *European Journal of Pharmaceutical Sciences*, 2013, **48**, 142-152.
92. G. Soni, K. Kale, S. Shetty, M. K. Gupta and K. S. Yadav, *Heliyon*, 2020, **6**, e03846.
93. S. Shafiq, F. Shakeel, S. Talegaonkar, F. J. Ahmad, R. K. Khar and M. Ali, *European Journal of Pharmaceutics and Biopharmaceutics*, 2007, **66**, 227-243.

94. V. Shah, M. Sharma, R. Pandya, R. K. Parikh, B. Bharatiya, A. Shukla and H.-C. Tsai, *Materials Science and Engineering C*, 2017, **75**, 1231-1241.
95. C. Hong, Y. Dang, G. Lin, Y. Yao, G. Li, G. Ji, H. Shen and Y. Xie, *International Journal of Pharmaceutics*, 2014, **477**, 251-260.
96. P. Urve, T. Ingrid, L. Ivo, L. Andres, K. Kalle, V. Peep, K. Karin and H. Jyrki, *BioMed Research International*, 2014, **2014**.
97. R. N. Shamma and M. Basha, *Powder Technology*, 2013, **237**, 406-414.
98. B. Y. Gajera, D. A. Shah and R. H. Dave, *International Journal of Pharmaceutics*, 2019, **559**, 348-359.
99. M. M. Kamal, A. Salawi, M. Lam, A. Nokhodchi, A. Abu-Fayyad, K. A. El Sayed and S. Nazzal, *Powder Technology*, 2020, **369**, 137-145.
100. A. Homayouni, M. Amini, M. Sohrabi, J. Varshosaz and A. Nokhodchi, *International Journal of Pharmaceutics*, 2019, **562**, 124-134.
101. T. Reintjes, Solubility Enhancement with BASF Pharma Polymers – Solubilizer Compendium, BASF SE Pharma Ingredients & Services, 2011. https://pharmaceutical.basf.com/global/images/b_03_110921e_solubility_enhance_compendium.pdf (accessed in October 23, 222)
102. Y. Wang, Y. Zheng, L. Zhang, Q. Wang and D. Zhang, *Journal of Controlled Release*, 2013, **172**, 1126-1141.
103. R. K. Chang, A. Raw, R. Lionberger and L. Yu, *AAPS Journal*, 2013, **15**, 674-683.
104. S. C. Raposo, S. D. Simoes, A. J. Almeida and H. M. Ribeiro, *Expert Opinion on Drug Delivery*, 2013, **10**, 857-877.
105. A. Gull, S. Ahmed, F. J. Ahmad, U. Nagaich and A. Chandra, *Journal of Drug Delivery Science and Technology*, 2020, **57**.
106. M. Leili, N. Shirmohammadi Khorram, K. Godini, G. Azarian, R. Moussavi and A. Peykhoshian, *Journal of Molecular Liquids*, 2020, **313**.
107. A. E. Sarrai, S. Hanini, N. K. Merzouk, D. Tassalit, T. Szabó, K. Hernádi and L. Nagy, *Materials*, 2016, **9**, 428.
108. A. A. Sağıroğlu, Y. Özsoy and Ö. Özer, *Journal of Drug Delivery Science and Technology*, 2020, **58**.
109. F. Pinto, D. P. C. de Barros, C. Reis and L. P. Fonseca, *Journal of Molecular Liquids*, 2019, **293**.
110. A. Witek-Krowiak, K. Chojnacka, D. Podstawczyk, A. Dawiec and K. Pokomeda, *Bioresource Technology*, 2014, **160**, 150-160.
111. B. A.-A. P. P. A. E. Hami, in *Embedded Mechatronic Systems* eds. A. E. Hami and P. Pougnet, Elsevier Ltd, 1 edn., 2015, vol. 2, Analysis of Failures, Modeling, Simulation and Optimization, ch. 6, pp. 151-179.
112. R. Verseput, I*nternational Journal of Statistics and Applications*, 5 (2015) 21-30.
113. M. Dutka, M. Ditaranto and T. Løvås, *Energies (19961073)*, 2015, **8**, 3606-3627.
114. National Institute of Standards and Technology (NIST), 5.3.3.6.1. Central Composite, e-Handbook of Statistical Methods, 2012. https://www.itl.nist.gov/div898/handbook/pri/section3/pri3361.htm (accessed in October 21, 2022)
115. L. Vera Candioti, M. M. De Zan, M. S. Cámara and H. C. Goicoechea, *Talanta*, 2014, **124**, 123-138.
116. H. Lambers, S. Piessens, A. Bloem, H. Pronk and P. Finkel, *International Journal of Cosmetic Science*, 2006, **28**, 359-370.

117. C. Surber, P. Humbert, C. Abels and H. Maibach, *Current Problems in Dermatology*, 2018, **54**, 1-10.
118. H. J. Lee, N. Y. Yoon, N. R. Lee, M. Jung, D. H. Kim and E. H. Choi, *Experimental Dermatology*, 2014, **23**, 736-741.
119. H. S. M. Ali, P. York and N. Blagden, *International Journal of Pharmaceutics*, 2009, **375**, 107-113.
120. H. S. M. Ali, P. York, A. M. A. Ali and N. Blagden, *Journal of Controlled Release*, 2011, **149**, 175-181.
121. M. A. Altamimi, E. M. Elzayat, W. Qamar, S. M. Alshehri, A. Y. Sherif, N. Haq and F. Shakeel, *Saudi Pharmaceutical Journal*, 2019, 629–636.
122. S. Patnaik, L. A. A. Chunduri, M. S. Akilesh, S. S. Bhagavatham and V. Kamisetti, *Journal of Experimental Nanoscience*, 2016, **11**, 916-929.
123. A. Sharma, D. K. Upadhyay, G. S. Sarma, N. Kaur, G. D. Gupta, R. K. Narang and V. K. Rai, *Journal of Drug Delivery Science and Technology*, 2020, **56**.
124. J. Deng, L. Huang and F. Liu, *International Journal of Pharmaceutics*, 2010, **390**, 242-249.
125. M. Lindner, M. Bäumler and A. Stäbler, *Coatings*, 2018, **8**, 469.
126. National Institute of Standards and Technology (NIST), 4.4.4. How can I tell if a model fits my data? e-Handbook of Statistical Methods, 2012. https://www.itl.nist.gov/div898/handbook/pri/section3/pri3361.htm (accessed in September 07, 2022).
127. National Institute of Standards and Technology (NIST), 5.2.4. Are the model residuals well-behaved?, e-Handbook of Statistical Methods, 2012. https://www.itl.nist.gov/div898/handbook/pmd/section4/pmd44.htm (accessed in September 07, 2022).
128. R. H. Müller and C. Jacobs, *International Journal of Pharmaceutics*, 2002, **237**, 151-161.
129. C. Jacobs and R. H. Müller, *Pharmaceutical Research*, 2002, **19**, 189-194.
130. R. Gadadare, L. Mandpe and V. Pokharkar, *AAPS PharmSciTech*, 2015, **16**, 787-799.
131. H. Yang, F. Teng, P. Wang, B. Tian, X. Lin, X. Hu, L. Zhang, K. Zhang, Y. Zhang and X. Tang, *International Journal of Pharmaceutics*, 2014, **477**, 88-95.
132. P. Shekhawat and V. Pokharkar, *International Journal of Pharmaceutics*, 2019, **567**, 118415-118415.
133. S. S. Gupta, A. Meena, T. Parikh and A. T. M. Serajuddin, *Journal of Excipients and Food Chemicals*, 2014, **5**, 32-45.
134. O. Popa, N. E. Băbeanu, I. Popa, S. Niță and C. E. Dinu-Pârvu, *BioMed Research International*, 2015, **2015**, 1-16.
135. M. A. Altamimi and S. H. Neau, *Saudi Pharmaceutical Journal*, 2017, **25**, 419-439.
136. D. W. Hall, S. N. Marshall, K. C. Gordon and D. P. Killeen, *Lipids*, 2016, **51**, 139-147.
137. L. Petrick and Y. Dubowski, *Indoor Air*, 2009, **19**, 381-391.
138. H. J. Chun, T. L. Weiss, T. P. Devarenne and J. Laane, *Journal of Molecular Structure*, 2013, **1032**, 203-206.
139. J. K. Kauppinen, D. J. Moffatt, H. H. Mantsch and D. G. Cameron, *Applied Spectroscopy*, 1981, **35**, 271-276.
140. A. Sadat and I. J. Joye, *Applied Sciences*, 2020.

141. V. Suitchmezian, I. Jess and C. Naether, *Journal of Pharmaceutical Sciences*, 2008, **97**, 4516-4527.
142. C. Jianxin, W. Jingkang, U. Joachim, Y. Qiuxiang and X. Lvzhong, *Crystal Growth & Design*, 2008, **8**, 1490-1494.
143. H. Yu, D. Xia, Q. Zhu, C. Zhu, D. Chen and Y. Gan, *European Journal of Pharmaceutics and Biopharmaceutics*, 2013, **85**, 1325-1336.
144. K. M. Huh, S. C. Lee, Y. W. Cho, J. Lee, J. H. Jeong and K. Park, *Journal of Controlled Release*, 2005, **101**, 59-68.
145. M. Linn, E.-M. Collnot, D. Djuric, K. Hempel, E. Fabian, K. Kolter and C.-M. Lehr, *European Journal of Pharmaceutical Sciences*, 2012, **45**, 336-343.
146. B. N. Estevinho, R. Mota, J. P. Leite, P. Tamagnini, L. Gales and F. Rocha, *Powder Technology*, 2019, **343**, 644-651.
147. Y. Zhang, M. Huo, J. Zhou, A. Zou, W. Li, C. Yao and S. Xie, *AAPS Journal*, 2010, **12**, 263-271.
148. L. Pourtalebi Jahromi, M. Ghazali, H. Ashrafi and A. Azadi, *Heliyon*, 2020, **6**, e03451.
149. V. Papadopoulou, K. Kosmidis, M. Vlachou and P. Macheras, *International Journal of Pharmaceutics*, 2006, **309**, 44-50.
150. A. M. E. Ribeiro, Berta Rocha, F., *Food and Bioprocess Technology*, 2019, **12**, 1381-1394.
151. T. N. D. Silva, F. Reynaud, P. H. S. Picciani, K. G. de Holanda E Silva and T. N. Barradas, *International Journal of Biological Macromolecules*, 2020, **164**, 2558-2568.
152. M. L. Bruschi, in *Strategies to Modify the Drug Release from Pharmaceutical Systems*, Woodhead Publishing, United Kingdom, 1 edn., 2015, ch. 5, pp. *63-86*.
153. B. H. Estevinho, Ioana-Luiza Blaga, Alexandra-Cristina Rocha, Fernando, *Food and Bioprocess Technology*, 2021, **14**, 1503-1517.
154. M. Miranda, M. T. Cruz, C. Vitorino and C. Cabral, *Materials Science and Engineering: C*, 2019, **103**, 109804-109804.
155. J. Hadgraft, *Skin Pharmacology and Applied Skin Physiology*, 2001, **14**, 72.
156. C. Vitorino, J. Almeida, L. M. Gonçalves, A. J. Almeida, J. J. Sousa and A. A. C. C. Pais, *Journal of Controlled Release*, 2013, **167**, 301-314.
157. A. M. Alambiaga-Caravaca, M. A. Calatayud-Pascual, V. Rodilla, A. Concheiro, A. López-Castellano and C. Alvarez-Lorenzo, *Pharmaceutics*, 2020, **12**, 702.
158. A. R. Fernandes, N. R. Ferreira, J. F. Fangueiro, A. C. Santos, F. J. Veiga, C. Cabral, A. M. Silva and E. B. Souto, *Saudi Pharmaceutical Journal*, 2017, **25**, 1117-1124.
159. D. Lerche and T. Sobisch, *Journal of Dispersion Science and Technology*, 2011, **32**, 1799-1811.
160. J.-J. Wang, K. C. Sung, O. Y.-P. Hu, C.-H. Yeh and J.-Y. Fang, *Journal of Controlled Release*, 2006, **115**, 140-149.
161. H. Chung, T. W. Kim, M. Kwon, I. C. Kwon and S. Y. Jeong, *Journal of Controlled Release*, 2001, **71**, 339-350.
162. C. E. Navarro Chica, B. J. de Haan, M. M. Faas, A. M. Smink, L. Sierra, P. de Vos and B. L. López, *International Journal of Pharmaceutics*, 2020, **590**, 119893.
163. J. Lee, J. Y. Choi and C. H. Park, *International Journal of Pharmaceutics*, 2008, **355**, 328-336.
164. L. Gao, D. Zhang and M. Chen, *Journal of Nanoparticle Research*, 2008, **10**, 845-862.

165. T. Tol, N. Kadam, N. Raotole, A. Desai and G. Samanta, *Journal of Chromatography A*, 2016, **1432**, 26-38.
166. T. Tol, H. Tawde, S. Gorad, A. Jagdale, A. Kulkarni, A. Kasbale, A. Desai and G. Samanta, *Journal of Pharmaceutical and Biomedical Analysis*, 2020, **178**, 112943.
167. S. Orlandini, B. Pasquini, M. Del Bubba, S. Pinzauti and S. Furlanetto, *Journal of Chromatography A*, 2015, **1380**, 177-185.

CRediT author statement

Ana Simões: Conceptualization, Writing - Original Draft preparation; **Ricardo Castro:** Conceptualization, Writing – Reviewing**; Francisco Veiga**: Conceptualization, Supervision, Project management, Funding acquisition; **Carla Vitorino**: Conceptualization, Writing - Reviewing, Supervision, Project management, Funding acquisition.

Declaration of interests

☐ The authors declare that they have no known competing financial interests or personal relationships that could have appeared to influence the work reported in this paper.

☒ The authors declare the following financial interests/personal relationships which may be considered as potential competing interests:

Ana Simoes reports financial support was provided by Fundação para a Ciência e a Tecnologia.

Table 1. Independent variables of the experimental design and respective codification.

Independent variables	Level				
	-α	-1	0	+1	-α
x_1: Squalene concentration (%, w/v)	0.000	0.750	1.875	3.00	3.800
x_2: Soluplus concentration (%, w/v)	0.5	1.5	3.0	4.5	5.5
x_3: HPH time (min)	2.4	7.5	15.0	22.5	27.6

Table 2. Experimental planning according to rotatable circumscribed central composite design (CCCD).

ID	x_1 (%)	x_2 (%)	x_3 (min)
F_1	1.875	0.5	15.0
F_2	0.750	4.5	22.5
F_3	1.875	3.0	2.4
F_4	1.875	3.0	15.0
F_5	0.750	1.5	22.5
F_6	1.875	3.0	15.0
F_7	0.750	1.5	7.5
F_8	0.750	4.5	7.5
F_9	1.875	5.5	15.0
F_{10}	3.000	1.5	22.5
F_{11}	0.000	3.0	15.0
F_{12}	3.000	1.5	7.5
F_{13}	3.000	4.5	7.5
F_{14}	3.000	4.5	22.5

F_{15}	1.875	3.0	27.6
F_{16}	3.800	3.0	15.0

Table 3. Quality target product profile (QTPP) of a hydrocortisone nanocrystal-based formulation.

QTPP element	Target	Is it a CQA ?	Justification
Dosage form	Nanosuspension	-	To improve drug bioavailability and skin permeation.
Route of administration	Topical	-	Local administration avoids systemic side effects. Non-invasive, convenient and painless administration. High patient compliance.
Dosage strength	1% w/v	-	1% w/v of hydrocortisone safeguards formulation efficacy.
Dosage form design	Nanocrystals	-	.
***Assay*[a]**	≥ 65 % of the labelled claim* RSD NMT 5.0%	Yes	Impact on therapeutic efficacy and safety.
Physicochemical attributes			
Appearance	White liquid	No	Not directly related with safety and efficacy. Required to ensure patient compliance and acceptance.
Color	No addition of artificial colors	No	
Odor	No objectionable odor	No	
pH	3.5 - 4.5	Yes	Within an appropriate pH range to guarantee product stability and skin compatibility.
Colloidal properties			
Dx(50)	≤ 350 nm	Yes	To improve hydrocortisone solubility. To ensure a uniform particle size distribution. Impact on physical stability. Impact on hydrocortisone release pattern and skin permeation. To understand the impact of formulation and/or process parameters variability.
Span value	≤ 8	Yes	
Zeta potential[b]	Steric stabilization (≥|20| mV)** / Steric stabilization (<|20| mV)*** / Electrostatic stabilization (>|30| mV)	Yes	Impact on product physical stability.
Solid state properties			

Polymorphic form	Form I	Yes	Thermodynamically more stable. Impact on hydrocortisone solubility, bioavailability and performance. Impact on physical stability.
Relative area %	≥ 9 %	Yes	Impact on hydrocortisone solubility, bioavailability and performance. Impact on physical stability.
X_c	≥ 13%	Yes	To understand the impact of formulation and/or process parameters variability.
Product performance			
IVRT			
IVRR[a]	≥ 230 µg/cm^2/√t, R^2	Yes	To demonstrate that hydrocortisone is released at a higher extent when in the form of nanocrystals. Dissolution and solubility testing.
R_{6h}[a]	≥ 9.3 %	Yes	
R_{24h}[a]	≥ 18 %	Yes	Critical to inspect the kinetic mechanism describing hydrocortisone release. Impact on therapeutic efficacy. To understand the impact of formulation and/or process parameters variability.
IVPT			
J_{ss}[a]	≥ 0.03 µg/cm^2/h	Yes	Impact on therapeutic efficacy. Critical to detect differences regarding the hydrocortisone permeation rate and extent through the skin. To understand the impact of formulation and/or process parameters variability.
k_p[a]	≥ 2.11 x 10^{-5} cm/h	Yes	
Q_{6h}[a]	≥ 0.4 µg/cm^2	Yes	
Q_{24h}[a]	≥ 0.5 0µg/cm^2	Yes	
Q_{48h}	≥ 1.5 µg/cm^2	Yes	
Physical stability			
t = 0 days			
Instability index[a]	≤ 0.7	Yes	Critical to ensure long-term product physical stability. Impact on therapeutics during the storage period.
Separation velocity[a]	< |33.3| µm/s	Yes	
t= 30 days			
Dx(50)	≤ 385 nm	Yes	Impact on long-term physical stability. Impact on long-term product
Span value	≤ 10	Yes	

Zeta potential[b]	Steric stabilization (≥ |20| mV)** / Steric stabilization (<|20| mV)*** / Electrostatic stabilization (>|30| mV)	Yes	performance.

Key: NMT, Not more than; RSD, Relative standard deviation.
The investigated CQAs are highlighted (in bold).
[a] Thresholds were set up according to the behavior of the negative control formulation, NC_{HC}.
[b] [17]
* Note that this range reflects the yield of HPH process.
** Low MW stabilizer.
*** High MW stabilizer.

Table 4. Failure Mode, Effects and Criticality Analysis (FMECA) tool exhibiting initial risk assessment levels of individual formulation and manufacturing process.

Risk area	Variables	Failure mode	Failure cause	Failure effect	S	P	D	RPN	Strategy
Formulation	API	High drug hardness Large size of the starting materials Low/excessive concentration	Weighing error Lack of scientific knowledge Lack of raw materials physicochemical properties knowledge Lack of excipients function Lack of detail formulation understanding Lack of the required *in vivo* performance understanding	Undesirable particle size. Polydisperse distribution. Clogging of the narrow homogenization gap. Insufficient bioavailability. Inadequate drug performance.	4	3	1	12	Establish through preliminary study.
	Stabilizing agent			Undesirable particle size. Polydisperse distribution. Zeta potential. Physical instability. Amorphous state. Skin irritancy. Insufficient bioavailability. Inadequate drug performance.	5	4	3	40	Evaluate through RSM
	Permeation enhancer			Undesirable particle size. Polydisperse distribution. Amorphous state. Skin irritancy.	5	4	1	20	Evaluate through RSM
Manufacturing process	High shear starrier type	Inappropriate mixing	Malfunction of the equipment	Undesirable particle size. Polydisperse distribution.	5	3	1	15	Establish through preliminary study.

	mechanism	Lack of process monitoring Lack of scientific knowledge Lack of equipment specifications knowledge	Clogging of the narrow homogenization gap.				
Pre-mixing rate	Low/excessive pre-mixing rate		Undesirable particle size. Polydisperse distribution. Clogging of the narrow homogenization gap.				Establish through preliminary study.
Pre-mixing time	Low/excessive pre-mixing/HPH time		Undesirable particle size. Polydisperse distribution. Clogging of the narrow homogenization gap.	5	3	1	15	Establish through preliminary study.
Pre-mixing temperature	Low/excessive pre-mixing/HPH temperature		Chemical instability.	5	3	1	15	Establish through preliminary study.
HPH temperature			Chemical instability.	5	3	1	15	Establish through preliminary study.
HPH time	Low/excessive HPH pressure Equipment stops inadvertently		Undesirable particle size. Polydisperse distribution. Physical instability. Amorphous state. Impurities. Chemical instability. Insufficient bioavailability. Inadequate drug performance.	5	4	1	20	Evaluate through RSM
HPH pressure			Undesirable particle size. Polydisperse distribution. Physical instability. Amorphous state. Insufficient bioavailability. Inadequate drug performance.	5	2	1	10	Establish through preliminary study.

Key: API, Active pharmaceutical ingredient; D, Detectability; HPH, High-pressure homogenization; P, Probability; RSM, Response Surface Methodology; RPN, Risk Priority Number; S, Severity.

Table 5. Physicochemical attributes of experimental formulations as a function of independent variables.

ID	Assay / RSD %	pH	Dx(10)[a] nm	Dx(50)[a] nm	Dx(90)[a] nm	Span value[a]	$d_{3,2}$ nm	$d_{4,3}$ nm	Residual %	Weighted Residual %	ZP[a] mV
F_1	69.9 ± 0.5/ 0.8 C	3.96 ± 0.04	82.4 ± 1.4	317 ± 10 C	6,445 ±	20.0 ± 2.4	196.7 ±	3,144 ± 15	3.62 ± 2	0.60 ± 0.16	-12.3 ± 0.4
F_2	70.4 ± 0.4 / 0.5	3.96 ± 0.02	28.9 ± 0.5	261 ± 41 C	3,534 ± 52	13.7 ± 1.8	86.9 ± 2.3	1,799 ±	1.45 ± 1	0.29 ± 0.05	-3.0 ± 0.2
F_3	70 ± 2/ 2.5 C	3.923 ± 05 C	347 ± 12	3,282 ± 255	21,994 ± 94	6.6 ± 0.5 C	1,027 ± 40	6,608 ±	1.51 ± 1	0.373 031	-4.38 ± 9 C
F_4	70 ± 2 / 2.9 C	3.900 ± 08 C	75.7 ± 2.0	353 ± 13	3,822 ±	10.62 ± 0.32	188.9 ±	2,307 ±	2.79 ± 4	0.40 ± 0.06	-3.25 ± 6 C
F_5	67.0 ± 1.3 / 2.0	4.00 ± 0.02	41.8 ± 1.2	306 ± 25 C	3,467 ±	11.3 ± 0.6	117.8 ±	2,974 ±	2.11 ± 4	0.40 ± 0.09	-4.0 ± 0.2
F_6	71.7 ± 0.4/ 0.6 C	3.950 ± 08 C	51.9 ± 2.0	309 ± 16 C	3,734 ±	11.92 ± 0.42	136.2 ±	2,765 ±	2.67 ± 6	0.42 ± 0.09	-3.49 ± 3 C
F_7	64.9 ± 0.6/ 0.9 C*	3.97 ± 0.02	80 ± 7	1,148 ± 96	5,044 ±	4.4 ± 0.4 C	219 ± 16	3,292 ±	1.76 ± 8	0.38 ± 0.10	-3.48 ± 8 C
F_8	67 ± 2/ 3.0 C	3.927 ± 05 C	57.4 ± 3.9	1,534 ± 69	6,294 ±	4.07 ± 0.15	176 ± 11	3,324 ±	1.35 ± 5	0.32 ± 0.12	-2.19 ± 5 C
F_9	59 ± 3/ 4.9 NC	3.877 ± 12 C	41.6 ± 1.0	294 ± 13 C	4,384 ±	14.8 ± 0.7	116.3 ±	2,951 ±	2.37 ± 3	0.29 ± 0.07	-2.7 ± 0.2
F_{10}	76.4 ± 0.4 / 0.5	3.950 ± 08 C	138 ± 3	311.8 ± 1.5	732 ± 49	1.91 ± 0.17	257 ± 7	903 ± 74	0.7 ± 0.3	1.31 ± 0.05	-4.7 ± 0.4
F_{11}	77.3 ± 1.7/ 2.2 C	4.13 ± 0.02	1,289 ± 31	2,407 ± 35	4,849 ±	1.48 ± 0.05	2,182 ± 39	3,486 ±	0.82 ± 4	0.27 ± 0.07	-4.3 ± 0.2
F_{12}	65 ± 2/ 3.4 NC*	3.937 ± 05 C	142.5 ±	335.8 ± 2.0	861 ± 76	2.14 ± 0.22	276.9 ±	1,029 ± 61	1.5 ± 0.8	1.16 ± 0.05	-5.97 ± 7 C
F_{13}	71 ± 2 / 2.9 C	3.870 ±	114.9 ±	513 ± 16	11,094 ±	21.4 ± 1.0	292.7 ±	3,055 ± 32	2.40 ±	0.49 ± 0.11	-3.2 ± 0.2

		08 C								
F_{14}	67 ± 5/ 7.7 NC	3.810 ± 14 C	61 ± 13	245 ± 17 C	2,243 ± 76	9.0 ± 0.8 NC	145.5 ± 5	1,878 ± 0	1.7 ± 0.4	0.66 ± 0.10	-2.60 ± 2 C
F_{15}	73 ± 5 / 6.4 NC	3.893 ± 12 C	32.08 ± 6	174 ± 5 C	2,358 ± 5	13.4 ± 0.6	86.3 ± 0.9	1,720 ± 3	3.00 ± 4	0.388 ± 34	-3.3 ± 0.2
F_{16}	66 ± 2 / 3.6 C	3.867 ± 05 C	46 ± 15	212 ± 48 C	2,177 ± 95	9.6 ± 3.7 NC	115 ± 33	1,627 ± 5	3.0 ± 1.5	0.54 ± 0.11	-3.4 ± 0.2

Key: C, Compliant with QTPP; NC, Noncompliant with QTPP; RSD, Relative standard deviation.

[a] t = 0 days

* Note that this response result is borderline.

Table 6. Hydrocortisone crystallinity as a function of independent variables.

ID	Relative area %	X_c %
F_1	22.19 C	69 C
F_2	7.06 NC	35 C
F_3	9.71 C	40 C
F_4	10.00 C	35 C
F_5	12.48 C	67 C
F_6	9.83 C	43 C
F_7	11.74 C	64 C
F_8	7.33 NC	34 C
F_9	4.29 NC	27 C
F_{10}	13.26 C	42 C
F_{11}	14.66 C	64 C
F_{12}	13.31 C	31 C
F_{13}	8.66 NC	22 C
F_{14}	8.40 NC	21 C
F_{15}	10.05 C	39 C
F_{16}	9.31 C	22 C

Key: C, Compliant with QTPP; NC, Noncompliant with QTPP.

Table 7. Hydrocortisone release profile as a function of independent variables. Data are expressed as mean ± SD (n=3).

ID	IVRR $\mu g/cm^2/\sqrt{t}$	R_{6h} %	R_{24h} %
F_1	516 ± 37 C	61 ± 3 C	75 ± 5 C
F_2	369 ± 23 C	45 ± 3 C	70 ± 6 C
F_3	360 ± 60 C	44 ± 5 C	65 ± 16 C
F_4	389 ± 4 C	47 ± 2 C	72 ± 2 C
F_5	370 ± 7 C	49 ± 3 C	64 ± 4 C
F_6	375 ± 8 C	44 ± 3 C	67.6 ± 1.3 C
F_7	394 ± 24 C	53 ± 2 C	73 ± 6 C
F_8	316 ± 21 C	41.2 ± 1.0 C	63 ± 8 C
F_9	328 ± 33 C	48 ± 5 C	77 ± 5 C
F_{10}	441 ± 18 C	49 ± 3 C	70 ± 2 C
F_{11}	384 ± 15 C	42 ± 2 C	64 ± 2 C
F_{12}	381 ± 22 C	53 ± 3 C	69 ± 6 C
F_{13}	342 ± 39 C	41 ± 5 C	68 ± 7 C
F_{14}	365 ± 25 C	46 ± 4 C	75 ± 3 C
F_{15}	406 ± 30 C	45 ± 4 C	68 ± 6 C
F_{16}	357 ± 21 C	46 ± 4 C	70 ± 3 C

Key: C, Compliant with QTPP; NC, Noncompliant with QTPP.

Table 8. Hydrocortisone permeation profile as a function of independent variables. Data are expressed as mean ± SD (n=3).

ID	J_{ss} µg/cm²/h	ER	K_p (x10 $^{-5}$) cm/h	Q_{6h} µg/cm²	Q_{24h} µg/cm²	Q_{48h} µg/cm²	t_{lag} h
F_1	0.30 ± 0.06 C	0.68	8.02 C	0.620 ± 0.009 C	3.6 ± 0.7 C	12 ± 2 C	9.5
F_2	0.25 ± 0.09 C	0.56	7.03 C	0.64 ± 0.7 C	3.3 ± 0.8 C	10 ± 3 C	8
F_3	0.38 ± 0.14 C	0.85	10.6 C	0.59 ± 0.09 C	4.5 ± 1.2 C	15 ± 5 C	9.4
F_4	0.44 ± 0.15 C	1.01	12.7 C	0.8 ± 0.2 C	6 ± 2 C	18 ± 6 C	9.3
F_5	0.248 ± 0.012 C	0.56	7.38 C	0.51 ± 0.04 C	2.9 ± 0.2 C	10.3 ± 0.4 C	9.9
F_6	0.226 ± 0.003 C	0.51	6.27 C	0.55 ± 0.07 C	3.7 ± 1.3 C	9.1 ± 0.6 C	5
F_7	0.34 ± 0.09 C	0.78	10.5 C	1.0 ± 0.5 C	5 ± 2 C	15 ± 4 C	8
F_8	0.16 ± 0.02 C	0.37	4.84 C	0.44 ± 0.06 NC*	2.0 ± 0.2 C	6.9 ± 1.0 C	8.9
F_9	0.27 ± 0.07 C	0.60	8.96 C	0.73 ± 0.16 C	3.9 ± 1.2 C	11 ± 3 C	7.7
F_{10}	0.278 ± 0.006 C	0.63	7.25 C	0.56 ± 0.12 C	3.5 ± 0.3 C	11.5 ± 0.4 C	9.1
F_{11}	1.2 ± 0.5 C	2.77	31.4 C	2.4 ± 0.7 C	22 ± 7 C	61 ± 17 C	6.9
F_{12}	0.32 ± 0.09 C	0.74	10.0 C	0.8 ± 0.2 C	4.3 ± 1.4 C	14 ± 4 C	8.6
F_{13}	0.5 ± 0.2 C	1.24	15.4 C	1.5 ± 0.7 C	7 ± 3 C	24 ± 8 C	8.1
F_{14}	0.28 ± 0.03 C	0.63	8.17 C	0.65 ± 0.09 C	3.5 ± 0.5 C	11.5 ± 1.2 C	9.0
F_{15}	0.26 ± 0.08 C	0.58	6.92 C	0.59 ± 0.11 C	3.3 ± 0.8 C	11 ± 3 C	8
F_{16}	0.38 ± 0.10 C	0.87	11.6 C	0.7 ± 0.2 C	4.6 ± 1.5 C	16 ± 4	9.8

Key: C, Compliant with QTPP; NC, Noncompliant with QTPP.
* Note that this response result is borderline.

Table 9. Physical stability attributes of experimental formulations as a function of independent variables.

ID	Instability index[a]	Separation velocity[a] µm/s	Dx(10)[b] nm	Dx(50)[b] nm	Dx(90)[b] nm	Span value[b]	ZP[b] mV
F_1	0.739 ± 0.004 NC	-7.44 ± 0.05 C	89.5 ± 3.0	448 ± 51 NC	27,956 ± 6,104	62 ± 10 NC	-11.9 ± 0.2 C
F_2	0.6683 ± 0.0012 C	-6.44 ± 0.06 C	70.3 ± 0.8	190 ± 6 C	607 ± 66	2.8 ± 0.2 C	-1.82 ± 0.07 C
F_3	0.708 ± 0.0005 NC	-7.2 ± 0.4 C	239 ± 8	1,154 ± 132 NC	23,717 ± 2,084	20.4 ± 0.9 NC	-2.7 ± 0.2 C
F_4	0.655 ± 0.005 C	-6.29 ± 0.02 C	122 ± 6	321 ± 4 C	1,208 ± 550	3.4 ± 1.7 C	-2.5 ± 0.4 C
F_5	0.770 ± 0.005 NC	-10.3 ± 0.2 C	101 ± 5	284 ± 6 C	1,170 ± 354	3.8 ± 1.2 C	-4.5 ± 0.3 C
F_6	0.630 ± 0.012 C	-6.41 ± 0.02 C	103 ± 12	287 ± 8 C	854 ± 126	2.6 ± 0.5 C	-2.6 ± 0.2 C
F_7	0.782 ± 0.3005 NC	-12.8 ± 0.3 C	110 ± 8	397 ± 15 NC	3,435 ± 966	8.3 ± 2.3 C	-5.26 ± 0.15 C
F_8	0.7337 ± 0.0009 NC	-9.4 ± 0.5 C	95.3 ± 2.9	377 ± 14 C	11,535 ± 3,450	30 ± 8 NC	-1.7 ± 0.4 C
F_9	0.595 ± 0.005 C	-5.20 ± 0.04 C	61 ± 8	244 ± 11 C	985 ±153	3.8 ± 0.6	-1.06 ± 0.09 C
F_{10}	0.605 ± 0.007 C	-5.71 ± 0.08 C	85 ± 8	301 ± 8 C	2,611 ± 317	8.4 ± 1.1 C	-5.9 ± 0.4 C
F_{11}	0.901 ± 0.004 NC	41.5 ± 0.7 C	75.4 ± 2.9	509 ± 112 NC	1,602 ± 175	3.1 ± 0.4 C	-1.28 ± 0.17 C
F_{12}	0.642 ± 0.011 C	-5.78 ± 0.09 C	110 ± 4	364 ± 15 C	3,426 ± 532	9.1 ± 1.2 C	-7.2 ± 0.2 C

F_{13}	0.567 ± 0.013 C	-5.60 ± 0.03 C	114 ± 2	372 ± 10 C	9,870 ± 575	26.5 ± 1.2 NC	-2.317 ± 0.017 C
F_{14}	0.539 ± 0.007 C	-4.971 ± 0.007 C	119.9 ± 1.1	276 ± 6 C	585 ± 50	1.68 ± 0.14 C	-3.09 ± 0.12 C
F_{15}	0.624 ± 0.004 C	-5.93 ± 0.04 C	106.9 ± 0.9	255.8 ± 1.3 C	562 ± 14	1.78 ± 0.05 C	-2.20 ± 0.14 C
F_{16}	0.521 ± 0.002 C	-4.617 ± 0.013 C	117.0 ± 3.2	278.1 ± 3.0 C	645 ± 74	1.90 ± 0.26 C	-2.28 ± 0.05 C

Key: C, Compliant with QTPP; NC, Noncompliant with QTPP.
[a] t = 0 days
[b] t = 30 days

Table S1. Detailed characterization of unprocessed drug powder, NC_{HC}, SH_{CB} and EH_{CB}.

CQAs	Unprocessed HC powder	NC_{HC}	S_{BHC}	E_{BHC}
pH	N.A.	4.123 ± 0.012	4.44 ± 0.02	4.17 ± 0.05
Dx(10) (nm)	3,526 ± 256	1,918 ± 60	N.A.	N.A.
Dx(50) (nm)	8,095 ± 350	9,131 ± 718	N.A.	N.A.
Dx(90) (nm)	2,1911 ± 6579	35,233 ± 3303	N.A.	N.A.
Span value	2.28 ± 0.89	3.65 ± 0.26	N.A.	N.A.
$d_{3,2}$ (nm)	5,625 ± 553	5,032 ± 237	N.A.	N.A.
$d_{4,3}$ (nm)	14,950 ± 3141	17,889 ± 3975	N.A.	N.A.
Residual	0.451 ± 0.012	0.45 ± 0.08	N.A.	N.A.
Weighted Residual	0.240 ± 0.027	0.39 ± 0.17	N.A.	N.A.
T_{onset} (°C)	225.3	N.A.	N.A.	N.A.
T_{peak} (°C)	227.7	N.A.	N.A.	N.A.
Δ_H (J/g)	-122.3	N.A.	N.A.	N.A.
Relative area % (%)	18.77	9.44	N.A.	N.A.
Xc (%)	99.0	13.0	N.A.	N.A.
IVRR (µg/cm²/√t)	N.A.	270 ± 40	0.54 ± 0.15	0.63 ± 0.03
R_{6h} (%)	N.A.	10.4 ± 1.1	0.23 ± 0.05	0.311 ± 0.003
R_{24h} (%)	N.A.	24 ± 6	0.32 ± 0.36	0.36 ± 0.02
J_{ss} (µg/cm²/h)	N.A.	0.032 ± 0.002	0.0044 ± 0.0012	0.0077 ± 0.0015
K_p (x10^{-5}) (cm/h)	N.A.	2.11	0.439	0.773
Q_{6h} (µg/cm²)	N.A.	0.402 ± 0.006	0.35 ± 0.03	0.371 ± 0.015
Q_{24h} (µg/cm²)	N.A.	0.525 ± 0.001	0.42 ± 0.06	0.47 ± 0.03
Q_{48h} (µg/cm²)	N.A.	1.6 ± 0.08	0.54 ± 0.08	0.68 ± 0.05
Instability index	N.A.	0.803 ± 0.007	N.A.	0.095 ± 0.002
Separation velocity (µm/s)	N.A.	-33.3 ± 1.1	N.A.	-0.63 ± 0.07

Key: E_{HCB}, Commercial emulsion of hydrocortisone butyrate salt; HC, Hydrocortisone; N.A, Not applicable; NC_{Hc}, Negative control; S_{HCB}, Commercial solution of hydrocortisone butyrate salt.

Table S2. ANOVA summary.

CQAs	Regression			Lack of fit	
	F_1	Prob>F	R^2	F_2	Prob>F
Assay	0.6963	0.700	0.510854	14.1784	0.1988
pH	4.6347	0.0378*	0.874246	1.2994	0.5795
Dx(50)[a]	2.1019	0.1891	0.759204	617.1797	0.0306*
Span value[a]	1.6590	0.2768	0.713342	37.8301	0.1228
ZP[a]	1.7990	0.2444	0.729621	158.0736	0.0603
Relative area %	2.4270	0.1464	0.784503	730.4669	0.0281*
Xc %	19.1938	0.0009*	0.966432	0.6532	0.7291
IVRR	2.2639	0.1661	0.772511	15.0373	0.1932
R_{6h}	24.6179	0.0005*	0.973633	0.2680	0.8888
R_{24h}	6.1397	0.0193*	0.902052	0.3408	0.8526
J_{ss}	0.6628	0.7222	0.498539	3.5295	0.3827
k_p	0.7424	0.6700	0.526869	2.4371	0.4500
Q_{6h}	0.6850	0.7075	0.506779	11.1717	0.2232
Q_{24h}	0.7266	0.6802	0.521499	11.4812	0.2202
Q_{48h}	0.7148	0.6879	0.517434	5.6593	0.9835
Instability index[a]	12.9237	0.0028*	0.950945	4.5286	0.3418
Separation velocity[a]	1.6575	0.2772	0.713154	9487.429	0.0078*
Dx(50)[b]	1.1911	0.4306	0.6411	91.6444	0.0791

Span value[b]	0.9530	0.5450	47 0.588388	1225.753	0.0217*
ZP [b]	8.6364	0.0081*	0.928339	335.6324	0.0414*

* Statistically significant
[a] t = 0 days
[b] t = 30 days

Table S3. Coefficient values and respective fit summary of the investigated independent variables.

	Assay	Prob>|t|	pH	Prob>|t|	Dx(50)[a]	Prob>|t|	Span value [a]	Prob>|t|	ZP [a]	Prob>|t|
β_0	70.836	<.0001*	3.9275	<.0001*	401.285	0.4505	11.4680	0.0199*	-3.5467	0.0416*
β_1	-0.711712	0.6267	-0.0534	0.0025*	-407.724	0.0764	1.1319	0.4492	-0.1738	0.7527
β_2	-1.202459	0.4221	-0.0309	0.0280*	30.457	0.879	1.4491	0.3423	1.7149	0.0177*
β_3	1.4394	0.3408	-0.0023	0.8368	-559.058	0.0264*	1.1311	0.4502	0.1770	0.7487
β_{12}	-1	0.602	-0.0166	0.2791	-28.850	0.9117	3.0213	0.1498	0.3238	0.6551
β_{13}	0.35	0.8536	-0.0141	0.3511	227.900	0.3962	-3.6313	0.0944	0.4013	0.5816
β_{23}	-1.675	0.3922	-0.0084	0.5708	-84.400	0.7467	-1.1938	0.5383	-0.1338	0.8525
β_{11}	0.0573	0.9738	0.0216	0.1441	205.580	0.4055	-2.5571	0.1800	0.2016	0.7615
β_{22}	-2.462161	0.2007	-0.0062	0.6560	-152.656	0.5404	1.6166	0.3848	-1.1048	0.1399
β_{33}	0.2892	0.8697	-0.0097	0.4814	355.600	0.1762	-1.0228	0.5697	0.2080	0.7564
	Relative area %	Prob>|t|	Xc	Prob>|t|	IVRR	Prob>|t|	R_{6h}	Prob>|t|	R_{24h}	Prob>|t|
β_0	10.129	0.0029*	39.501	<.0001*	384.5360	<.0001*	45.5447	<.0001*	69.8810	<.0001*
β_1	-0.296	0.7243	-11.305	0.0001*	2.7152	0.7853	0.5650	0.1656	1.6386	0.0272*
β_2	-3.628	0.0041*	-11.951	<.0001*	-37.4262	0.0079*	-3.8705	<.0001*	0.2459	0.6798
β_3	0.054	0.9490	0.903	0.5106	13.872	0.1965	0.1818	0.6304	0.809	0.2024

β_{12}	0.040	0.9708	4	0.0554	0 - 4.5000	0.7306	0.1000	0.8380	1 1.000 0	0.2245
β_{13}	-0.098	0.9290	0.75	0.6721	6.7500	0.6079	0.1500	0.7596	1.250 0	0.1415
β_{23}	-0.153	0.8891	-1.75	0.3394	5.0000	0.7024	2.1000	0.0042 *	2.750 0	0.0098 *
β_{11}	0.337	0.7395	0.444	0.7845	- 9.0396	0.4613	-0.6752	0.1686	- 1.189 1	0.1310
β_{22}	0.808	0.4452	2.161	0.2230	9.3335	0.4575	3.0768	0.0004 *	2.024 1	0.0271 *
β_{33}	-0.391	0.7025	-0.871	0.5986	- 4.5675	0.7073	-0.5126	0.2837	- 1.371 1	0.0928
	J_{ss}	Prob>|t|	K_p	Prob>|t|	Q_{6h}	Prob>|t|	Q_{24h}	Prob>|t|	Q_{48h}	Prob>|t|
β_0	0.3553	0.1053	10.1E-05	0.0774	0.7102	0.1135	5.3201	0,1873	14.81 85	0.1812
β_1	-0.0751	0.3374	-1.62E- 05	0.3914	-0.1467	0.357	-1.8060	0,2359	- 4.279 0	0.2982
β_2	-0.0034	0.9642	0.138E- 05	0.9422	0.0401	0.7953	0.0443	0,9754	- 0.004 9	0.999
β_3	-0.0341	0.6533	-1.25E- 05	0.518	-0.1011	0.518	-0.5215	0,7173	- 1.709 1	0.6658
β_{12}	0.0450	0.6502	1.54E-05	0.5417	0.1525	0.4582	0.6625	0,7246	2.300 0	0.6564
β_{13}	-0.0325	0.7422	-1.13E- 05	0.6518	-0.1	0,.218	-0.4375	0,8155	-1.675	0.745
β_{23}	0.0005	0.9959	0.104E- 05	0.9667	0.0100	0.9602	0.0875	0,9627	-0.275	0.9572
β_{11}	0.1159	0.2308	3.12E-05	0.2045	0.4254 1	0,.015	2.1566	0,2397	6.571 2	0.197
β_{22}	-0.0616	0.5145	-1.44E- 05	0.5447	-0.0503	0.791	-1.1992	0,5049	- 2.901 0	0.5544
β_{33}	-0.0477	0.6064	-1.3E-05	0.576	-0.0790	0.6743	-1.1172	0,528	- 2.297 1	0.6332
	Instability Index[a]	Prob>|t|	Separation velocity[a]	Prob>|t|	Dx(50)[b]	Prob>|t|	Span value[b]	Prob>|t|	ZP[b]	Prob>|t|
β_0	0.6456	<.0001 *	7.0556	0.2327	323.54 8	0.0717	3.4724	0.7793	- 2.516 2	0.0234 *
β_1	-0.0910	<.0001 *	-5.8544	0.0284 *	-22.801	0.7022	0.3457	0.9418	- 0.505 1	0.1651

β_2	-0.0392	0.0063 *	-0.8788	0.6830	-34.303	0.5702	-4.3987	0.3727	2.3508	0.0003 *
β_3	-0.0208	0.0713	-0.6077	0.7761	-144.644	0.0441*	-6.9331	0.1786	0.1532	0.6494
β_{12}	0.0011	0.9307	0.7926	0.7764	12.875	0.8682	-0.5566	0.9285	0.1788	0.6840
β_{13}	0.0016	0.9047	0.5951	0.8309	16.875	0.828	0.0891	0.9885	-0.0113	0.9794
β_{23}	-0.0056	0.6703	-0.1274	0.9635	-14.125	0.8556	-6.5859	0.3104	-0.3763	0.4030
β_{11}	0.0193	0.1425	4.6798	0.1055	-9.248	0.897	-1.2068	0.8329	0.2031	0.6170
β_{22}	0.0035	0.7758	-1.2068	0.6483	-26.980	0.7136	9.6932	0.1344	-1.4870	0.0093 *
β_{33}	0.0031	0.7946	-1.0863	0.6767	101.189	0.1937	1.8367	0.751	-0.0399	0.9216

* Statistically significant coefficients, as extracted from Student`s *t*-test analysis.
[a] t = 0 days
[b] t = 30 days

Table S4. Statistical parameters resulting from the fitting of different mathematical kinetic models to the release profiles.

ID	Zero order - $k_0.t$						
	k_0	R^2	R^2adj	MSE	RMSE	SS	*AIC*
F_1	4.682	0.4155	0.4155	525.4069	22.9218	5254.0691	96.2343
F_2	3.983	0.5775	0.5775	253.9064	15.9344	2539.0639	88.2351
F_3	3.769	0.5231	0.5231	258.8394	16.0885	2588.3941	88.4467
F_4	4.156	0.5678	0.5678	287.1501	16.9455	2871.5006	89.5885
F_5	3.946	0.3857	0.3857	365.7595	19.1248	3657.5945	92.2502
F_6	3.886	0.5623	0.5623	254.6978	15.9593	2546.9776	88.2693
F_7	4.382	0.4656	0.4656	394.5554	19.8634	3945.5538	93.0838
F_8	3.610	0.5559	0.5559	216.9071	14.7278	2169.0707	86.5026
F_9	4.311	0.5898	0.5898	284.6151	16.8705	2846.1513	89.4910

F_{10}	4.134		0.5374	0.5374	313.6671	17.7106	3136.6711	90.5601
F_{11}	3.678		0.5507	0.5507	233.9447	15.2953	2339.4472	87.3344
F_{12}	4.211		0.3981	0.3981	411.5871	20.2876	4115.8708	93.5487
F_{13}	3.759		0.6575	0.6575	185.6101	13.6239	1856.1010	84.7886
F_{14}	4.180		0.6333	0.6333	244.7550	15.6446	2447.5500	87.8313
F_{15}	3.914		0.5856	0.5856	258.3713	16.0739	2583.7135	88.4268
F_{16}	4.053		0.5427	0.5427	286.2102	16.9177	2862.1016	89.5524
NC_{HC}	1.171		0.8601	0.8601	7.7394	2.7820	77.3943	49.8380
ID	**First order - $F_{max}.(1-e^{k_1.t})$**							
	k_1	***F_{max}***	**R^2**	**R^2adj**	**MSE**	**RMSE**	**SS**	***AIC***
F_1	0.200	80.517	0.9841	0.9824	15.8428	3.9803	142.5854	58.5594
F_2	0.158	72.150	0.9986	0.9984	0.9434	0.9713	8.4902	27.5280
F_3	0.174	66.555	0.9976	0.9973	1.4446	1.2019	13.0014	32.2156
F_4	0.162	74.892	0.9980	0.9977	1.5028	1.2259	13.5254	32.6503
F_5	0.213	66.396	0.9955	0.9950	2.9715	1.7238	26.7435	40.1492
F_6	0.163	69.854	0.9975	0.9972	1.6405	1.2808	14.7646	33.6145
F_7	0.188	75.976	0.9959	0.9954	3.3612	1.8334	30.2506	41.5047
F_8	0.165	64.599	0.9989	0.9988	0.5754	0.7585	5.1782	22.0891
F_9	0.155	78.398	0.9993	0.9992	0.5521	0.7430	4.9690	21.6354
F_{10}	0.168	73.936	0.9928	0.9920	5.4254	2.3292	48.8286	46.7715
F_{11}	0.166	65.784	0.9974	0.9971	1.4863	1.2192	13.3771	32.5290
F_{12}	0.210	71.027	0.9943	0.9937	4.3330	2.0816	38.9967	44.2983
F_{13}	0.137	71.139	0.9990	0.9989	0.5974	0.7729	5.3767	22.5028
F_{14}	0.144	77.864	0.9984	0.9982	1.2035	1.0970	10.8315	30.2071
F_{15}	0.156	71.468	0.9907	0.9897	6.4143	2.5326	57.7288	48.6133
F_{16}	0.168	72.286	0.9982	0.9980	1.2673	1.1257	11.4053	30.7748

NC_{HC}	0.080	27.609	0.9992	0.9991	0.0488	0.2210	0.4396	-5.0409
ID	**Higuchi – $k_H.t^{0.5}$**							
	k_H		**R^2**	**R^2adj**	**MSE**	**RMSE**	**SS**	***AIC***
F_1	20.319		0.8602	0.8602	70.5830	8.4014	494.0812	51.6216
F_2	17.121		0.9416	0.9416	27.0699	5.2029	243.6294	56.9565
F_3	16.638		0.9405	0.9405	26.0632	5.1052	234.5685	56.5775
F_4	17.995		0.9373	0.9373	32.6844	5.7170	294.1599	58.8412
F_5	18.425		0.9447	0.9447	28.7877	5.3654	259.0889	57.5717
F_6	16.869		0.9359	0.9359	29.4265	5.4246	264.8385	57.7912
F_7	18.581		0.8971	0.8971	39.4502	6.2809	276.1511	46.9676
F_8	15.639		0.9460	0.9460	20.4840	4.5259	184.3561	54.1687
F_9	17.964		0.9312	0.9312	29.2139	5.4050	233.7111	51.0868
F_{10}	17.723		0.9008	0.9008	44.8277	6.6953	358.6215	54.9404
F_{11}	16.053		0.9369	0.9369	26.1551	5.1142	235.3960	56.6127
F_{12}	19.508		0.9215	0.9215	40.2436	6.3438	321.9489	53.9695
F_{13}	15.510		0.9348	0.9348	25.4865	5.0484	229.3789	56.3538
F_{14}	17.455		0.9357	0.9357	31.5589	5.6177	284.0303	58.4908
F_{15}	16.913		0.9103	0.9103	44.8932	6.7002	404.0388	62.0151
F_{16}	17.737		0.9414	0.9414	29.1986	5.4036	262.7875	57.7135
NC_{HC}	4.433		0.9477	0.9477	2.8951	1.7015	28.9515	39.0218
ID	**Korsmeyer–Peppas - $k_{KP}.t^n$**							
	k_{KP}	***n***	**R^2**	**R^2adj**	**MSE**	**RMSE**	**SS**	***AIC***
F_1	11.144	0.963	0.9936	0.9925	3.7879	1.9462	22.7272	28.9885
F_2	11.686	0.716	0.9884	0.9870	6.0345	2.4565	48.2762	42.7694
F_3	11.555	0.707	0.9845	0.9825	7.6557	2.7669	61.2453	45.1489
F_4	12.091	0.725	0.9872	0.9857	7.4813	2.7352	59.8506	44.9185

F_5	13.738	0.667	0.9764	0.9734	13.8417	3.7204	110.7338	51.0713
F_6	11.317	0.726	0.9862	0.9844	7.1519	2.6743	57.2151	44.4682
F_7	11.684	0.862	0.9946	0.9937	2.4049	1.5508	14.4291	25.3540
F_8	11.094	0.695	0.9860	0.9843	5.9536	2.4400	47.6290	42.6344
F_9	12.173	0.752	0.9910	0.9897	4.3638	2.0890	30.5464	34.7732
F_{10}	10.495	0.837	0.9904	0.9890	4.9615	2.2274	34.7306	35.9286
F_{11}	10.855	0.721	0.9856	0.9838	6.7105	2.5905	53.6842	43.8312
F_{12}	13.311	0.748	0.9806	0.9778	11.3874	3.3745	79.7120	43.4058
F_{13}	10.124	0.741	0.9898	0.9885	4.4946	2.1201	35.9569	39.8232
F_{14}	11.650	0.728	0.9868	0.9851	7.3070	2.7032	58.4563	44.6828
F_{15}	10.130	0.788	0.9822	0.9799	10.0382	3.1683	80.3053	47.8584
F_{16}	12.152	0.714	0.9877	0.9862	6.8986	2.6265	55.1891	44.1077
NC_{HC}	3.092	0.652	0.9851	0.9835	0.9150	0.9566	8.2354	27.1929

ID	**Hixson-Crowell – 100.[1-(1-k_{HC} . t)^3**						
	k_{HC}	**R^2**	**R^2adj**	**MSE**	**RMSE**	**SS**	***AIC***
F_1	0.040	0.9227	0.9227	69.4396	8.3330	694.3958	73.9735
F_2	0.025	0.8800	0.8800	72.1290	8.4929	721.2902	74.3915
F_3	0.024	0.8824	0.8824	68.6842	8.2876	686.8420	73.8531
F_4	0.028	0.8970	0.8970	68.4547	8.2737	684.5472	73.8163
F_5	0.028	0.7871	0.7871	126.7725	11.2593	1267.7254	80.5948
F_6	0.024	0.8605	0.8605	81.1902	9.0106	811.9025	75.6932
F_7	0.034	0.8953	0.8953	77.3121	8.7927	773.1207	75.1548
F_8	0.021	0.8236	0.8236	86.1479	9.2816	861.4788	76.3452
F_9	0.029	0.9216	0.9216	54.3652	7.3733	543.6520	71.2814
F_{10}	0.028	0.8824	0.8824	79.7562	8.9306	797.5616	75.4971
F_{11}	0.022	0.8286	0.8286	89.2350	9.4464	892.3504	76.7324

F_{12}	0.032		0.8415	0.8415	108.4046	10.4118	1084.0464	78.8730
F_{13}	0.021		0.8926	0.8926	58.2133	7.6298	582.1332	72.0337
F_{14}	0.027		0.9222	0.9222	51.9348	7.2066	519.3478	70.7783
F_{15}	0.025		0.8717	0.8717	80.0066	8.9446	800.0655	75.5316
F_{16}	0.027		0.8746	0.8746	78.5029	8.8602	785.0285	75.3229
NC_{HC}	0.004		0.8926	0.8926	5.9409	2.4374	59.4086	46.9288
ID	**Hopfenberg – $100.[1-(1-k_{HB}.t)^n]$**							
	k_{HB}	***n***	**R^2**	**R^2adj**	**MSE**	**RMSE**	**SS**	***AIC***
F_1	6.22E-05	2147.513	0.9446	0.9385	55.3114	7.4372	497.8022	72.3122
F_2	1.69E-05	5119.044	0.9365	0.9295	42.3927	6.5110	381.5339	69.3862
F_3	1.71E-05	4854.903	0.9383	0.9315	40.0303	6.3269	360.2723	68.7555
F_4	1.90E-05	4994.296	0.9465	0.9405	39.5233	6.2868	355.7095	68.6153
F_5	1.93E-05	4910.382	0.8661	0.8513	88.5576	9.4105	797.0185	77.4897
F_6	1.29E-05	6473.822	0.9223	0.9136	50.2573	7.0892	452.3160	71.2582
F_7	2.91E-05	3846.415	0.9389	0.9321	50.1589	7.0823	451.4302	71.2366
F_8	1.05E-05	6889.101	0.8950	0.8833	56.9986	7.5497	512.9876	72.6428
F_9	1.63E-05	6114.064	0.9632	0.9592	28.3314	5.3227	254.9829	64.9532
F_{10}	1.76E-05	5464.667	0.9336	0.9263	49.9950	7.0707	449.9554	71.2006
F_{11}	2.71E-05	2797.418	0.8986	0.8873	58.6881	7.6608	528.1930	72.9641
F_{12}	2.87E-05	3746.449	0.9010	0.8900	75.1955	8.6715	676.7599	75.6905
F_{13}	1.04E-05	7151.899	0.9448	0.9387	33.2165	5.7634	298.9484	66.7030
F_{14}	2.28E-05	4018.270	0.9642	0.9602	26.5689	5.1545	239.1202	64.2466
F_{15}	2.00E-05	4222.725	0.9271	0.9191	50.4690	7.1042	454.2207	71.3044
F_{16}	2.86E-05	3196.692	0.9318	0.9242	47.4230	6.8864	426.8067	70.6196
NC_{HC}	2.19E-05	620.334	0.9071	0.8968	5.7068	2.3889	51.3614	47.3278
ID	**Weibull – $F_{max}.(1-e^{\beta t/\alpha})$**							
	α	***β***	***F_{max}***	**R^2**	**R^2adj**	**MSE**	**RMSE**	**SS**	***AIC***

F_1	7.771	1.403	75.348	0.9995	0.9994	0.5270	0.7259	4.2159	21.8276
F_2	6.839	1.074	70.626	0.9994	0.9992	0.4535	0.6734	3.6278	20.1748
F_3	6.830	1.043	70.736	0.9987	0.9983	0.9834	0.9917	7.8673	28.6898
F_4	6.948	1.106	72.781	0.9996	0.9995	0.3274	0.5722	2.6191	16.5911
F_5	5.586	1.178	63.943	0.9995	0.9994	0.3791	0.6157	3.0331	18.2053
F_6	6.967	1.117	67.739	0.9994	0.9993	0.4213	0.6491	3.3703	19.3651
F_7	6.397	1.173	73.159	0.9998	0.9998	0.1603	0.4004	1.2826	8.7376
F_8	6.416	1.053	63.604	0.9994	0.9992	0.3869	0.6220	3.0953	18.4287
F_9	6.589	1.023	77.806	0.9994	0.9992	0.5492	0.7411	4.3933	22.2810
F_{10}	7.808	1.237	70.256	0.9997	0.9996	0.2852	0.5340	2.2815	15.0730
F_{11}	6.873	1.122	63.751	0.9995	0.9994	0.3025	0.5500	2.4199	15.7208
F_{12}	5.750	1.197	68.092	0.9990	0.9987	0.8893	0.9431	7.1148	27.5839
F_{13}	7.752	1.059	69.674	0.9995	0.9994	0.3304	0.5748	2.6432	16.6919
F_{14}	7.397	1.060	76.315	0.9989	0.9986	0.9087	0.9533	7.2696	27.8207
F_{15}	8.726	1.265	67.337	0.9992	0.9990	0.6399	0.8000	5.1194	23.9633
F_{16}	6.677	1.104	70.360	0.9997	0.9997	0.1972	0.4441	1.5775	11.0145
NC_{HC}	12.534	1.006	27.450	0.9992	0.9990	0.0547	0.2338	0.4373	-3.0991

ID	**Gompertz - $Fmax.e^{-\alpha e^{-\beta.\log(t)}}$**								
	α	***β***	F_{max}	**R^2**	**R^2adj**	**MSE**	**RMSE**	**SS**	***AIC***
F_1	3.078	2.739	84.711	0.9897	0.9871	11.5991	3.4057	92.7927	55.8340
F_2	2.519	1.476	99.153	0.9963	0.9953	2.7954	1.6720	22.3636	40.1818
F_3	2.542	1.399	102.277	0.9984	0.9980	1.1760	1.0844	9.4082	30.6574
F_4	2.527	1.581	98.510	0.9965	0.9956	2.9260	1.7106	23.4084	40.6840
F_5	2.215	2.030	76.333	0.9942	0.9927	4.3342	2.0819	34.6733	45.0057
F_6	2.540	1.640	89.867	0.9965	0.9957	2.5107	1.5845	20.0855	39.0000

F_7	2.420	1.904	90.324	0.9928	0.9909	6.6855	2.5856	53.4841	49.7732
F_8	2.431	1.456	89.124	0.9969	0.9961	1.8875	1.3739	15.1001	35.8617
F_9	2.491	1.303	117.566	0.9974	0.9968	2.2384	1.4961	17.9070	37.7371
F_{10}	2.839	2.072	85.316	0.9932	0.9916	5.7262	2.3929	45.8096	48.0694
F_{11}	2.519	1.659	84.105	0.9958	0.9948	2.7338	1.6534	21.8701	39.9363
F_{12}	-1.901	3.686	72.544	0.9994	0.9993	0.4720	0.6871	3.7764	20.6164
F_{13}	2.735	1.308	108.471	0.9978	0.9972	1.5143	1.2306	12.1142	33.4382
F_{14}	2.666	1.398	112.013	0.9981	0.9976	1.6190	1.2724	12.9521	34.1738
F_{15}	3.088	2.136	81.360	0.9959	0.9949	3.2096	1.7915	25.6770	41.7016
F_{16}	2.466	1.595	94.378	0.9953	0.9941	3.6744	1.9169	29.3948	43.1890
NC_{HC}	3.949	0.740	98.033	0.9992	0.9990	0.0532	0.2307	0.4260	-3.3878